Single-Crystal Plasticity at Finite Strains: A Computational Investigation of Hardening Relations

---

Timothy M. Povall

A dissertation presented for the degree of Master of Science
in the Department of Mathematics and Applied Mathematics,
Faculty of Science,
University of Cape Town,
South Africa.

Supervisor: Prof. B.D. Reddy

March 2013

Plagiarism Declaration

I know the meaning of plagiarism and declare that all of the work in this dissertation, save for that which is properly acknowledged, is my own.

Signed:_____

Date:__/__/2013

Abstract

This dissertation has two main objectives. The first is to develop and implement a numerical algorithm to solve the system of equations that describe single-crystal viscoplasticity under finite strains. The second objective is to use the computer code that is developed to examine three hardening laws that have been proposed. The first is an isotropic hardening law. The second is a hardening law that is expressed implicitly. The third is a novel hardening law in which the slip resistance is expressed explicitly in terms of the accumulated slip on each slip-system. The numerical method uses a predictor-corrector type algorithm and is coupled with a finite element method. The numerical method is validated by comparing with results from the literature. After calibrating the hardening rules, two different model problems are examined: A spherical indentation problem and a three dimensional shear problem. For both problems, the numerical code is run with the three hardening rules. For each hardening rule three types of crystal are examined: A crystal with only one slip system, a crystal with two slip systems and a front centered cubic (FCC) crystal. All three hardening rules show very similar results.

Acknowledgements

I am grateful to my supervisor, Prof. Daya Reddy, for his guidance and his patience. I gratefully acknowledge the South African National Research Foundation (NRF) for their financial support through the research chair in computational and applied mechanics. I am thankful for the working and social environment I have had in the Centre for Computational and Applied Mechanics (CERECAM). In particular I would like to thank Jean-Paul Pelteret and Dr Andrew McBride for the many hours of help they have given me. I am grateful to my parents, Mark and Julie Povall, my sisters and my friends for their amazing support and their unwavering (alas, mostly unsuccessful) attempts to understand the topic of this dissertation. Lastly, I am very thankful to my partner, Raissa Philibert, who has been incredibly supportive.

Contents

List of Figures

List of Tables

1. Introduction

The study of the plasticity of metals dates back to the mid 19^{th} century with the work of Tresca, Lévy and St. Venant. These works laid much of the foundation of the theory of plasticity, including the concept of a yield condition, perfect plasticity and basic constitutive relations[1]. In 1913 von Mises [41] derived the general equations for plasticity. In addition to this, he described a pressure-insensitive yield condition that was based purely on mathematical considerations. A decade later Prandtl [29] extended the equations for the plane continuum problem to include the elastic component of strain and in 1930 Reuss extended this to three dimensions [32]. In 1928 von Mises [42] extended his generalized theory to include a general yield function and formally introduced the concept of using the yield function as a plastic potential in the incremental stress-strain relations of the flow theory.

Further work on incremental constitutive relations for hardening materials was done in 1928 by Prandtl [30], who tried to formulate general relations for hardening behaviour. The work of Drucker and Prager, in the middle of the 20^{th} century, allowed for a more fundamental understanding of hardening materials [28, 11].

In 1923 Taylor and Elam [37] described an experiment in which they measured the distortion of an aluminium crystal under tensile stress. The results of the experiment agreed with the theory that the slip bands that appear on the aluminium during the test coincide with the planes of the crystals. In other words, the aluminium was deforming plastically along the slip planes. Taylor and Elam repeated the tension experiment and suggested the concept of a slip resistance [38]. The material, they argued, must have some kind of resistance which increases as the material slips. If not, the material would simply continue slipping along one plane and break. It was observed that the material would deform along one shear band for a while following which the deformations would become more prominent on a new shear band. In 1938 [39], Taylor expanded the theory to crystal aggregates, also called polycrystals. In the paper he described how the friction at the boundaries between the crystals inside the aggregate play a major role in the way the aggregates deform. In the 1960s Mandel [24] and Hill [17] formulated the constitutive equations for elastoplastic behaviour of ductile single crystals undergoing small deformations. This was extended to finite deformations by Rice [33], Hill and Rice [19], Asaro and Rice [2] and Asaro [3, 4]. In 1985 Asaro and Needleman [5] developed a model of rate-dependent crystal plasticity.

The work of Wilkins [44] and Maenchen and Sacks [23] in 1964 on algorithmic strategies for perfect plasticity led to the development of the elasto-plastic return mapping algorithm. Numerous approaches were proposed for this algorithm (see the overview in [34]). In 1985 Simo and Taylor [35] proposed the consistent tangent modulus, which is obtained by enforcing the consistency condition on the discrete algorithmic problem, rather than the continuum problem.

[1] Much of the history here is based on the summaries in [16], [34] and [18].

This allows for a quadratic rate of convergence of the Newton method. In 1990 Weber and Anand [43] developed a new time integration procedure for the plastic evolution equation. In 1996 Miehe [25] presented a stress update algorithm for large-strain rate-independant single-crystal plasticity. In the same year Steinmann and Stein [36] outlined an algorithm for modelling a viscoplastic (rate-dependent) single crystal, with an isotropic hardening rule, under finite strains. The algorithm that was described by Steinmann and Stein forms the foundation of the algorithm that will be used in this project.

There are two main objectives in this project. The first is to develop a numerical algorithm that will solve for a system that describes single-crystal viscoplasticity under large deformations. The second objective is to use this code to examine a few of the hardening laws that have been proposed for this type of problem. The numerical scheme that will be used to solve the problem is a predictor-corrector scheme. The elastic problem will be solved using the Finite Element Method (FEM). This will be done using the Differential Equation Analysis Library (DEAL.II) [7], which is a finite element library written in the C++ programming language. DEAL.II provides a comprehensive framework of functions and data structures on which a finite element model can be built.

This thesis is divided into four parts. In the first part the theory of finite strain single-crystal plasticity is discussed. Chapters 1 to 6 describe the mathematical basis of continuum mechanics and its application to elasticity. Chapter 6 provides a description of single crystals and a mathematical theory of single-crystal viscoplasticity. The last chapter in Part I gives a description of the various hardening rules that were modelled.

The second part of the thesis provides details of the numerical algorithms used to solve the problem described. Chapter 8 gives an overview the numerical method and an outline of the problem in time-discrete form. Chapter 9 describes the finite element method (FEM) and how it is applied to the elastic problem. Chapter 10 describes the algorithms used in the corrector part of the problem. Chapter 11 is a discussion of the programming language and libraries that were used in the numerical method.

The third part shows the results of the numerical method. The numerical method is first validated with two two-dimensional, plane strain, problems, the results of which are compared with results in the literature. Two model problems are then examined. The first is a spherical indentation problem, in which a spherically shaped indenter presses down onto a block. The second problem is a three-dimensional-shear problem, in which a bar is sheared, sheared back to the original position, and then sheared again. All of these problems are run with various types of crystal structures, and with three hardening rules. The first of three hardening rules is the isotropic rule described by Steinmann and Stein [36]. The second is an implicit hardening rule, as first described by Asaro in 1983 [4]. The last rule is a novel hardening rule that is described by Gurtin and Reddy in [14]. The new hardening rule of Gurtin and Reddy is developed in the context of strain-gradient plasticity, here specialised to the conventional case. It is not implicitly dependent on the flow resistance, rather it is dependent on the accumulated slip on each slip-system. This makes the solution much easier to find. A comparison between the results from the hardening rules will therefore be of interest.

Part I.

Theory and continuum formulation of Single-Crystal Plasticity

Notation

Scalars, vectors and tensors

The field variables used in continuum mechanics can be scalar, vector- and tensor-valued. These are generally represented by lower-case, bold lower-case and bold upper-case characters, respectively, e.g.

$$\begin{aligned} \text{scalars} \quad & a, b, \rho, \cdots \\ \text{vectors} \quad & \mathbf{u}, \boldsymbol{\chi}, \cdots \\ \text{tensors (second-order)} \quad & \mathbf{F}, \mathbf{C}, \cdots \\ \text{tensors (fourth-order)} \quad & \mathbb{A}, \mathbb{C}, \cdots \end{aligned}$$

Vectors and tensors are also represented in indicial form relative to a fixed Cartesian basis $\mathbf{e}_i,\ i = 1, 2, 3$, e.g.

$$\begin{aligned} \mathbf{u} &= u_i \mathbf{e}_i, \\ \mathbf{C} &= C_{ij} \mathbf{e}_i \otimes \mathbf{e}_j, \\ \mathbb{A} &= A_{ijkl} \mathbf{e}_i \otimes \mathbf{e}_j \otimes \mathbf{e}_k \otimes \mathbf{e}_l. \end{aligned}$$

The convention in index notation is that the sum is taken over repeated subscripts, i.e.

$$C_{ij} x_j = \sum_{j=1}^{N_{\text{dim}}} C_{ij} x_j$$

Generally a lower case index and symbol (e.g. $\mathbf{e}_i$) represents a basis in the current configuration and an upper case index and symbol (e.g. $\mathbf{E}_i$) represents a basis in the reference configuration. A Greek index (e.g. $\mathbf{m}_\alpha$) represents a basis in some other configuration (such as an intermediate configuration). Tensors are linear transformations of scalars, vectors and other tensors. A second-order tensor is a linear transformation of a vector to another vector, e.g.

$$\mathbf{C}\mathbf{x} = \mathbf{b} \text{ or } C_{ij} x_j = b_i.$$

A fourth-order tensor is a linear transformation of a second-order tensor to another second-order tensor, e.g.

$$\mathbb{A}\mathbf{C} = \mathbf{D} \text{ or } A_{ijkl} C_{kl} = D_{ij}.$$

Derivatives, gradient and divergence

The derivatives of scalar, vector and tensor fields are defined by

$$\begin{aligned}
\frac{\partial a}{\partial \mathbf{x}} &= \frac{\partial a}{\partial x_j}\mathbf{e}_j \\
\frac{\partial \mathbf{u}}{\partial \mathbf{x}} &= \frac{\partial u_i}{\partial x_j}\mathbf{e}_i \otimes \mathbf{e}_j \\
\frac{\partial \mathbf{u}}{\partial \mathbf{C}} &= \frac{\partial u_i}{\partial C_{jk}}\mathbf{e}_i \otimes \mathbf{e}_j \otimes \mathbf{e}_k \\
\frac{\partial \mathbf{F}}{\partial \mathbf{C}} &= \frac{\partial F_{ij}}{\partial C_{kl}}\mathbf{e}_i \otimes \mathbf{e}_j \otimes \mathbf{e}_k \otimes \mathbf{e}_l.
\end{aligned}$$

The gradient operator is the derivative of a field with respect to either the reference or current configuration. The gradients of an arbitrary scalar field a relative to the reference and current configurations are, respectively, denoted by

$$\boldsymbol{\nabla} a \equiv \frac{\partial a}{\partial \mathbf{X}} = \frac{\partial a}{\partial X_A}\mathbf{E}_A$$

and

$$\boldsymbol{\nabla}_{\mathbf{x}} a \equiv \frac{\partial a}{\partial \mathbf{x}} = \frac{\partial a}{\partial x_i}\mathbf{e}_i.$$

The gradients of an arbitrary vector field $\mathbf{u}$ relative to the reference and current configurations are, respectively, denoted by

$$\boldsymbol{\nabla} \mathbf{u} \equiv \frac{\partial \mathbf{u}}{\partial \mathbf{X}} = \frac{\partial u_i}{\partial X_B}\mathbf{e}_i \otimes \mathbf{E}_B$$

and

$$\boldsymbol{\nabla}_{\mathbf{x}} \mathbf{u} \equiv \frac{\partial \mathbf{u}}{\partial \mathbf{x}} = \frac{\partial u_i}{\partial x_j}\mathbf{e}_i \otimes \mathbf{e}_j.$$

The divergence of an arbitrary vector field $\mathbf{u}$ relative to the reference and configurations are, respectively, denoted by

$$\mathrm{Div}\,(\mathbf{u}) = \frac{\partial u_A}{\partial X_A} \text{ and } \mathrm{div}\,(\mathbf{u}) = \frac{\partial u_i}{\partial x_i}.$$

The divergence of an arbitrary tensor field $\mathbf{T}$ relative to the reference and configurations are, respectively, denoted by

$$\mathrm{Div}\,(\mathbf{T}) = \frac{\partial T_{iA}}{\partial X_A}\mathbf{e}_i \text{ and } \mathrm{div}\,(\mathbf{T}) = \frac{\partial T_{ij}}{\partial x_j}\mathbf{e}_i.$$

1. Kinematics

A fundamental assumption of continuum mechanics is that of the continuum. Matter such as solid, liquid or gas is made up of atoms and molecules. Relative to the size of these particles the space between them is vast, making matter inherently discrete. Due to the vast numbers of these particles at a macroscopic scale, however, material quantities can be represented as smooth functions of position and time. In this chapter an overview of the mathematics that is used to describe a continuum is given.

1.1. Motion

Define the body B_0 as an object that occupies a region of Euclidean space $\mathcal{E}$ in some fixed configuration called the reference configuration, also called the material configuration. The choice of a reference configuration is arbitrary. B_0 is referred to as the reference body, and to a point $\mathbf{X}$ in B_0 as a material point or particle. A motion of B_0 is a smooth bijective function $\boldsymbol{\chi}$ that assigns to each material point $\mathbf{X}$ and at time t a point

$$\mathbf{x} = \boldsymbol{\chi}(\mathbf{X}, t), \tag{1.1}$$

where $\mathbf{x}$ is referred to as the spatial (or current) point occupied by $\mathbf{X}$ at time t. The displacement ($\mathbf{u}$) is defined to be the difference between the spatial and reference points, i.e.

$$\begin{aligned} \mathbf{u}(\mathbf{X}, t) &= \mathbf{x} - \mathbf{X} \\ &= \boldsymbol{\chi}(\mathbf{X}, t) - \mathbf{X}. \end{aligned} \tag{1.2}$$

The velocity ($\mathbf{v}$) is defined as the rate of change in time of the displacement, i.e.

$$\mathbf{v}(\mathbf{X}, t) = \dot{\mathbf{u}} = \frac{\partial \mathbf{u}}{\partial t}. \tag{1.3}$$

1.2. Deformation tensors

The tensor field

$$\mathbf{F} := \boldsymbol{\nabla}\boldsymbol{\chi} = \frac{\partial \chi_i}{\partial X_A} \mathbf{e}_i \otimes \mathbf{E}_A, \tag{1.4}$$

is referred to as the deformation gradient. Note use of lower case and upper case in the index notation and the basis vectors, lower-case and upper-case characters represent basis vectors in the spatial and material configurations, respectively. The deformation gradient may be considered as a mapping of an infinitesimal line segment located at $\mathbf{X}$ to an infinitesimal line segment located at $\mathbf{x}$

$$\mathbf{dx} = \mathbf{F}\,(\mathbf{X}, t)\,\mathbf{dX}. \tag{1.5}$$

The deformation gradient can also be used to relate infinitesimal areas in the spatial and reference configurations using Nanson's relation

$$\mathbf{n}\,da = J\mathbf{F}^{-T}\mathbf{N}\,dA, \tag{1.6}$$

where da and dA are infinitesimal areas in the spatial and reference configurations, respectively. $\mathbf{n}$ and $\mathbf{N}$ are the vectors normal to the areas da and dA, respectively. J is the determinant of $\mathbf{F}$ (the Jacobian)

$$J = \det \mathbf{F}. \tag{1.7}$$

Matter should not be able to interpenetrate, so

$$J > 0. \tag{1.8}$$

Two important deformation tensors derived from the deformation gradient are the right and left Cauchy–Green deformation tensors. The right Cauchy-Green tensor is defined as

$$\mathbf{C} = \mathbf{F}^T\mathbf{F}, \quad C_{AB} = F_{iA}F_{iB}, \tag{1.9}$$

and the left Cauchy-Green tensor is defined as

$$\mathbf{B} = \mathbf{F}\mathbf{F}^T, \quad B_{ij} = F_{iA}F_{jA}. \tag{1.10}$$

It is worth noting that $\mathbf{B}$ and $\mathbf{C}$ have the same principal invariants and eigenvalues, but different principal directions (eigenvectors). These principal invariants are defined as

$$I_1(\mathbf{B}) = I_1(\mathbf{C}) = \lambda_1^2 + \lambda_2^2 + \lambda_3^2 \tag{1.11}$$

$$I_2(\mathbf{B}) = I_2(\mathbf{C}) = \lambda_1^2\lambda_2^2 + \lambda_1^2\lambda_3^2 + \lambda_2^2\lambda_3^2 \tag{1.12}$$

$$I_3(\mathbf{B}) = I_3(\mathbf{C}) = \lambda_1^2\lambda_2^2\lambda_3^2, \tag{1.13}$$

where λ_1^2, λ_2^2 and λ_3^2 are the eigenvalues of $\mathbf{B}$ and $\mathbf{C}$.

1.3. Material, spatial and mixed tensor fields

Material and spatial tensors are defined in terms of their mapping properties.

- A spatial tensor field maps spatial vectors to spatial vectors.
- A material tensor field maps material vectors to material vectors.
- A mixed tensor field maps either spatial vectors to material vectors or vice versa.

The deformation gradient is an example of a mixed tensor:

- $\mathbf{F}$ and $\mathbf{F}^{-T}$ map material vectors to spatial vectors.

- $\mathbf{F}^{-1}$ and $\mathbf{F}^T$ map spatial vectors to material vectors.

The right and left Cauchy–Green tensors are material and spatial tensor fields respectively.

1.4. Velocity gradient

The velocity gradient is the tensor field defined by

$$\mathbf{L} = \boldsymbol{\nabla}_{\mathbf{x}}\mathbf{v}. \tag{1.14}$$

If the time derivative of the deformation gradient is taken

$$\begin{aligned}\dot{F}_{iA} &= \frac{\partial}{\partial t}\left(\frac{\partial \chi_i}{\partial X_A}\right)\\ &= \frac{\partial}{\partial X_A}\left(\frac{\partial \chi_i}{\partial t}\right)\\ &= \frac{\partial}{\partial X_A}\left(v_i\right)\\ &= \frac{\partial v_i}{\partial \chi_j}\frac{\partial \chi_j}{\partial X_A},\end{aligned} \tag{1.15}$$

which leads to the differential equation

$$\dot{F}_{iA} = L_{ij}F_{jA}. \tag{1.16}$$

Rearranging this gives the identity

$$\mathbf{L} = \dot{\mathbf{F}}\mathbf{F}^{-1}. \tag{1.17}$$

These results can be used to express the rate of change of the Jacobian $\dot{J}$ in terms of the velocity as follows

$$\begin{aligned}\dot{J} &= \frac{\partial \det(\mathbf{F})}{\partial \mathbf{F}} : \dot{\mathbf{F}}\\ &= \det(\mathbf{F})\mathbf{F}^{-T} : \mathbf{L}\mathbf{F}\\ &= J\mathbf{I} : \mathbf{L}\\ &= J\mathbf{I} : \boldsymbol{\nabla}_{\mathbf{x}}\mathbf{v}\\ &= J\mathrm{div}(\mathbf{v}).\end{aligned} \tag{1.18}$$

2. Stress and Balance Relations

2.1. Body force and traction

Consider a body which is undergoing a deformation, as shown in figure 2.1. Consider an infinitesimal surface area inside the body in the current configuration, da. The relationship between the infinitesimal internal force, $d\mathbf{f}$, and the infinitesimal surface area is given by

$$d\mathbf{f} = \mathbf{t}da = \mathbf{T}dA, \tag{2.1}$$

where $\mathbf{t}$ is the Cauchy traction, which exists in the current configuration, $\mathbf{T}$ is the first Piola–Kirchhoff traction, which exists in the reference configuration and dA is an infinitesimal surface area in the reference configuration. Cauchy's postulate states that the two tractions are dependent on their respective normals, their position and time, i.e.

$$\mathbf{T} = \mathbf{T}(\mathbf{X}, t, \mathbf{N}) \text{ and } \mathbf{t} = \mathbf{t}(\mathbf{x}, t, \mathbf{n}). \tag{2.2}$$

The force per unit current volume that is applied to the entire body is denoted as $\mathbf{b}$.

2.2. Stress

Cauchy's stress theorem postulates a linear relationship between the Cauchy traction, $\mathbf{t}$ and the normal, $\mathbf{n}$. There exists a spatial tensor field $\boldsymbol{\sigma}$, called the Cauchy stress, such that

$$\mathbf{t} = \boldsymbol{\sigma}\mathbf{n}. \tag{2.3}$$

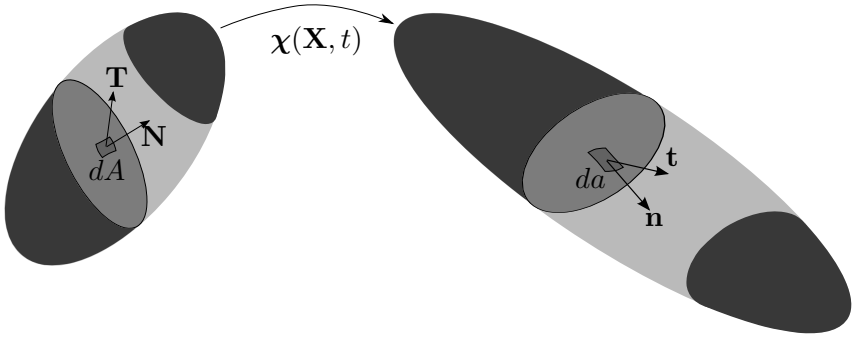

Figure 2.1.: A body undergoing a deformation.

Similarly in the reference configuration there exists a mixed tensor field $\mathbf{P}$, called the first Piola–Kirchhoff stress, such that

$$\mathbf{T} = \mathbf{P}\mathbf{N}. \tag{2.4}$$

These two stresses can be related to one another using Nanson's relation (equation 1.6)

$$\begin{aligned} \mathbf{t}\, da &= \mathbf{T}\, dA \\ \Rightarrow \boldsymbol{\sigma}\mathbf{n}\, da &= \mathbf{P}\mathbf{N}\, dA \\ \Rightarrow \boldsymbol{\sigma} J\mathbf{F}^{-T}\mathbf{N}\, dA &= \mathbf{P}\mathbf{N}\, dA \\ \Rightarrow \mathbf{P} &= \boldsymbol{\sigma} J\mathbf{F}^{-T}. \end{aligned} \tag{2.5}$$

In addition to these two stress measures the second Piola–Kirchhoff stress is used, this exists in the reference configuration

$$\mathbf{S} = \mathbf{F}^{-1}\mathbf{P} \tag{2.6}$$

and the Kirchhoff stress ($\boldsymbol{\tau}$), which is the push-forward of the second Piola–Kirchhoff stress, $\mathbf{S}$, from the material into the spatial configuration

$$\boldsymbol{\tau} = \mathbf{F}\mathbf{S}\mathbf{F}^{T} = J\boldsymbol{\sigma}. \tag{2.7}$$

2.3. Momentum balance

The balance of linear momentum in the spatial configuration is given by

$$\rho\dot{\mathbf{v}} = \mathrm{div}\boldsymbol{\sigma} + \mathbf{b}, \tag{2.8}$$

where $\dot{\mathbf{v}}$ is the acceleration, and ρ is the spatial density. The inertial terms are assumed to be negligible, i.e.

$$\rho\dot{\mathbf{v}} \approx \mathbf{0}. \tag{2.9}$$

This results in the quasi-static balance law (equilibrium equation)

$$\mathrm{div}\boldsymbol{\sigma} + \mathbf{b} = \mathbf{0}. \tag{2.10}$$

It can be shown via the balance of angular momentum that the Cauchy stress is symmetric

$$\boldsymbol{\sigma} = \boldsymbol{\sigma}^{T}, \tag{2.11}$$

and consequently

$$\boldsymbol{\tau} = J\boldsymbol{\sigma} = \boldsymbol{\tau}^{T}, \tag{2.12}$$

$$\mathbf{S} = J\mathbf{F}^{-1}\boldsymbol{\sigma}\mathbf{F}^{-T} = \mathbf{S}^{T} \tag{2.13}$$

and

$$\mathbf{P} = J\boldsymbol{\sigma}\mathbf{F}^{-T} \neq \mathbf{P}^{T}. \tag{2.14}$$

2.4. Boundary conditions

At time t the boundary conditions applied on the surface of the body (∂B) are imposed via the tractions or the displacements, or both. The region on the boundary with traction applied is denoted by ∂B_σ and the region with displacement applied is denoted by ∂B_u. These regions must satisfy the following constraints:

$$\partial B_\sigma \cup \partial B_u = \partial B \tag{2.15}$$

$$\partial B_\sigma \cap \partial B_u = \emptyset \tag{2.16}$$

The Neumann boundary condition enforces the traction

$$\mathbf{t} = \boldsymbol{\sigma}\mathbf{n} \ \text{ on } \partial B_\sigma, \tag{2.17}$$

and the Dirichlet boundary condition enforces displacement

$$\mathbf{u}(\mathbf{X}, t) = \bar{\mathbf{u}} \ \text{ on } \partial B_u. \tag{2.18}$$

2.5. Second law of thermodynamics

The second law of thermodynamics states that the entropy in a closed system is always non-decreasing. A consequence of this is the Clausius-Planck inequality

$$\mathbf{P} : \dot{\mathbf{F}} - \dot{\psi} \geq 0, \tag{2.19}$$

where ψ is the strain energy and the system is assumed to be isothermal. This is also referred to as the dissipation inequality.

3. Elastic constitutive relations

3.1. Strain energy function

A hyperelastic material is defined as a material for which the strain energy is a function of the deformation gradient, i.e.

$$\psi = \psi(\mathbf{F}). \tag{3.1}$$

The dissipation inequality (equation 2.19) can then be rewritten as

$$\mathbf{P} : \dot{\mathbf{F}} - \frac{\partial \psi}{\partial \mathbf{F}} : \dot{\mathbf{F}} \geq 0. \tag{3.2}$$

Rearranging and taking note of the arbitrariness of $\dot{\mathbf{F}}$ gives the relation for the first Piola–Kirchhoff stress

$$\begin{aligned} \left(\mathbf{P} - \frac{\partial \psi}{\partial \mathbf{F}}\right) : \dot{\mathbf{F}} \geq 0 \\ \Rightarrow \mathbf{P} = \frac{\partial \psi}{\partial \mathbf{F}}. \end{aligned} \tag{3.3}$$

3.2. Hyperelasticity

The main assumption of hyperelasticity is that the stress can be derived from a scalar potential. Equation 3.1 satisfies this assumption. Thus it is assumed that the strain energy function is the scalar potential. A second assumption is that the deformation is independent of path taken, thus rigid body motion should not contribute to the strain energy. Given an isotropic material, a consequence of material frame indifference is that the strain energy is dependent on the left or right Cauchy–Green tensors or their invariants, as these are measures of non-rigid body motion

$$\psi_1(\mathbf{C}) = \psi_2(I_C, II_C, III_C) = \psi_3(I_B, II_B, III_B) = \psi_4(\mathbf{B}). \tag{3.4}$$

The strain energy function that will be used is the St. Venant–Kirchhoff strain energy function,

$$\psi(\mathbf{C}) = \frac{\lambda}{8}(\mathrm{tr}(\mathbf{C} - \mathbf{I}))^2 + \frac{\mu}{2}(\mathrm{tr}(\mathbf{C} - \mathbf{I})). \tag{3.5}$$

4. Single crystals

4.1. Poly- and single crystals

Metals are made up of a polycrystalline aggregate, which is composed of grains, which are separated by grain boundaries. Figure (4.1) shows a photomicrograph of a metal, showing the polycrystalline structure. The grains in the polycrystal have been found to have an almost perfect

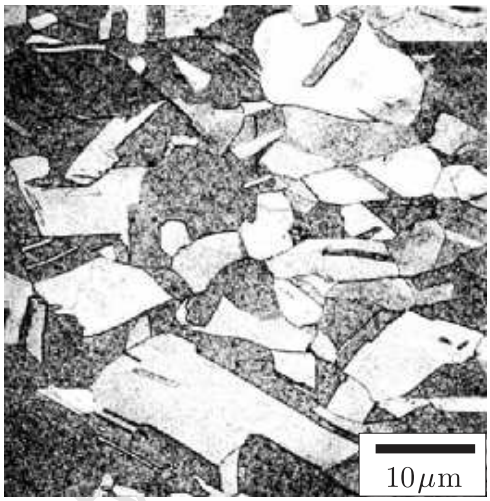

Figure 4.1.: Photomicrograph of a metal [15].

lattice structure. A single crystal is idealized as having this perfect lattice structure. The model of a single crystal, therefore, should approximate very well the grains inside a polycrystal.

4.2. Screw and edge dislocations

If one considers a crystal lattice, where atoms are connected via atomic bonds, an elastic deformation is seen as being due to stretching of these bonds. A plastic deformation is associated with the severing of bonds and the formation of new ones. It is useful to consider the dislocations in a lattice that are caused by the plastic deformations. The two types of dislocations that can occur are called edge and screw. Figures 4.2 and 4.3 show examples of edge and screw dislocations, respectively.

4.3. Slip directions and slip planes

Plastic deformation in single crystals is assumed to occur via the motion of dislocations along crystallographic slip directions on crystallographic slip planes. Two sets of vectors that describe

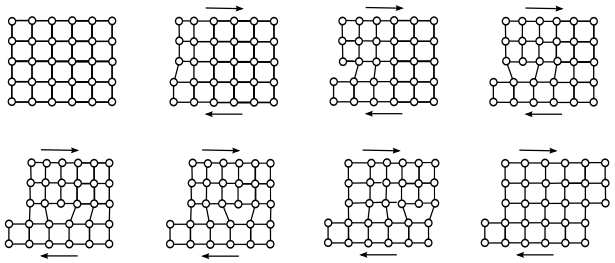

Figure 4.2.: An edge dislocation travels through a two-dimensional lattice. The top face of the lattice undergoes a shear deformation to the right, and the bottom face is sheared to the left. The dislocation first appears on the left face. It then travels through the lattice to emerge on the right face.

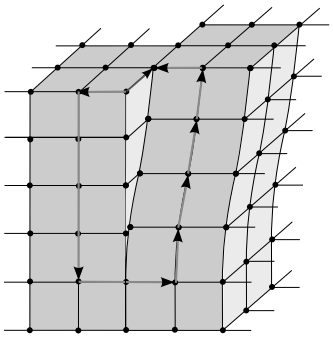

Figure 4.3.: A screw dislocation in a three-dimensional lattice.

the slip systems are introduced. Dislocations occur along preferred slip directions

$$\mathbf{s}^\alpha, \quad \alpha = 1, 2, \ldots, N, \tag{4.1}$$

on preferred slip planes, which are identified by their normals

$$\mathbf{m}^\alpha, \quad \alpha = 1, 2, \ldots, N, \tag{4.2}$$

where $\mathbf{s}^\alpha$ and $\mathbf{m}^\alpha$ are orthonormal vectors in the intermediate (lattice) configuration, i.e.

$$\mathbf{s}^\alpha \cdot \mathbf{m}^\alpha = 0, \quad |\mathbf{s}^\alpha| = |\mathbf{m}^\alpha| = 1. \tag{4.3}$$

The crystal is made up of N independent slip systems, denoted by lower-case Greek superscripts. Note that there is no summation convention for the Greek superscripts.

4.4. Examples of crystal structures

The slip planes in a crystal are the generally the planes in which the atoms in the crystal are most closely packed. The face centre cubic (FCC) crystal is a common crystal structure. The atoms are arranged in a cube so that there is an atom at each vertex and at the centre of each face on the cube. The arrangement is shown in Figure 4.4.

The slip directions and normals for a FCC crystal are shown in Table 4.1. A hypothetical toy crystal is useful for testing the model. This crystal is made up of only two slip planes with one

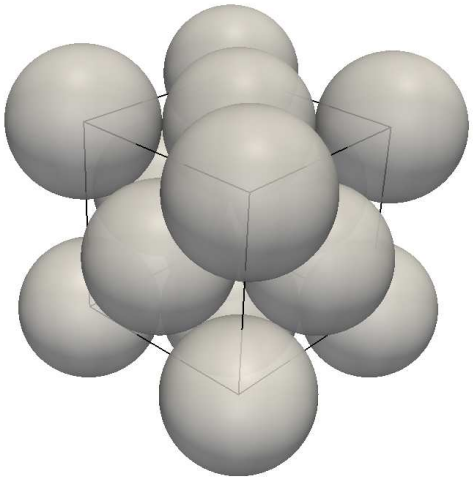

Figure 4.4.: Arrangement of atoms in unit cell of a FCC crystal.

α	$\mathbf{s}^\alpha$	$\mathbf{m}^\alpha$	α	$\mathbf{s}^\alpha$	$\mathbf{m}^\alpha$	α	$\mathbf{s}^\alpha$	$\mathbf{m}^\alpha$
1	[0 1 $\bar{1}$]	(1 1 1)	5	[1 0 1]	($\bar{1}$ 1 1)	9	[$\bar{1}$ $\bar{1}$ 0]	($\bar{1}$ 1 $\bar{1}$)
2	[$\bar{1}$ 0 1]	(1 1 1)	6	[$\bar{1}$ $\bar{1}$ 0]	($\bar{1}$ 1 1)	10	[0 1 1]	(1 1 $\bar{1}$)
3	[1 $\bar{1}$ 0]	(1 1 1)	7	[0 1 1]	($\bar{1}$ 1 $\bar{1}$)	11	[1 $\bar{1}$ 0]	(1 1 $\bar{1}$)
4	[0 1 $\bar{1}$]	($\bar{1}$ 1 1)	8	[1 0 $\bar{1}$]	($\bar{1}$ 1 $\bar{1}$)	12	[1 0 1]	(1 1 $\bar{1}$)

Table 4.1.: The slip directions and normals for a face centre cubic (FCC) crystal in Miller notation. In Miller notation a normal to a plane is expressed in terms of the basis of the reciprocal lattice vectors and is denoted with round brackets, e.g. $(i\ j\ k)$. A direction in the basis of direct lattice vectors is denoted with square brackets, e.g. $[i\ j\ k]$. Also, note that $\bar{1} = -1$.

slip direction each. Table 4.2 shows the slip planes and slip plane normals.

α	$\mathbf{s}^\alpha$	$\mathbf{m}^\alpha$
1	[0 1 1]	(0 $\bar{1}$ 1)
2	[0 $\bar{1}$ 1]	(0 1 1)

Table 4.2.: The slip directions and normals for a toy crystal.

4.5. Slip rate

Gurtin [12] argues that it is more meaningful in a large strain context to have the slip rate, rather than the slip, as the primary variable for describing the plastic deformation. The slip rate is denoted by ν^α and has dimension of $[\text{time}]^{-1}$. The slip is the integral of the slip rate over time

$$\gamma^\alpha = \int_{t_0}^{t} \nu^\alpha \, dt. \tag{4.4}$$

4.6. Resolved shear stress

The resolved shear stress of a slip system is the traction on a slip plane resolved in the slip direction in the current configuration [13]

$$\tau^{\alpha} = \bar{\mathbf{s}}^{\alpha} \cdot \boldsymbol{\sigma} \bar{\mathbf{m}}^{\alpha}, \tag{4.5}$$

where $\bar{\mathbf{s}}^{\alpha}$ and $\bar{\mathbf{m}}^{\alpha}$ are the slip directions and normals pushed forward into the spatial configuration

$$\bar{\mathbf{s}}^{\alpha} = \mathbf{F}^{\mathrm{e}} \mathbf{s}^{\alpha} \quad \text{and} \quad \bar{\mathbf{m}}^{\alpha} = \mathbf{F}^{\mathrm{e}-T} \mathbf{m}^{\alpha}. \tag{4.6}$$

Figure (4.5) gives a graphical representation of the resolved shear stress.

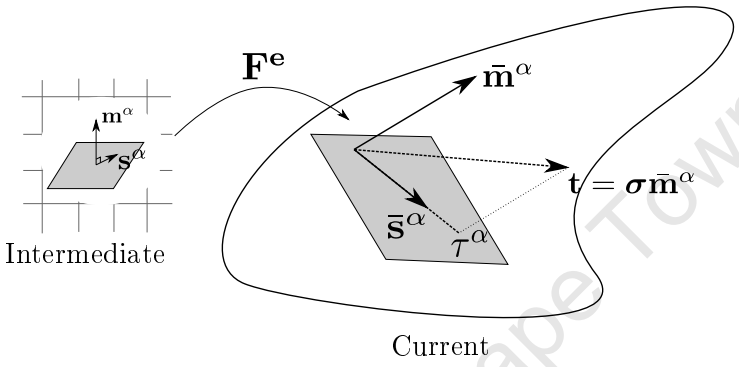

Figure 4.5.: The resolved shear stress on slip plane α.

5. Kinematics of plastic deformation

5.1. Kröner-Lee decomposition

The deformation gradient is split, multiplicatively, into an elastic and a plastic part as:

$$\mathbf{F} = \mathbf{F}^{\mathrm{e}}\mathbf{F}^{\mathrm{p}}, \quad F_{iA} = F^{\mathrm{e}}_{i\alpha}F^{\mathrm{p}}_{\alpha A}, \tag{5.1}$$

where $\mathbf{F}^{\mathrm{e}}$ is the elastic deformation gradient and $\mathbf{F}^{\mathrm{p}}$ is the plastic deformation gradient. This is known as the Kröner-Lee decomposition [21, 22]. Consistent with the requirement that the Jacobian is positive, it is assumed that

$$\det \mathbf{F}^{\mathrm{e}} > 0 \quad \text{and} \quad \det \mathbf{F}^{\mathrm{p}} > 0, \tag{5.2}$$

which means that they are both invertible. In addition to this we assume that plastic flow is volume preserving, i.e.

$$\det \mathbf{F}^{\mathrm{p}} = 1. \tag{5.3}$$

Recall that the deformation gradient maps an infinitesimal neighbourhood of the undeformed body onto an infinitesimal neighbourhood on the deformed body. This is summarized by equation (1.5), which can now be rewritten as

$$\mathbf{dx} = \mathbf{F}^{\mathrm{e}}\mathbf{F}^{\mathrm{p}}\mathbf{dX}. \tag{5.4}$$

The vector $\mathbf{dl}$ is denoted as

$$\mathbf{dl} = \mathbf{F}^{\mathrm{p}}\mathbf{dX}, \tag{5.5}$$

then

$$\mathbf{dx} = \mathbf{F}^{\mathrm{e}}\mathbf{dl}. \tag{5.6}$$

From equations (5.6) and (5.5) it can be seen that $\mathbf{dl}$ can be viewed as an infinitesimal neighbourhood in a new, intermediate, configuration. $\mathbf{F}^{\mathrm{p}}$ maps vectors from the material configuration to the intermediate configuration, and $\mathbf{F}^{\mathrm{e}}$ maps vectors from the intermediate configuration into the spatial configuration. The intermediate configuration represents the structural space that is being modelled by the plastic part, in this case the space is an undistorted crystal lattice. Figure (5.1) gives a visual explanation of the Kröner-Lee decomposition. Note the Greek subscripts used in the index notation in equation (5.1). From here on subscripts with Greek characters will be used to denote tensors that exist in the intermediate configuration. From the elastic deformation tensor, the right and left elastic Cauchy–Green tensors are defined as

$$\mathbf{C}^{\mathrm{e}} = \mathbf{F}^{\mathrm{e}T}\mathbf{F}^{\mathrm{e}} \text{ and } \mathbf{B}^{\mathrm{e}} = \mathbf{F}^{\mathrm{e}}\mathbf{F}^{\mathrm{e}T}, \tag{5.7}$$

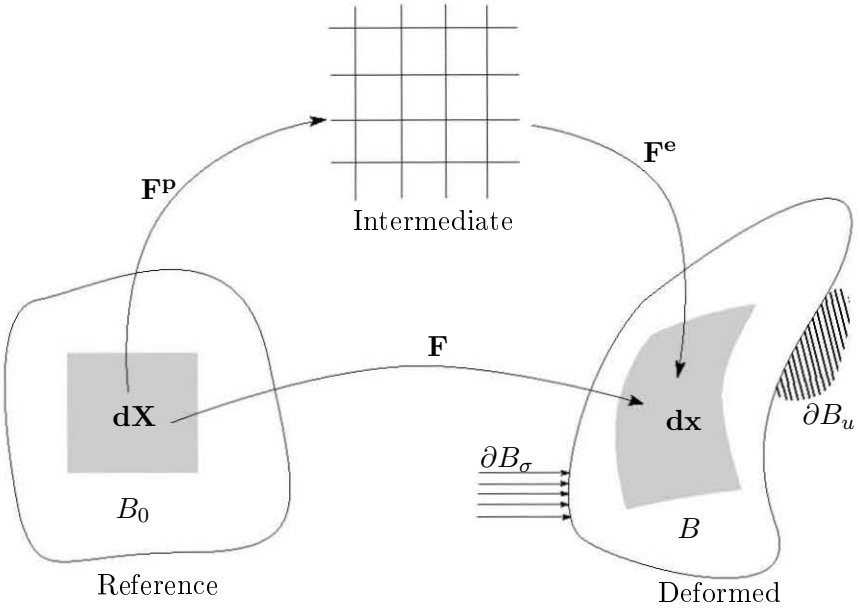

Figure 5.1.: The Kröner-Lee decomposition.

respectively. Similarly the right and left plastic Cauchy–Green tensors are defined, respectively, as

$$\mathbf{C}^{\mathrm{p}} = \mathbf{F}^{\mathrm{p}T}\mathbf{F}^{\mathrm{p}} \text{ and } \mathbf{B}^{\mathrm{p}} = \mathbf{F}^{\mathrm{p}}\mathbf{F}^{\mathrm{p}T}. \tag{5.8}$$

5.2. Elastic and plastic distortion rate

Recall equation (1.17), which relates the velocity gradient to the deformation gradient and its derivative in time. Given the Kröner-Lee decomposition (equation 5.1), the time derivative of the deformation gradient is

$$\dot{\mathbf{F}} = \dot{\mathbf{F}}^{\mathrm{e}}\mathbf{F}^{\mathrm{p}} + \mathbf{F}^{\mathrm{e}}\dot{\mathbf{F}}^{\mathrm{p}}, \tag{5.9}$$

and the inverse is

$$\mathbf{F}^{-1} = \mathbf{F}^{\mathrm{p}-1}\mathbf{F}^{\mathrm{e}-1}. \tag{5.10}$$

Substituting these into equation (1.17) results in

$$\begin{aligned}\mathbf{L} &= \left(\dot{\mathbf{F}}^{\mathrm{e}}\mathbf{F}^{\mathrm{p}} + \mathbf{F}^{\mathrm{e}}\dot{\mathbf{F}}^{\mathrm{p}}\right)\left(\mathbf{F}^{\mathrm{p}-1}\mathbf{F}^{\mathrm{e}-1}\right) \\ &= \dot{\mathbf{F}}^{\mathrm{e}}\mathbf{F}^{\mathrm{e}-1} + \mathbf{F}^{\mathrm{e}}\dot{\mathbf{F}}^{\mathrm{p}}\mathbf{F}^{\mathrm{p}-1}\mathbf{F}^{\mathrm{e}-1}.\end{aligned} \tag{5.11}$$

Now define the elastic and plastic distortion rates, respectively, as

$$\mathbf{L}^{\mathrm{e}} = \dot{\mathbf{F}}^{\mathrm{e}}\mathbf{F}^{\mathrm{e}-1} \text{ and } \mathbf{L}^{\mathrm{p}} = \dot{\mathbf{F}}^{\mathrm{p}}\mathbf{F}^{\mathrm{p}-1}. \tag{5.12}$$

Note that elastic distortion rate is in the current configuration while the plastic distortion rate is in the intermediate configuration.Using these equations, equation 5.11 becomes

$$\mathbf{L} = \mathbf{L}^{\mathrm{e}} + \mathbf{F}^{\mathrm{e}}\mathbf{L}^{\mathrm{p}}\mathbf{F}^{\mathrm{e}-1}, \tag{5.13}$$

it is useful to note in the second term of the right-hand side of the equation the push forward of the plastic distortion rate into the current configuration.

6. Finite strain single crystal plasticity

6.1. Reduced dissipation inequality

For a perfectly elastic material it is assumed that the dissipation is zero. Plasticity, however, is not a reversible process, so the dissipation should be non-zero. Recall the dissipation inequality (equation 2.19)

$$\begin{aligned}\mathbf{P} : \dot{\mathbf{F}} - \dot{\psi} \geq 0 \\ \Rightarrow \mathbf{P} : \mathbf{L}\mathbf{F} - \dot{\psi} \geq 0.\end{aligned}$$

Now the decomposotion of the velocity gradient into elastic and plastic parts (equation 5.13) is substituted into the dissipation inequality

$$\begin{aligned}&\Rightarrow \mathbf{P} : \left(\mathbf{L}^{\mathrm{e}} + \mathbf{F}^{\mathrm{e}}\mathbf{L}^{\mathrm{p}}\mathbf{F}^{\mathrm{e}-1}\right)\mathbf{F} - \dot{\psi} \geq 0 \\ &\Rightarrow J\boldsymbol{\sigma}\mathbf{F}^{-T} : \mathbf{L}^{\mathrm{e}}\mathbf{F} + \mathbf{P} : \mathbf{F}^{\mathrm{e}}\mathbf{L}^{\mathrm{p}}\mathbf{F}^{\mathrm{e}-1}\mathbf{F} - \dot{\psi} \geq 0 \\ &\Rightarrow J\boldsymbol{\sigma} : \mathbf{L}^{\mathrm{e}} + J\boldsymbol{\sigma}\mathbf{F}^{-T} : \mathbf{F}^{\mathrm{e}}\mathbf{L}^{\mathrm{p}}\mathbf{F}^{\mathrm{e}-1}\mathbf{F} - \dot{\psi} \geq 0 \\ &\Rightarrow J\boldsymbol{\sigma} : \dot{\mathbf{F}}^{\mathrm{e}}\mathbf{F}^{\mathrm{e}-1} + J\boldsymbol{\sigma} : \mathbf{F}^{\mathrm{e}}\mathbf{L}^{\mathrm{p}}\mathbf{F}^{\mathrm{e}-1} - \dot{\psi} \geq 0 \\ &\Rightarrow J\mathbf{F}^{\mathrm{e}-1}\boldsymbol{\sigma}\mathbf{F}^{\mathrm{e}-T} : \mathbf{F}^{\mathrm{e}T}\dot{\mathbf{F}}^{\mathrm{e}} + J\mathbf{F}^{\mathrm{e}T}\mathbf{F}^{\mathrm{e}}\mathbf{F}^{\mathrm{e}-1}\boldsymbol{\sigma}\mathbf{F}^{\mathrm{e}-T} : \mathbf{L}^{\mathrm{p}} - \dot{\psi} \geq 0 \qquad (6.1)\end{aligned}$$

The intermediate second Piola–Kirchhoff stress ($\mathbf{S}^{\mathrm{p}}$) is defined as the pull back of the Kirchhoff stress into the intermediate configuration, i.e.

$$\mathbf{S}^{\mathrm{p}} = J\mathbf{F}^{\mathrm{e}-1}\boldsymbol{\sigma}\mathbf{F}^{\mathrm{e}-T}. \qquad (6.2)$$

Substituting this into equation 6.1 gives

$$\mathbf{S}^{\mathrm{p}} : \mathbf{F}^{\mathrm{e}T}\dot{\mathbf{F}}^{\mathrm{e}} + \mathbf{C}^{\mathrm{e}}\mathbf{S}^{\mathrm{p}} : \mathbf{L}^{\mathrm{p}} - \dot{\psi} \geq 0. \qquad (6.3)$$

Due to the symmetry of the Kirchhoff stress, the intermediate second Piola–Kirchhoff stress is symmetric. The dissipation inequality can thus be rewritten as

$$\begin{aligned}\mathbf{S}^{\mathrm{p}} : (\mathbf{F}^{\mathrm{e}T}\dot{\mathbf{F}}^{\mathrm{e}})^{\mathrm{SYM}} + \mathbf{C}^{\mathrm{e}}\mathbf{S}^{\mathrm{p}} : \mathbf{L}^{\mathrm{p}} - \dot{\psi} \geq 0 \\ \Rightarrow \mathbf{S}^{\mathrm{p}} : \frac{1}{2}\dot{\mathbf{C}}^{\mathrm{e}} + \mathbf{C}^{\mathrm{e}}\mathbf{S}^{\mathrm{p}} : \mathbf{L}^{\mathrm{p}} - \dot{\psi} \geq 0. \qquad (6.4)\end{aligned}$$

It is assumed that the strain energy is dependent not only on the non-rigid elastic deformation but on the plastic deformation as well. It is also assumed that any hardening mechanism is uncoupled from the elastic deformation [34]. The strain energy function is thus of the following

form

$$\psi = \psi^e(\mathbf{C}^{\mathrm{e}}) + \psi^p(\xi^\alpha), \tag{6.5}$$

where $\xi^\alpha,\ \alpha = 1, 2, \cdots, N$, is a set of internal plastic variables. The time derivative of the strain energy is thus

$$\dot{\psi} = \frac{\partial \psi^e(\mathbf{C}^{\mathrm{e}})}{\partial \mathbf{C}^{\mathrm{e}}} : \dot{\mathbf{C}}^{\mathrm{e}} + \sum_{\alpha=1}^{N} \frac{\partial \psi^p(\xi^\alpha)}{\partial \xi^\alpha} \dot{\xi}^\alpha. \tag{6.6}$$

Equation 6.4 now becomes

$$\begin{aligned} &\mathbf{S}^{\mathrm{p}} : \frac{1}{2}\dot{\mathbf{C}}^{\mathrm{e}} + \mathbf{C}^{\mathrm{e}}\mathbf{S}^{\mathrm{p}} : \mathbf{L}^{\mathrm{p}} - \frac{\partial \psi^e(\mathbf{C}^{\mathrm{e}})}{\partial \mathbf{C}^{\mathrm{e}}} : \dot{\mathbf{C}}^{\mathrm{e}} - \sum_{\alpha=1}^{N} \frac{\partial \psi^p(\xi^\alpha)}{\partial \xi^\alpha} \dot{\xi}^\alpha \geq 0 \\ \Rightarrow &\left(\frac{1}{2}\mathbf{S}^{\mathrm{p}} - \frac{\partial \psi^e(\mathbf{C}^{\mathrm{e}})}{\partial \mathbf{C}^{\mathrm{e}}} \right) : \dot{\mathbf{C}}^{\mathrm{e}} + \mathbf{C}^{\mathrm{e}}\mathbf{S}^{\mathrm{p}} : \mathbf{L}^{\mathrm{p}} - \sum_{\alpha=1}^{N} \frac{\partial \psi^p(\xi^\alpha)}{\partial \xi^\alpha} \dot{\xi}^\alpha \geq 0. \end{aligned} \tag{6.7}$$

Following the argument of Truesdell and Noll [40] produces the relation

$$\mathbf{S}^{\mathrm{p}} = 2\frac{\partial \psi^e(\mathbf{C}^{\mathrm{e}})}{\partial \mathbf{C}^{\mathrm{e}}}, \tag{6.8}$$

which results in the reduced dissipation inequality

$$\mathbf{C}^{\mathrm{e}}\mathbf{S}^{\mathrm{p}} : \mathbf{L}^{\mathrm{p}} - \sum_{\alpha=1}^{N} \frac{\partial \psi^p(\xi^\alpha)}{\partial \xi^\alpha} \dot{\xi}^\alpha \geq 0. \tag{6.9}$$

The force quantity conjugate to the internal variable is defined as

$$S^\alpha = \frac{1}{J} \frac{\partial \psi^p(\xi^\alpha)}{\partial \xi^\alpha}. \tag{6.10}$$

The reduced dissipation inequality now becomes

$$\mathcal{D} = \mathbf{C}^{\mathrm{e}}\mathbf{S}^{\mathrm{p}} : \mathbf{L}^{\mathrm{p}} - \sum_{\alpha=1}^{N} J S^\alpha \dot{\xi}^\alpha \geq 0. \tag{6.11}$$

6.2. Single-crystal hypothesis

The single-crystal hypothesis states that the plastic distortion rate is composed of the sum of the slip rates on their respective slip planes [33]

$$\mathbf{L}^{\mathrm{p}} = \sum_{\alpha=1}^{N} \nu^\alpha \mathbf{s}^\alpha \otimes \mathbf{m}^\alpha. \tag{6.12}$$

Substituting this into the reduced dissipation inequality (equation 6.11) gives

$$\mathcal{D} = \mathbf{C}^{\mathrm{e}}\mathbf{S}^{\mathrm{p}} : \sum_{\alpha=1}^{N} \nu^\alpha \mathbf{s}^\alpha \otimes \mathbf{m}^\alpha - \sum_{\alpha=1}^{N} J S^\alpha \dot{\xi}^\alpha \geq 0. \tag{6.13}$$

Rearranging this gives

$$\mathcal{D} = \sum_{\alpha=1}^{N} \left(J\boldsymbol{\sigma} : \nu^{\alpha} \mathbf{F}^{\mathrm{e}} \mathbf{s}^{\alpha} \otimes \mathbf{F}^{\mathrm{e}-T} \mathbf{m}^{\alpha} - J S^{\alpha} \dot{\xi}^{\alpha} \right) \geq 0. \tag{6.14}$$

Recalling the resolved shear stress (equation 4.5), this can be rewritten as

$$\mathcal{D} = \sum_{\alpha=1}^{N} \left(\tau^{\alpha} \nu^{\alpha} - S^{\alpha} \dot{\xi}^{\alpha} \right) \geq 0. \tag{6.15}$$

6.3. Rate-independent theory

6.3.1. Yield function

Classical elasto-plastic theory assumes that there is a point at which an elastic material yields and starts deforming plastically. The elastic domain $\mathbb{E}$ is defined as the convex region of stresses for which there results only an elastic deformation. It is assumed that there exists a set of yield functions $\phi^{\alpha}(\tau^{\alpha}, S^{\alpha})$ (dependent on the stress and an internal variable S^{α}) that have a negative value when inside the elastic domain and are zero-valued when on the surface of the elastic domain. Plastic deformation occurs on the surface of the elastic domain. A common example of a yield function is

$$\phi^{\alpha}(\tau^{\alpha}, S^{\alpha}) = |\tau^{\alpha}| - S^{\alpha}. \tag{6.16}$$

6.3.2. Maximum dissipation, associativity and the normality law

The principle of maximum dissipation is the assumption that among the possible plastic configurations that satisfy the dissipation inequality (equation 6.11), the actual configuration is the one that maximizes the value of $\mathcal{D}$ [10]. The assumption of associativity between the rate measures and the normal of the yield surfaces is made, i.e.

$$\nu^{\alpha} = \lambda^{\alpha} \frac{\partial \phi^{\alpha}}{\partial \tau^{\alpha}} \text{ and } \dot{\xi}^{\alpha} = \lambda^{\alpha} \frac{\partial \phi^{\alpha}}{\partial (-S^{\alpha})}, \; 0 \leq \alpha \leq N, \tag{6.17}$$

where $\lambda^{\alpha} \geq 0$. It can be shown that this assumption is equivalent to the assumption of maximum dissipation. If the set of yield functions in equation 6.16 is used the normals can be written as

$$\begin{aligned} \nu^{\alpha} &= \lambda^{\alpha} \frac{\partial \phi^{\alpha}}{\partial \tau^{\alpha}} = \lambda^{\alpha} \mathrm{sgn}(\tau^{\alpha}) \\ \dot{\xi}^{\alpha} &= \lambda^{\alpha} \frac{\partial \phi^{\alpha}}{\partial (-S^{\alpha})} = \lambda^{\alpha} \\ \Rightarrow \dot{\xi}^{\alpha} &= |\nu^{\alpha}| \end{aligned} \tag{6.18}$$

6.3.3. Karush–Kuhn–Tucker conditions

Plasticity only occurs on the surface of the elastic domain, where the yield function is zero. In addition to this if there is no plasticity the set of parameters $\lambda^{\alpha} = 0$ and the yield function $\phi^{\alpha}(\tau^{\alpha}, S^{\alpha}) < 0$. These constraints are incorporated into the Karush–Kuhn–Tucker (KKT)

conditions, given as

$$\lambda^\alpha \geq 0,\ \phi^\alpha(\tau^\alpha, S^\alpha) \leq 0 \text{ and } \lambda^\alpha \phi^\alpha(\tau^\alpha, S^\alpha) = 0. \tag{6.19}$$

6.4. Rate-dependent theory

Rate-dependent theory can be expressed as a regularization of the rate-independent theory. This is useful from an algorithmic standpoint, as solving a problem with multiple yield surfaces is complex. The regularization is done using of a Norton–Hoff viscoplastic approximation.

6.4.1. Penalty method

A penalty method is applied to the reduced dissipation inequality (equation 6.15)

$$\min \mathcal{L}(\tau^\alpha, S^\alpha) = -\sum_{\alpha=1}^{N} \left(\tau^\alpha \nu^\alpha - S^\alpha \dot{\xi}^\alpha\right) + d_0 \sum_{\alpha=1}^{N} P(\tau^\alpha, S^\alpha), \tag{6.20}$$

where d_0 is a positive parameter and $P(\tau^\alpha, S^\alpha)$ is a non-negative penalty function. The penalty function is chosen in the sense of a Norton-Hoff creep law [36]

$$P(\tau^\alpha, S^\alpha) = \frac{S^\alpha}{\frac{1}{m}+1}\left(\frac{|\tau^\alpha|}{S^\alpha}\right)^{\frac{1}{m}+1}. \tag{6.21}$$

The Lagrangian $\mathcal{L}$ is at a minimum at the stationary point

$$\begin{aligned} \frac{\partial \mathcal{L}}{\partial \tau^\alpha} &= 0 \\ \frac{\partial \mathcal{L}}{\partial S^\alpha} &= 0. \end{aligned} \tag{6.22}$$

Which results in the relations

$$\nu^\alpha = d_0 \left(\frac{|\tau^\alpha|}{S^\alpha}\right)^{\frac{1}{m}} \operatorname{sgn}(\tau^\alpha) \tag{6.23}$$

$$\dot{\xi}^\alpha = \nu^\alpha \frac{\frac{1}{m}}{\frac{1}{m}+1}\left(\frac{|\tau^\alpha|}{S^\alpha}\right) \operatorname{sgn}(\tau^\alpha). \tag{6.24}$$

For a small value of $m \ll 1$, the following approximations may be made for equation 6.24

$$\text{As } m \to 0\ \frac{\frac{1}{m}}{\frac{1}{m}+1} \approx 1, \left(\frac{|\tau^\alpha|}{S^\alpha}\right) \approx 1, \tag{6.25}$$

and therefore

$$\dot{\xi}^\alpha \approx |\nu^\alpha|, \tag{6.26}$$

which is identical to the rate independent result in equation 6.18. This shows that if the rate-sensitivity parameter in the constitutive equation (equation 6.23) is made to be very small, $m \ll 1$, then the constitutive equation approximates a rate-independent model. As mentioned earlier, rate-independent models are not simple, in an algorithmic sense, to solve. This is due

to the fact that not every slip system may have yielded and started deforming plastically. This makes very low values of the rate sensitivity parameter interesting, as successfully solving with these low values may provide a way of avoiding the algorithmic trouble that is encountered in the purely rate-independent case. This was, however, beyond the scope of this project, since the main aim is to examine the different rules for hardening, which governs the evolution of the flow resistance (S^α). The rate-sensitivity parameter was kept to be a value of $m = 0.5$ making the power law parabolic.

The penalty parameter in the constitutive equation for the slip rate (equation 6.23), d_0 is taken to be the initial slip-rate and, unless otherwise stated, has a value of $d = 0.001$. S^α is the flow resistance (described in more detail in the next chapter).

7. Hardening theory

In general terms, hardening dictates the resistance to plastic flow in a material. In crystal plasticity hardening is governed by the flow resistance S^α. There are numerous hardening rules that govern the flow resistance. In this project all of the hardening rules evolve according to

$$\dot{S}^\alpha = \sum_\beta h^{\alpha\beta} |\nu^\beta|, \; S^\alpha|_{t=0} = S_0 \tag{7.1}$$

where S_0 is the initial flow resistance and the hardening moduli $h^{\alpha\beta}$ describe the rate of increase of the deformation resistance on slip system α due to shearing on slip system β [1]. In this project various types of hardening relations will be compared. The hardening equations that were examined are shown in the following sections.

7.1. Implicit hardening

In this theory the hardening moduli are assumed to be dependent on the slip resistance S^β, and are made up of two parts [27]

- Self-hardening, which arises from interactions between slip systems that share the same slip plane.
- Latent-hardening, which arises from interactions between slip systems that do not share the same slip plane.

The coplanarity moduli $\chi^{\alpha\beta}$ are a useful measure of interaction between slip systems. Slip systems α and β are referred to as coplanar if $|\mathbf{m}^\alpha \times \mathbf{m}^\beta| = 0$, and non-coplanar if $|\mathbf{m}^\alpha \times \mathbf{m}^\beta| \neq 0$. The coplanarity moduli are thus

$$\chi^{\alpha\beta} = \begin{cases} 1 & \text{for } \alpha \text{ and } \beta \text{ coplanar} \\ 0 & \text{for } \alpha \text{ and } \beta \text{ noncoplanar.} \end{cases} \tag{7.2}$$

The hardening moduli are given as

$$h^{\alpha\beta}\left(S^\beta\right) = \underbrace{\chi^{\alpha\beta} h\left(S^\beta\right)}_{\text{self-hardening}} + \underbrace{q\left(1-\chi^{\alpha\beta}\right) h\left(S^\beta\right)}_{\text{latent hardening}}, \tag{7.3}$$

where $q > 0$ is an interaction constant and $h(S^\beta)$ is a self-hardening function, given by

$$h(S^\beta) = \begin{cases} h_0 \left(1 - \frac{S^\beta}{S^*}\right)^a & \text{for } S_0 \leq S^\beta \leq S^* \\ 0 & \text{for } S^\beta > S^* \end{cases}, \tag{7.4}$$

with a, S_0, S^* and h_0 being material constants. The self-hardening function shown above was first proposed by Anand and Kothari [1]. They proposed the values $q = 1.4$, $a = 2.25$, $S^* = 148\text{MPa}$, $S_0 = 16\text{MPa}$ and $h_0 = 180\text{MPa}$ for annealed copper.

7.2. Hardening theory of Gurtin and Reddy

Gurtin and Reddy [14] propose a new formulation for self- and latent-hardening in the context of a gradient theory of crystal plasticity. The special case of conventional plasticity is considered here[1]. The proposed hardening rule has the hardening moduli dependent on the accumulated slip, rather than the slip resistance. As with the hardening rule in section 7.1, the hardening moduli can be written in terms of self and latent parts. It also makes use of the coplanarity moduli (equation 7.2). In addition to this a new set of moduli are defined and used in the latent part of the hardening. The latent part of the hardening moduli is intended to represent the contribution to hardening from slip systems that are not coplanar. Gurtin and Reddy argue that using the coplanarity moduli seems to be "too rough" an approximation, because it treats all non-coplanar slip systems equally. The angle between the slip directions should also contribute to the degree with which they interact. The interaction moduli takes into account the angle between the slip directions, it is defined as

$$\iota^{\alpha\beta} = |\mathbf{s}^\alpha \cdot \mathbf{s}^\beta||\mathbf{m}^\alpha \times \mathbf{m}^\beta|. \tag{7.5}$$

The hardening law takes the form

$$S^\alpha\left(\boldsymbol{\gamma}_{\text{acc}}\right) = S_0 + S_S\left(m^\alpha_{\text{slf}}\right) + S_L\left(m^\alpha_{\text{lat}}\right), \tag{7.6}$$

where S_S and S_L are the self- and latent-hardening contributions. These functions are found by calibrating this hardening rule with the single-slip case of the implicit rule and then extending to multiple slip. They are given by

$$S_S\left(m^\alpha_{\text{slf}}\right) = (S - S_0)\left(1 - \frac{1}{1 + \frac{S^* - S_0}{S^*}\frac{h_0}{S^*}m^\alpha_{\text{slf}}}\right) \tag{7.7}$$

$$S_L\left(m^\alpha_{\text{lat}}\right) = q(S - S_0)\left(1 - \frac{1}{1 + \frac{S^* - S_0}{S^*}\frac{h_0}{S^*}m^\alpha_{\text{lat}}}\right), \tag{7.8}$$

with q, a, S_0, S^* and h_0 being the same material constants defined after equation (7.4). m^α_{slf} and m^α_{lat} are self and latent hardening measures, respectively. They are defined as

$$m^\alpha_{\text{slf}} \overset{\text{def}}{=} \sum_\beta \chi^{\alpha\beta}\gamma^\beta_{\text{acc}}, \tag{7.9}$$

$$m^\alpha_{\text{lat}} \overset{\text{def}}{=} \sum_\beta \iota^{\alpha\beta}\gamma^\beta_{\text{acc}}, \tag{7.10}$$

[1] Cf. sections 5.3 and 5.4 of [14]

where $\boldsymbol{\gamma}_{\text{acc}} = (\gamma^0_{\text{acc}}, \gamma^1_{\text{acc}}, \cdots, \gamma^N_{\text{acc}})$ is the a vector of the accumulated slips. The accumulated slip on slip system β is given by

$$\dot{\gamma}^\beta_{\text{acc}} = |\dot{\gamma}^\beta| = |\nu^\beta|. \tag{7.11}$$

Equation 7.6 is equivalent to

$$\dot{S}^\alpha = \sum_\beta \left(\chi^{\alpha\beta} H_S\left(m^\alpha_{\text{slf}}\right) + \iota^{\alpha\beta} H_L\left(m^\alpha_{\text{lat}}\right)\right)|\nu^\beta|,\ S|_{t=0} = S_0 \tag{7.12}$$

where $H_S\left(m^\alpha_{\text{slf}}\right) = S'_S\left(m^\alpha_{\text{slf}}\right)$ and $H_L\left(m^\alpha_{\text{lat}}\right) = S'_L\left(m^\alpha_{\text{lat}}\right)$. Since this is written in the general form of equation 7.1, the numerical solution will use this form. H_S and H_L are given as

$$H_S\left(m^\alpha_{\text{slf}}\right) = h_0\left(\frac{S^* - S_0}{S^*}\right)^2\left(1 + \frac{S^* - S_0}{S^*}\frac{h_0}{S^*}m^\alpha_{\text{slf}}\right)^{-2} \tag{7.13}$$

$$H_L\left(m^\alpha_{\text{lat}}\right) = qh_0\left(\frac{S^* - S_0}{S^*}\right)^2\left(1 + \frac{S^* - S_0}{S^*}\frac{h_0}{S^*}m^\alpha_{\text{lat}}\right)^{-2}. \tag{7.14}$$

7.2.1. Example with two slip-systems

As an example consider a simple two dimensional crystal with two slip-systems, with slip directions oriented at 60° to each other, i.e.

$$\begin{aligned} \mathbf{m}^1 &= \tfrac{1}{\sqrt{5}}(-2,1), & \mathbf{s}^1 &= \tfrac{1}{\sqrt{5}}(1,2), \\ \mathbf{m}^2 &= \tfrac{1}{\sqrt{5}}(2,1), & \mathbf{s}^2 &= \tfrac{1}{\sqrt{5}}(-1,2). \end{aligned} \tag{7.15}$$

The coplanarity moduli then take the form

$$\chi = \begin{pmatrix} 1 & 0 \\ 0 & 1 \end{pmatrix} \tag{7.16}$$

and the interaction moduli are

$$\iota = \begin{pmatrix} 0 & \frac{12}{25} \\ \frac{12}{25} & 0 \end{pmatrix}. \tag{7.17}$$

The self- and latent-hardening measures are thus

$$\begin{aligned} m^1_{\text{slf}} &= \gamma^1_{\text{acc}}, & m^1_{\text{lat}} &= \tfrac{12}{25}\gamma^2_{\text{acc}}, \\ m^2_{\text{slf}} &= \gamma^2_{\text{acc}}, & m^2_{\text{lat}} &= \tfrac{12}{25}\gamma^1_{\text{acc}}. \end{aligned} \tag{7.18}$$

The hardening laws for the two slip systems take the following form:

$$\begin{pmatrix} S^1 \\ S^2 \end{pmatrix} = (S^* - S_0)\begin{pmatrix} -\left(1 + \frac{S^*-S_0}{S^*}\frac{h_0}{S^*}\gamma^1_{\text{acc}}\right)^{-1} - q\frac{25}{12}\left(1 + \frac{S^*-S_0}{S^*}\frac{h_0}{S^*}\frac{12}{25}\gamma^2_{\text{acc}}\right)^{-1} \\ -q\frac{25}{12}\left(1 + \frac{S^*-S_0}{S^*}\frac{h_0}{S^*}\frac{12}{25}\gamma^1_{\text{acc}}\right)^{-1} - \left(1 + \frac{S^*-S_0}{S^*}\frac{h_0}{S^*}\gamma^2_{\text{acc}}\right)^{-1} \\ +(1 + q\frac{25}{12}) \\ +(1 + q\frac{25}{12}) \end{pmatrix} + \begin{pmatrix} S_0 \\ S_0 \end{pmatrix} \tag{7.19}$$

7.3. Isotropic Taylor hardening

In addition to the previously described hardening. The model that was used by Steinmann and Stein [36] is also used, as a way of verifying the numerical algorithm. The hardening rule is an isotropic Taylor hardening. The assumption of isotropy means that

$$S = S^{\alpha} = S^{\alpha}(\gamma), \tag{7.20}$$

where

$$\dot{\gamma} = \sum_{\alpha} |\dot{\gamma}^{\alpha}| = \sum_{\alpha} |\nu^{\alpha}|. \tag{7.21}$$

the approximation

$$h^{\alpha\beta}(\gamma) = h(\gamma). \tag{7.22}$$

is also made. The hardening equations are then defined as

$$S(\gamma) = \tau_0 + (\tau_\infty - \tau_0) \tanh\left(\frac{h_0\gamma}{\tau_\infty - \tau_0}\right)$$
$$h(\gamma) = h_0 \cosh^{-2}\left(\frac{h_0\gamma}{\tau_\infty - \tau_0}\right),$$

where τ_0, τ_∞ and h_0 are material constants. τ_0 is the initial flow resistance, thus

$$\tau_0 = S_0. \tag{7.23}$$

The other two parameters are not given as they will be used to calibrate this hardening rule with the rules described in the previous two sections.

7.4. Constant hardening

Constant hardening moduli are useful for testing the numerical algorithms, these are simply

$$h^{\alpha\beta} = \begin{cases} h_0 & \alpha = \beta \\ \rho h_0 & \alpha \neq \beta \end{cases}, \tag{7.24}$$

where h_0 and ρ are material constants. In all calculations presented here $\rho = 1$. To conclude this part of the thesis the system of equations for finite strain single crystal plasticity is shown in table 7.1.

Governing equation and boundary conditions	$\mathrm{div}\boldsymbol{\sigma} + \mathbf{b} = \mathbf{0}$ $\mathbf{u}(\mathbf{X}, t) = \bar{\mathbf{u}} \quad \text{on } \partial B_u$ $\mathbf{t} = \boldsymbol{\sigma}\mathbf{n}, \quad \text{on } \partial B_\sigma$
Kröner-Lee decomposition	$\mathbf{F} = \mathbf{F}^{\mathrm{e}}\mathbf{F}^{\mathrm{p}}$
Single crystal kinematics	$\dot{\mathbf{F}}^{\mathrm{p}} = \sum_{\alpha=1}^{N} \nu^\alpha \mathbb{S}^\alpha \mathbf{F}^{\mathrm{p}}$ $\mathbb{S}^\alpha = \mathbf{s}^\alpha \otimes \mathbf{m}^\alpha$ $\mathbf{s}^\alpha \cdot \mathbf{m}^\alpha = 0, \quad \lvert\mathbf{s}^\alpha\rvert = \lvert\mathbf{m}^\alpha\rvert = 1.$
Constitutive relations	$\boldsymbol{\sigma} = \frac{1}{J}\mathbf{F}^{\mathrm{e}} 2 \frac{\partial \psi^e(\mathbf{C}^{\mathrm{e}})}{\partial \mathbf{C}^{\mathrm{e}}} \mathbf{F}^{\mathrm{e}T}$ $\nu^\alpha = d_0 \left(\frac{\lvert\tau^\alpha\rvert}{S^\alpha}\right)^{\frac{1}{m}} \mathrm{sgn}\left(\tau^\alpha\right)$ $\mathrm{sgn}(\nu^\alpha) = \mathrm{sgn}(\tau^\alpha)$ $\tau^\alpha = \mathbf{F}^{\mathrm{e}}\mathbf{s}^\alpha \cdot \boldsymbol{\sigma}\mathbf{F}^{\mathrm{e}-T}\mathbf{m}^\alpha$
Hardening relations	
Implicit	$\dot{S}^\alpha = \sum_\beta \left(\chi^{\alpha\beta} h\left(S^\beta\right) + q\left(1 - \chi^{\alpha\beta}\right) h\left(S^\beta\right)\right) \lvert\nu^\beta\rvert$ $h(S^\beta) = \begin{cases} h_0 \left(1 - \frac{S^\beta}{S^*}\right)^a & \text{for } S_0 \le S^\beta \le S^* \\ 0 & \text{for } S^\beta > S^* \end{cases}$ $\chi^{\alpha\beta} = \begin{cases} 1 & \text{for } \alpha \text{ and } \beta \text{ coplanar} \\ 0 & \text{for } \alpha \text{ and } \beta \text{ noncoplanar} \end{cases}$
Gurtin and Reddy [14]	$\dot{S}^\alpha = \sum_\beta \left(\chi^{\alpha\beta} H_s\left(m^\alpha_{\mathrm{slf}}\right) + \iota^{\alpha\beta} H_L\left(m^\alpha_{\mathrm{lat}}\right)\right) \lvert\nu^\beta\rvert$ $\iota^{\alpha\beta} = \lvert\mathbf{s}^\alpha \cdot \mathbf{s}^\beta\rvert\lvert\mathbf{m}^\alpha \times \mathbf{m}^\beta\rvert$ $H_S\left(m^\alpha_{\mathrm{slf}}\right) = h_0 \left(\frac{S^* - S_0}{S^*}\right)^2 \left(1 + \frac{S^* - S_0}{S^*} \frac{h_0}{S^*} m^\alpha_{\mathrm{slf}}\right)^{-2}$ $H_L\left(m^\alpha_{\mathrm{lat}}\right) = q h_0 \left(\frac{S^* - S_0}{S^*}\right)^2 \left(1 + \frac{S^* - S_0}{S^*} \frac{h_0}{S^*} m^\alpha_{\mathrm{lat}}\right)^{-2}$ $m^\alpha_{\mathrm{slf}} = \sum_\beta \chi^{\alpha\beta}\gamma^\beta_{\mathrm{acc}}, \quad m^\alpha_{\mathrm{lat}} = \sum_\beta \iota^{\alpha\beta}\gamma^\beta_{\mathrm{acc}}$
Isotropic	$S\left(\gamma\right) = \tau_0 + \left(\tau_\infty - \tau_0\right) \tanh\left(\frac{h_0\gamma}{\tau_\infty - \tau_0}\right)$ $\dot{\gamma} = \sum_\alpha \lvert\nu^\alpha\rvert$
Constant	$S\left(\gamma\right) = \sum_\beta h_0 \lvert\nu^\beta\rvert$

Table 7.1.: The continuous system of equations governing finite strain single-crystal plasticity with viscoplastic flow.

Part II.

Finite Element Method

8. Overview and time discretization

The system that has been described was solved using a predictor-corrector Newton–Raphson scheme. The predictor solves the elastic part of the problem using the finite element method. At each time step the predictor assumes that there is no change in plastic deformation since the last time step. Once the elastic part is solved, the plastic deformation is then updated by the corrector. The elastic problem is nonlinear, hence it requires a Newton–Raphson scheme to solve. The predicting and correcting occurs at each iteration in the Newton–Raphson scheme.

8.1. Time discretization

The time domain is discretized into a number of equally space time increments $t_0 < t_1 < \cdots < t_N$, with $t_{\mathrm{n+1}}{=}\Delta t + t_n$ and Δt being the time increment.

8.1.1. Balance of momentum

The time discrete form of the balance of linear momentum (equation 2.10) is

$$\mathrm{div}\boldsymbol{\sigma}_{n+1} + \mathbf{b}_{n+1} = \mathbf{0}, \tag{8.1}$$

8.1.2. Plastic deformation gradient

Recall from section 5.2 that the plastic deformation gradient and the plastic distortion rate are related by:

$$\dot{\mathbf{F}}^{\mathrm{p}} = \mathbf{L}^{\mathrm{p}}\mathbf{F}^{\mathrm{p}}. \tag{8.2}$$

This is discretized semi-implicitly [36] as

$$\mathbf{F}^{\mathrm{p}}{}_{\mathrm{n+1}} = \exp(\boldsymbol{\Lambda})\mathbf{F}^{\mathrm{p}}{}_{\mathrm{n}}, \tag{8.3}$$

where $\boldsymbol{\Lambda} = \Delta t\mathbf{L}^{\mathrm{p}}$ and $\exp(\Lambda)$ is the tensor exponential

$$\exp(\Lambda) \approx (\mathbf{I} - \theta\boldsymbol{\Lambda})^{-1} \cdot (\mathbf{I} + (1-\theta)\,\boldsymbol{\Lambda}) = \bar{\mathbf{F}}^{\mathrm{p}}. \tag{8.4}$$

The value of θ $(0 \leq \theta \leq 1)$ in the tensor exponential determines the type of time integration being done :

- $\theta = 0$: Forward Euler (Explicit)
- $\theta = \frac{1}{2}$: Midpoint
- $\theta = 1$: Backward Euler (Implicit)

In the case of this project the midpoint rule was used.

8.1.3. Hardening rules

The hardening law (equation 7.1) is discretized using an implicit first order scheme,

$$^{\mathrm{n+1}}S^{\alpha} =^{n} S^{\alpha} + \Delta t \sum_{\beta=1}^{N} h^{\alpha\beta} |^{\mathrm{n+1}}\nu^{\beta}|. \tag{8.5}$$

Since the hardening moduli is different for the various hardening law, this scheme still lacks some information. The full discrete form for each hardening rule is shown in chapter 10.

8.1.4. Constitutive equation

The discretization of the constitutive equation for the slip rate (equation 6.23) is straight forward,

$$\nu^{\alpha}_{\mathrm{n+1}} = d_0 \left(\frac{|\tau^{\alpha}_{\mathrm{n+1}}|}{S^{\alpha}_{\mathrm{n+1}}} \right)^{\frac{1}{m}} \mathrm{sgn}\left(\tau^{\alpha}_{\mathrm{n+1}}\right). \tag{8.6}$$

9. Predictor

The finite element method (FEM) obtains approximate solutions to partial differential equations based upon their weak formulations. The domain (B) is partitioned into a mesh. The mesh is composed of a set of elements. Each element is either a line segment, a polygon, or a polyhedron depending on the dimension of the domain. In the case of this project the domain is three-dimensional, and the elements that comprise the mesh are all quadrilaterally-faced hexahedra.

9.1. Algorithmic variables

9.1.1. Trial elastic deformation gradient

The predictor part assumes no change in the plastic deformation gradient. For this purpose the trial elastic deformation gradient $\hat{\mathbf{F}}^{\mathrm{e}}{}_{\mathrm{n+1}}$ is used. This is an elastic deformation gradient that assumes no change in the plastic deformation since the previous time step

$$\begin{aligned}\hat{\mathbf{F}}^{\mathrm{e}}{}_{\mathrm{n+1}} &= \mathbf{F}_{\mathrm{n+1}}\mathbf{F}^{\mathrm{p}}{}_{\mathrm{n}}{}^{-1} \\ &= \mathbf{F}^{\mathrm{e}}{}_{\mathrm{n+1}}\bar{\mathbf{F}}^{\mathrm{p}},\end{aligned} \tag{9.1}$$

9.1.2. Trial elastic right Cauchy-Green tensor

Using the trial elastic deformation gradient, the trial elastic right Cauchy-Green tensor is given as

$$\hat{\mathbf{C}}^{\mathrm{e}} = \hat{\mathbf{F}}^{\mathrm{e}T}\hat{\mathbf{F}}^{\mathrm{e}}. \tag{9.2}$$

9.1.3. Trial second Piola–Kirchhoff tensor

The trial second Piola–Kirchhoff tensor is made by pushing back the current Kirchhoff tensor into the intermediate configuration

$$\bar{\mathbf{S}}_{\mathrm{n+1}} = \left(\hat{\mathbf{F}}^{\mathrm{e}}{}_{\mathrm{n+1}}\right)^{-1}\boldsymbol{\tau}_{\mathbf{n+1}}\left(\hat{\mathbf{F}}^{\mathrm{e}}{}_{n+1}\right)^{-T}. \tag{9.3}$$

9.1.4. Plastic right Cauchy–Green tensor

The plastic right Cauchy–Green tensor is defined as

$$\bar{\mathbf{C}}^{\mathrm{p}} = \bar{\mathbf{F}}^{\mathrm{p}T}\bar{\mathbf{F}}^{\mathrm{p}}. \tag{9.4}$$

9.2. Weak formulation

Consider the time discretized form of the balance of linear momentum, which can be rewritten in indicial form as

$$\frac{\partial}{\partial x_j}\left(\sigma_{n+1}\right)_{ij} + \left(b_{n+1}\right)_i = 0. \tag{9.5}$$

The weak form is obtained by multiplying by an arbitrary variation in the spatial field ($\delta\mathbf{u}$), and integrating over the entire domain in the spatial configuration (the time increment, $n+1$, is left out for brevity)

$$\begin{aligned}
&\int_B \left(\frac{\partial}{\partial x_j}\sigma_{ij} + b_i\right)\delta u_i dv = 0 \\
\Rightarrow &\int_B \left(\frac{\partial}{\partial x_j}\sigma_{ij}\right)\delta u_i dv + \int_B \left(b_i\right)\delta u_i dv = 0 \\
\Rightarrow &\int_B \frac{\partial}{\partial x_j}\left(\sigma_{ij}\delta u_i\right) ds - \int_B \sigma_{ij}\left(\frac{\partial}{\partial x_j}\delta u_i\right) dv + \int_B \left(b_i\right)\delta u_i dv = 0 \\
\Rightarrow &\int_{\partial B} \sigma_{ij}\delta u_i \hat{n}_j ds - \int_B \sigma_{ij}\left(\frac{\partial}{\partial x_j}\delta u_i\right) dv + \int_B \left(b_i\right)\delta u_i dv = 0 \\
\Rightarrow &\int_{\partial B_\sigma} t_i \delta u_i ds - \int_B \sigma_{ij}\left(\frac{\partial}{\partial x_j}\delta u_i\right) dv + \int_B \left(b_i\right)\delta u_i dv = 0,
\end{aligned} \tag{9.6}$$

which can be written in vector form as

$$\int_{\partial B_\sigma} \mathbf{t_{n+1}}\cdot\delta\mathbf{u} ds - \int_B \boldsymbol{\sigma_{n+1}} : \boldsymbol{\nabla_x}\delta\mathbf{u} dv + \int_B \mathbf{b_{n+1}}\cdot\delta\mathbf{u} dv = 0. \tag{9.7}$$

Now the trial second Piola–Kirchhoff tensor is introduced into the middle term

$$G = \int_{\partial B_\sigma} \mathbf{t}_{n+1}\cdot\delta\mathbf{u} ds - \int_B \frac{1}{J}\bar{\mathbf{S}}_{n+1} : \left(\hat{\mathbf{F}}^e \boldsymbol{\nabla_x}\delta\mathbf{u}\left(\hat{\mathbf{F}}^e\right)^T\right) dv + \int_B \mathbf{b}_{n+1}\cdot\delta\mathbf{u} dv = 0. \tag{9.8}$$

Equation (9.8) is the weak form of the elastic problem. This can be re-written as an integral over the domain in the reference configuration

$$G = \int_{\partial B_{0\sigma}} \mathbf{T}_{n+1}\cdot\delta\mathbf{u} dS - \int_{B_0} \bar{\mathbf{S}}_{n+1} : \left(\hat{\mathbf{F}}^e \boldsymbol{\nabla_x}\delta\mathbf{u}\left(\hat{\mathbf{F}}^e\right)^T\right) dV + \int_{B_0} \hat{\mathbf{b}}_{n+1}\cdot\delta\mathbf{u} dV = 0, \tag{9.9}$$

where Nanson's relation (equation 1.6) has been used in the first term and $\hat{\mathbf{b}}$ is the body force in the reference configuration.

9.2.1. Linearization

The linearization of the weak form is found by taking the directional derivative of the weak form in the direction of the incremental displacement ($\Delta\mathbf{u}$) [20]. Using the linearization operator

$\Delta\left(\bullet(\mathbf{x})\right) = \partial_\epsilon\left(\bullet\left(\mathbf{x}+\epsilon\Delta\mathbf{u}\right)\right)\big|_{\epsilon=0}$ gives

$$\Delta G = \int_B \boldsymbol{l}_\Delta : \boldsymbol{\mathcal{E}}^{\boldsymbol{a}}_{\boldsymbol{2}} : \boldsymbol{l}_\delta + \boldsymbol{\tau} : \left(\boldsymbol{l}_\Delta \cdot \boldsymbol{l}_\delta\right) dV, \tag{9.10}$$

where $\boldsymbol{l}_\delta = \partial_{\mathbf{x}}\delta\mathbf{u}$, $\boldsymbol{l}_\Delta = \partial_{\mathbf{x}}\Delta\mathbf{u}$ and $\boldsymbol{\mathcal{E}}^{\boldsymbol{a}}_{\boldsymbol{2}}$ is the algorithmic material operator in the spatial configuration [36, 35], and is given by

$$J\left(\mathcal{E}^a_2\right)_{ijkl} = \hat{F}^{\mathrm{e}}{}_{iA}\hat{F}^{\mathrm{e}}{}_{jB}\frac{2\partial\left(\bar{\Sigma}_p\right)_{AB}}{\partial\left(\partial\hat{C}^{\mathrm{e}}\right)_{CD}}\hat{F}^{\mathrm{e}}{}_{kC}\hat{F}^{\mathrm{e}}{}_{lD}. \tag{9.11}$$

This is shown in Appendix A to be

$$\begin{aligned} J\left(\mathcal{E}^a_2\right)_{ijkl} =& \lambda B^{\mathrm{e}}_{ij}B^{\mathrm{e}}_{kl} + \mu\left(B^{\mathrm{e}}_{ik}B^{\mathrm{e}}_{lj} + B^{\mathrm{e}}_{il}B^{\mathrm{e}}_{kj}\right) \\ &+ \sum_\beta\left(\underset{iAjBkClD}{\mathbb{F}}\left(\left(4\mu\frac{\partial\bar{C}^{\mathrm{p}-1}_{AE}}{\partial\nu^\beta}\hat{C}^{\mathrm{e}}{}_{EG}\bar{C}^{\mathrm{p}-1}_{GB}\right)^{\mathrm{SYM}} + 2\delta^{\mathrm{n}+1}_I\frac{\partial\bar{C}^{\mathrm{p}-1}_{AB}}{\partial\nu^\beta}\right)\right. \\ &\left.+\left(\lambda\hat{F}^{\mathrm{e}}{}_{kC}\hat{F}^{\mathrm{e}}{}_{lD}\hat{C}^{\mathrm{e}}{}_{MN}\frac{\partial\bar{C}^{\mathrm{p}-1}_{MN}}{\partial\nu^\beta}B^{\mathrm{e}}_{ij}\right)\right)\left(\frac{\partial\nu^\beta}{\partial\hat{C}^{\mathrm{e}}{}_{CD}}\right), \end{aligned} \tag{9.12}$$

where $\underset{iAjBkClD}{\mathbb{F}}$ is the 8th order tensor

$$\underset{iAjBkClD}{\mathbb{F}} = \hat{F}^{\mathrm{e}}{}_{iA}\hat{F}^{\mathrm{e}}{}_{jB}\hat{F}^{\mathrm{e}}{}_{kC}\hat{F}^{\mathrm{e}}{}_{lD}, \tag{9.13}$$

(from equation (52) in [36])

$$\frac{\partial\bar{C}^{\mathrm{p}-1}_{AB}}{\partial\nu^\beta} = 2\left(\frac{\partial\bar{F}^{\mathrm{p}-1}_{AC}}{\partial\nu^\beta}\bar{F}^{\mathrm{p}-1}_{BC}\right)^{\mathrm{sym}} \tag{9.14}$$

and (from equation (42) in [36])

$$\frac{\partial\bar{F}^{\mathrm{p}-1}_{AC}}{\partial\nu^\beta} = -\Delta t\left(\delta_{AD} + (1-\theta)\Lambda_{AD}\right)^{-1}(Z)_{DE}\left(\theta\delta_{EC} + (1-\theta)\bar{F}^{\mathrm{p}-1}_{EC}\right). \tag{9.15}$$

The derivative of the slip rate with respect to the right Cauchy–Green tensor, $\frac{\partial\nu^\beta}{\partial\hat{C}^{\mathrm{e}}{}_{CD}}$, is obtained by the equation (from equation (53) in [36])

$$J_{\alpha\beta}\frac{\partial\nu^\beta}{\partial\hat{C}^{\mathrm{e}}{}_{CD}} = \bar{F}^{\mathrm{p}-1}_{CE}\frac{\partial R^\alpha}{\partial\left(C_e\right)_{EF}}\left(\bar{F}^{\mathrm{p}-T}\right)_{FD}, \tag{9.16}$$

where

$$J_{\alpha\beta} = -\left.\frac{\partial R^\alpha}{\partial\nu^\beta}\right|_{\hat{C}^{\mathrm{e}}}. \tag{9.17}$$

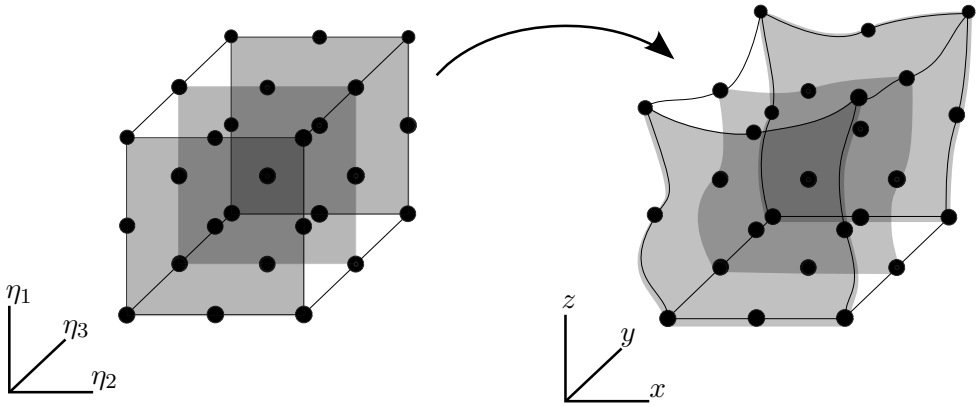

Figure 9.1.: Mapping from the reference element

9.3. Finite element discretization

9.3.1. Continuous elements

The domain (B) is decomposed into a set of M elements $E_1, E_2, \cdots, E_M$; $E_i \subset B$ such that $E_1 \cup E_2 \cup \cdots \cup E_M = B$ and $E_i \cap E_j = \emptyset$ for $j \neq i$. On each element shape functions are defined. Denote V as the set of continuous, differentiable functions that satisfy the Dirichlet boundary conditions. The finite element approximation is a finite-dimensional subspace $V^h \subset V$, the basis of which comprises the shape functions on each element. The shape functions must therefore be continuous. Polynomial shape functions of the following form were used

$$Q_k\left(E_i\right) = P_{k,k,k}\left(E_i\right), \tag{9.18}$$

where k is referred to as the order of the shape function and $P_{k,k,k}$ is defined by

$$P_{k_1,k_2,k_3}\left(E_i\right) = \{p\left(x_1,x_2,x_3\right) | p\left(x_1,x_2,x_3\right) = \sum_{\substack{h\leq k_1\\ i\leq k_2\\ j\leq k_3}} a_{hij} x_1^h x_2^i x_3^j\}, \tag{9.19}$$

which is the space of polynomials of degree $\leq k_1$ in x_1, $\leq k_2$ in x_2 and $\leq k_3$ in x_3 [8]. Shape functions of order $k = 2$ were used.

9.3.2. Reference element

Rather than defining the shape functions for each element in the domain, a reference element is used. The reference element is defined in a reference space, on the unit interval $[0,1]^3$. The reference element then maps onto the finite element space. This is illustrated in figure 9.1.

9.3.3. Finite element approximation

For an element E the finite element approximation assumes that

$$\mathbf{u}|_E \approx \mathbf{u}^h|_E = \sum_{i=0}^{N_{\mathbf{cell}}-1} \mathbf{\Phi}_i U_i, \tag{9.20}$$

where U_i and $\mathbf{\Phi}_i$ are scalar coefficients and vectorial shape functions for each degree of freedom, respectively. N_{cell} is the number of degrees of freedom on a cell. The shape functions ($\mathbf{\Phi}_i$) are defined as

$$\mathbf{\Phi}_i = \phi_{\text{base}(i)}(\mathbf{x})\mathbf{e}_{\text{comp}(i)}, \tag{9.21}$$

where $\phi_{\text{base}(i)}(\mathbf{x})$ are the scalar shape functions. This is not the conventional way of formulating finite elements, but it makes for an easier layout in the computer code [7]. In this formulation the vector shape functions $\mathbf{\Phi}_i$ have only one non-zero component. The function comp(i) determines which component is non zero and the function base(i) returns the index of the scalar shape function to be used [6], they are given as

$$\text{base}(i) = \text{floor}\left(\frac{3}{N_{\text{cell}}}i\right), \tag{9.22}$$

$$\text{comp}(i) = i \mod 3. \tag{9.23}$$

The displacement gradient is denoted as

$$\boldsymbol{\nabla}_{\mathbf{x}}\mathbf{u} \approx \boldsymbol{\nabla}_{\mathbf{x}}\mathbf{u}^h = \sum_{i=0}^{N_{\mathbf{cell}}-1} \boldsymbol{\nabla}_{\mathbf{x}}\mathbf{\Phi}_i U_i, \tag{9.24}$$

For the variation the same shape functions and gradients are used

$$\boldsymbol{\delta}\mathbf{x} \approx \boldsymbol{\delta}\mathbf{x}^h = \sum_{j=0}^{N_{\mathbf{cell}}-1} \mathbf{\Phi}_j V_j, \tag{9.25}$$

$$\boldsymbol{\nabla}_{\mathbf{x}}\boldsymbol{\delta}\mathbf{x} \approx \boldsymbol{\nabla}_{\mathbf{x}}\boldsymbol{\delta}\mathbf{x}^h = \sum_{j=0}^{N_{\mathbf{cell}}-1} \boldsymbol{\nabla}_{\mathbf{x}}\mathbf{\Phi}_j V_j, \tag{9.26}$$

where V_i are the degrees of freedom for the trial variable. Over a single element these approximations are then substituted into the weak form (equation (9.8)). For brevity the shorthand $\sum_i = \sum_{i=0}^{N_{\mathbf{cell}}-1}$ is used. The weak form becomes.

$$\begin{aligned} G = & \int_{\partial E_\sigma} \mathbf{t}_{\mathbf{n+1}} \cdot \sum_j \mathbf{\Phi}_j V_j dS - \int_E \frac{1}{J}\bar{\mathbf{S}}_{\mathbf{n+1}} : \left(\hat{\mathbf{F}}^{\text{e}} \sum_j \boldsymbol{\nabla}_{\mathbf{x}}\mathbf{\Phi}_j V_j \left(\hat{\mathbf{F}}^{\text{e}}\right)^T\right) dV \\ & + \int_E \mathbf{b}_{\mathbf{n+1}} \cdot \sum_j \mathbf{\Phi}_j V_j dV = 0 \\ \Rightarrow \quad & \sum_j V_j \left(\int_{\partial E_\sigma} \mathbf{t}_{\mathbf{n+1}} \cdot \mathbf{\Phi}_j dS - \int_{E_i} \frac{1}{J}\left(\hat{\mathbf{F}}^{\text{e}}\right) \bar{\mathbf{S}}_{\mathbf{n+1}} : \left(\hat{\mathbf{F}}^{\text{e}} \boldsymbol{\nabla}_{\mathbf{x}}\mathbf{\Phi}_j\right) dV \right. \\ & \left. + \int_E \mathbf{b}_{\mathbf{n+1}} \cdot \mathbf{\Phi}_j dV \right) = 0, \end{aligned} \tag{9.27}$$

where $\hat{\mathbf{F}}^{\mathrm{e}} = \hat{\mathbf{F}}^{\mathrm{e}}\left(\sum_i \boldsymbol{\Phi}_i U_i\right)$ and $\bar{\mathbf{S}}_{\mathrm{n+1}} = \bar{\mathbf{S}}_{\mathrm{n+1}}\left(\sum_i \boldsymbol{\Phi}_i U_i\right)$. The variation is arbitrary, this means that V_j are also arbitrary, and therefore

$$G_j = \left(\int_{\partial E_\sigma} \mathbf{t}_{\mathrm{n+1}} \cdot \boldsymbol{\Phi}_j dS - \int_E \frac{1}{J} \left(\hat{\mathbf{F}}^{\mathrm{e}}\right) \bar{\mathbf{S}}_{\mathrm{n+1}} : \left(\hat{\mathbf{F}}^{\mathrm{e}} \boldsymbol{\nabla}_{\mathbf{x}} \boldsymbol{\Phi}_j\right) dV + \int_E \mathbf{b}_{\mathrm{n+1}} \cdot \boldsymbol{\Phi}_j dV \right) = 0. \tag{9.28}$$

The linearized weak form is discretized in a similar fashion. First substitute the finite element approximations into equation (9.10) to get

$$\begin{aligned} \Delta G &= \int_B \sum_i \boldsymbol{\nabla}_{\mathbf{x}} \boldsymbol{\Phi}_i \Delta U_i : \boldsymbol{\mathcal{E}}_{\mathbf{2}}^{\boldsymbol{a}} : \sum_j \boldsymbol{\nabla}_{\mathbf{x}} \boldsymbol{\Phi}_j V_j + \boldsymbol{\tau} : \left(\sum_i \boldsymbol{\nabla}_{\mathbf{x}} \boldsymbol{\Phi}_i \Delta U_i \cdot \sum_j \boldsymbol{\nabla}_{\mathbf{x}} \boldsymbol{\Phi}_j V_j \right) dV \\ &= \sum_i \sum_j \Delta U_i V_j \left(k_{ij}\right), \end{aligned} \tag{9.29}$$

where

$$k_{ij} = \int_B \left(\boldsymbol{\nabla}_{\mathbf{x}} \boldsymbol{\Phi}_i : \boldsymbol{\mathcal{E}}_{\mathbf{2}}^{\boldsymbol{a}} : \boldsymbol{\nabla}_{\mathbf{x}} \boldsymbol{\Phi}_j + \boldsymbol{\tau} : \left(\boldsymbol{\nabla}_{\mathbf{x}} \boldsymbol{\Phi}_i \cdot \sum_j \boldsymbol{\nabla}_{\mathbf{x}} \boldsymbol{\Phi}_j \right) \right) dV, \tag{9.30}$$

and the finite element approximations are

$$\Delta \mathbf{x} \approx \Delta \mathbf{x}^h = \sum_i \boldsymbol{\Phi}_i \Delta U_i, \tag{9.31}$$

$$\boldsymbol{\nabla}_{\mathbf{x}} \Delta \mathbf{x} \approx \boldsymbol{\nabla}_{\mathbf{x}} \Delta \mathbf{x}^h = \sum_i \boldsymbol{\nabla}_{\mathbf{x}} \boldsymbol{\Phi}_i \Delta U_i, \tag{9.32}$$

and of course the algorithmic tangent is a function of the finite element approximation, $\boldsymbol{\mathcal{E}}_{\mathbf{2}}^{\boldsymbol{a}} = \boldsymbol{\mathcal{E}}_{\mathbf{2}}^{\boldsymbol{a}}\left(\sum_i \boldsymbol{\Phi}_i U_i\right)$.

9.3.4. Gaussian quadrature

The integrals in the weak form (equation 9.28) and the linearization (equation 9.29) must be approximated numerically. Gaussian quadrature is commonly used to do this in the finite element method. The Gaussian quadrature approximation of a volume integral is given as

$$\int_{\Omega_{\mathsf{G}}} f(\mathbf{x})\, dV \approx \sum_{i=1}^{N_{\mathsf{p}}} \sum_{j=1}^{N_{\mathsf{p}}} \sum_{k=1}^{N_{\mathsf{p}}} w_i w_j w_k \left. f(\mathbf{x}) \right|_{\mathbf{x}=(x_i, y_j, z_k)}, \tag{9.33}$$

where w_i, w_j and w_k are a set of weights that correspond to the N_{p}^3 integration points $\mathbf{x} = (x_i, y_j, z_k)$. The domain Ω_{G} is restricted to $(-1, 1)^3$. A useful property of this integration rule is that, depending on the number of integration points, it is possible integrate polynomials exactly. A Gaussian quadrature with N_{p}^3 integration points can integrate exactly a polynomial function of order $2N_{\mathsf{p}} - 1$ or less.

Algorithm 9.1 Outline of the Newton–Raphson method.

Initial values $\mathbf{d}_0 = \mathbf{d}_i$

1. Compute $\mathbf{K}(\mathbf{d}_i)$ and $\mathbf{F}(\mathbf{d}_i)$.
2. Compute increment $(\Delta\mathbf{d}_{i+1})$ by solving $\mathbf{K}(\mathbf{d}_i)\,\Delta\mathbf{d}_{i+1} = \mathbf{F}(\mathbf{d}_i)$.
3. Update solution $\mathbf{d}_{i+1} = \Delta\mathbf{d}_{i+1} + \mathbf{d}_i$.
4. Test for convergence.
   a) If $|\mathbf{F}(\mathbf{d}_{i+1})| >$ tolerance set $i \to i+1$ and go to step 1
   b) If $|\mathbf{F}(\mathbf{d}_{i+1})| <$ tolerance STOP

9.4. Newton–Raphson method

Due to the non-linear dependence on the degrees of freedom in the finite element problem, we need to use a root finding algorithm to find the solution. The Newton–Raphson method was used. Given some function $T : \mathbb{R}^n \to \mathbb{R}^n$, the root of

$$T(\mathbf{x}) = \mathbf{0} \tag{9.34}$$

can be approximated using the update formula

$$\left.\frac{\partial T(\mathbf{x})}{\partial \mathbf{x}}\right|_{\mathbf{x}=\mathbf{x}_i} (\mathbf{x}_{i+1} - \mathbf{x}_i) = T(\mathbf{x}_i), \tag{9.35}$$

where $\mathbf{x}_i$ is the i-th approximation of the root. The finite element equations can written as

$$G(\mathbf{d}) = 0 \tag{9.36}$$

where $\mathbf{d}$ is a vector containing the scalar coefficients for every degree of freedom in the domain. Applying the Newton–Raphson method then gives

$$\left.\frac{\partial G}{\partial \mathbf{d}}\right|_i \Delta\mathbf{d} = G_i. \tag{9.37}$$

This can also be written as

$$\mathbf{K}\Delta\mathbf{d} = \mathbf{F}, \tag{9.38}$$

where the global stiffness matrix $\mathbf{K}$ is assembled from the linearization of the weak form over each element in the system

$$\mathbf{K} = \mathop{\mathbf{A}}_{e=1}^{M} (k_{ij})_e\,, \tag{9.39}$$

the global residual $\mathbf{F}$ assembled from the weak form over each element in the system

$$\mathbf{F} = \mathop{\mathbf{A}}_{e=1}^{M} (G_j)_e\,, \tag{9.40}$$

and $\mathbf{d}$ is also written as an assemble over all of the elements

$$\mathbf{d} = \mathop{\mathbf{A}}_{e=1}^{M} (\Delta U_j)_e\,. \tag{9.41}$$

Algorithm 9.1 gives an outline of the procedure taken to find the solution.

10. Corrector

The corrector part of the numerical method solves for the plastic deformation, $\mathbf{F}^{\mathrm{p}}{}_{\mathrm{n+1}}$, at each integration point, given the previously calculated elastic deformation, $\mathbf{F}^{\mathrm{e}}{}_{\mathrm{n+1}}$. Recall from equation (8.3) that

$$\mathbf{F}^{\mathrm{p}}{}_{\mathrm{n+1}} = \exp(\mathbf{\Lambda})\mathbf{F}^{\mathrm{p}}{}_{\mathrm{n}}, \tag{10.1}$$

where

$$\mathbf{\Lambda} = \Delta t \sum_{\alpha=1}^{N} \nu^{\alpha}_{\mathrm{n+1}} \mathbb{S}^{\alpha}. \tag{10.2}$$

The unknowns in equation (10.1) that need to be found are the slip rates, $\nu^{\alpha}_{\mathrm{n+1}}$. Due to the differences between the hardening laws, the algorithm used for each one is different. In general terms, though, the algorithms for solving the slip rates involve using in combination a fixed point algorithm and a Newton–Raphson scheme.

10.1. The algorithmic residual

As mentioned previously, the residual is made in part by the constitutive equation governing the slip rate.

$$\nu^{\alpha}_{\mathrm{n+1}} = d_0 \left(\frac{|\tau^{\alpha}_{\mathrm{n+1}}|}{S^{\alpha}_{\mathrm{n+1}}} \right)^{\frac{1}{m}} \operatorname{sgn}\left(\tau^{\alpha}_{\mathrm{n+1}}\right). \tag{10.3}$$

A very small rate sensitivity parameter ($m \ll 1$) can cause issues when trying to solve this part. For example, if there is even a slight overshoot in $|\tau^{\alpha}_{\mathrm{n+1}}|/S^{\alpha}_{\mathrm{n+1}}$ the computer could potentially return a floating point error. Steinmann and Stein describe a solution to this problem in [36]. They propose reformulating the constitutive equation as

$$\left(\frac{\nu^{\alpha}_{\mathrm{n+1}}}{d_0 \operatorname{sgn}\left(\tau^{\alpha}_{\mathrm{n+1}}\right)} \right)^{m} = \frac{|\tau^{\alpha}_{\mathrm{n+1}}|}{S^{\alpha}_{\mathrm{n+1}}}. \tag{10.4}$$

This solves the problem of an overshoot in $|\tau^{\alpha}_{\mathrm{n+1}}|/S^{\alpha}_{\mathrm{n+1}}$, but unfortunately it creates a new problem. If the slip rate becomes very small ($\nu^{\alpha} \to 0$) the diagonal entry of the Jacobian will tend to infinity. The solution to this is to have both residuals, and then determine algorithmically which one to use for each slip system. The residual equation for the constitutive equation is thus

$$R^{\alpha}_{\nu} = \begin{cases} -\nu^{\alpha}_{\mathrm{n+1}} + d_0 \left(\frac{|\tau^{\alpha}_{\mathrm{n+1}}|}{S^{\alpha}_{\mathrm{n+1}}} \right)^{\frac{1}{m}} \operatorname{sgn}\left(\tau^{\alpha}_{\mathrm{n+1}}\right) & \text{if } \nu^{\alpha}_{\mathrm{n+1}} < \text{tol and } \frac{|\tau^{\alpha}_{\mathrm{n+1}}|}{S^{\alpha}_{\mathrm{n+1}}} < 1 \\ -\left(\frac{\nu^{\alpha}_{\mathrm{n+1}}}{d_0 \operatorname{sgn}\left(\tau^{\alpha}_{\mathrm{n+1}}\right)} \right)^{m} + \frac{\|\tau^{\alpha}_{\mathrm{n+1}}\|}{S^{\alpha}_{\mathrm{n+1}}} & \text{otherwise} \end{cases}. \tag{10.5}$$

10.2. Implicit hardening

Recall that this hardening law (equation 7.1) has hardening moduli that are dependent on the hardening variable. A fully-implicit discrete form is chosen in order to ensure stability

$$S^{\alpha}_{\mathrm{n+1}} = S^{\alpha}_{n} + \Delta t \sum_{\beta=1}^{N} \left(\chi^{\alpha\beta} + q\left(1-\chi^{\alpha\beta}\right)\right) h\left(S^{\beta}_{\mathrm{n+1}}\right) |\nu^{\beta}_{\mathrm{n+1}}|. \tag{10.6}$$

10.2.1. Residual

Since the discrete form of the hardening equation is implicitly dependent on the hardening variable, the hardening variable needs to be solved for at the same time as the slip rates. The residual is thus made of two parts

$$R = \begin{pmatrix} R_{\nu} \\ R_{S} \end{pmatrix}, \tag{10.7}$$

where $R_{\nu} = \left(R^{1}_{\nu}, R^{2}_{\nu}, \cdots, R^{n_{\mathrm{slips}}}_{\nu}\right)$ is the residual derived from the constitutive equation (equation 10.5) and $R_{S} = \left(R^{1}_{S}, R^{2}_{S}, \cdots, R^{n_{\mathrm{slips}}}_{S}\right)$ is the residual derived from the hardening equation, given by

$$R^{\lambda}_{S} = -S^{\lambda}_{\mathrm{n+1}} + S^{\beta}_{n} + \Delta t \sum_{\gamma} \left(\chi^{\lambda\gamma} + q\left(1-\chi^{\lambda\gamma}\right)\right) h\left(S^{\gamma}_{\mathrm{n+1}}\right) |\nu^{\gamma}_{\mathrm{n+1}}|. \tag{10.8}$$

The Newton scheme can now be re-written as

$$\begin{pmatrix} \Delta\nu^{\alpha} \\ \Delta S^{\mu} \end{pmatrix} = -J^{-1}_{i} \begin{pmatrix} R^{\beta}_{\nu} \\ R^{\lambda}_{S} \end{pmatrix}_{i}. \tag{10.9}$$

10.2.2. Jacobian

The Jacobian is

$$J = \begin{pmatrix} \frac{\partial R^{\beta}_{\nu}}{\partial \nu^{\alpha}} & \frac{\partial R^{\beta}_{\nu}}{\partial S^{\mu}} \\ \frac{\partial R^{\lambda}_{S}}{\partial \nu^{\alpha}} & \frac{\partial R^{\lambda}_{S}}{\partial \nu^{\mu}} \end{pmatrix} \tag{10.10}$$

The four blocks of the Jacobian are as follows

$$\frac{\partial R^{\lambda}_{S}}{\partial \nu^{\alpha}} = \Delta t \left(\chi^{\lambda\alpha} + q\left(1-\chi^{\lambda\alpha}\right)\right) h(S^{\alpha}) \mathrm{sgn}\left(\nu^{\alpha}\right) \tag{10.11}$$

$$\frac{\partial R^{\lambda}_{S}}{\partial S^{\mu}} = -\delta^{\mu\lambda} + \Delta t \left(\chi^{\lambda\mu} + q\left(1-\chi^{\lambda\mu}\right)\right) h'\left(S^{\mu}\right) \|\nu^{\mu}\| \tag{10.12}$$

$$\frac{\partial R^{\beta}_{\nu}}{\partial \nu^{\alpha}} = \begin{cases} -\delta^{\alpha\beta} + \frac{d_0}{m}\left(\frac{|\tau^{\beta}|}{S^{\beta}}\right)^{\frac{1}{m}-1} \frac{\partial \tau^{\beta}}{\partial \nu^{\alpha}} \frac{1}{S^{\beta}} & \text{if } \nu^{\alpha} < \mathrm{tol} \text{ and } \frac{|\tau^{\alpha}|}{S^{\alpha}} < 1 \\ -\delta^{\alpha\beta} m \left(\nu^{\beta}\right)^{m-1} \left(d_0 \mathrm{sgn}\left(\tau^{\beta}\right)\right)^{-(m-2)} + \frac{\mathrm{sgn}\left(\tau^{\beta}\right)}{S^{\beta}} \frac{\partial \tau^{\beta}}{\partial \nu^{\alpha}} & \text{otherwise} \end{cases} \tag{10.13}$$

$$\frac{\partial R^{\beta}_{\nu}}{\partial S^{\mu}} = \begin{cases} -\delta^{\mu\beta} \frac{d_0}{m}\left(\frac{\|\tau^{\beta}\|}{S^{\beta}}\right)^{\frac{1}{m}-1} \frac{\tau^{\beta}}{\left(S^{\beta}\right)^2} & \text{if } \nu^{\alpha}_{\mathrm{n+1}} < \mathrm{tol} \text{ and } \frac{|\tau^{\alpha}|}{S^{\alpha}} < 1 \\ -\delta^{\mu\beta} \frac{|\tau^{\beta}|}{\left(S^{\alpha}\right)^2} & \text{otherwise} \end{cases}. \tag{10.14}$$

Note that all variables are taken to be at time $t = t_{\mathrm{n+1}}$. The derivative $\partial\tau^{\beta}/\partial\nu^{\alpha}$ will be shown in section 10.6.

10.3. Gurtin-Reddy hardening

The discretized hardening in this case is

$$S^{\alpha}_{\mathrm{n+1}} = S^{\alpha}_{n} + \Delta t \sum_{\beta=1}^{N} \left(\chi^{\alpha\beta} H_s \left(m^{\alpha}_{\mathrm{slf}} \right)_{\mathrm{n+1}} + \iota^{\alpha\beta} H_L \left(m^{\alpha}_{\mathrm{lat}} \right)_{\mathrm{n+1}} \right) |\nu^{\beta}_{\mathrm{n+1}}|. \tag{10.15}$$

Unlike the previous hardening law, there is no implicit dependence on the hardening variable here. Solving for this case thus becomes a lot more straightforward. The residual is the algorithmically determined residual derived from the constitutive equation (equation 10.5).

10.3.1. Jacobian

The Jacobian for this residual is

$$\frac{\partial R^{\alpha}_{\nu}}{\partial \nu^{\beta}} = \begin{cases} -\delta^{\alpha\beta} + \frac{d_0}{m} \left(\frac{|\tau^{\alpha}|}{S^{\alpha}} \right)^{\frac{1}{m}-1} \left(\frac{1}{S^{\alpha}} \frac{\partial \tau^{\alpha}}{\partial \nu^{\beta}} + \frac{\tau^{\alpha}}{(S^{\alpha})^2} \frac{\partial S^{\alpha}}{\partial \nu^{\beta}} \right) & \text{if } \nu^{\alpha} < \text{tol and } \frac{|\tau^{\alpha}|}{S^{\alpha}} < 1 \\ -\delta^{\alpha\beta} \frac{m}{d_0 \mathrm{sgn}(\tau^{\alpha})} \left(\frac{\nu^{\alpha}}{d_0 \mathrm{sgn}(\tau^{\alpha})} \right)^{m-1} + \frac{\partial \tau^{\alpha}}{\partial \nu^{\beta}} \frac{\mathrm{sgn}(\tau^{\alpha})}{S^{\alpha}} + \frac{|\tau^{\alpha}|}{(S^{\alpha})^2} \frac{\partial S^{\alpha}}{\partial \nu^{\beta}} & \text{otherwise.} \end{cases} \tag{10.16}$$

As before, all variables above are taken to be at time $t = t_{\mathrm{n+1}}$. The derivative of the hardening variable with respect to the slip-rate is

$$\frac{\partial S^{\alpha}}{\partial \nu^{\beta}} = \Delta t \left(\chi^{\alpha\beta} H_s \left(m^{\alpha}_{\mathrm{slf}} \right) + \iota^{\alpha\beta} H_L \left(m^{\alpha}_{\mathrm{lat}} \right) \right) \mathrm{sgn} \left(\nu^{\beta} \right). \tag{10.17}$$

10.4. Constant hardening

The parameter ρ is kept to be $\rho = 1$ in equation (7.24), so the discretized form of the hardening equation is

$$S^{\alpha}_{\mathrm{n+1}} = S^{\alpha}_{\mathrm{n}} + \Delta t \sum_{\beta=1}^{N} h_0 |^{\mathrm{n+1}} \nu^{\beta}|. \tag{10.18}$$

The residual is derived from the constitutive equation (equation (10.5)). The Jacobian is identical to that of the Gurtin-Reddy theory, equation (10.16). With

$$\frac{\partial S^{\alpha}}{\partial \nu^{\beta}} = \Delta t \mathrm{sgn} \left(\nu^{\beta} \right) h_0. \tag{10.19}$$

10.5. Isotropic hardening

The isotropic hardening law is expressed explicitly

$$S(\gamma) = \tau_0 + (\tau_\infty - \tau_0) \tanh \left(\frac{h_0 \gamma}{\tau_\infty - \tau_0} \right), \tag{10.20}$$

$$h(\gamma) = h_0 \cosh^{-2} \left(\frac{h_0 \gamma}{\tau_\infty - \tau_0} \right), \tag{10.21}$$

so the only residual derived from the constitutive equation (equation 10.5) is needed.

10.5.1. Jacobian

The Jacobian is similar to the one used for the Gurtin-Reddy theory

$$\frac{\partial R^{\alpha}_{\nu}}{\partial \nu^{\beta}} = \begin{cases} -\delta^{\alpha\beta} + \frac{d_0}{m}\left(\frac{|\tau^{\alpha}|}{S}\right)^{\frac{1}{m}-1}\left(\frac{1}{S}\frac{\partial \tau^{\alpha}}{\partial \nu^{\beta}} + \frac{\tau^{\alpha}}{S^2}\frac{\partial S}{\partial \nu^{\beta}}\right) & \text{if } \nu^{\alpha} < \text{tol and } \frac{|\tau^{\alpha}|}{S} < 1 \\ -\delta^{\alpha\beta}\frac{m}{d_0 \operatorname{sgn}(\tau^{\alpha})}\left(\frac{\nu^{\alpha}}{d_0 \operatorname{sgn}(\tau^{\alpha})}\right)^{m-1} + \frac{\partial \tau^{\alpha}}{\partial \nu^{\beta}}\frac{\operatorname{sgn}(\tau^{\alpha})}{S} + \frac{|\tau^{\alpha}|}{S^2}\frac{\partial S}{\partial \nu^{\beta}} & \text{otherwise.} \end{cases} \tag{10.22}$$

Again, all variables above are taken to be at time $t = t_{\mathrm{n+1}}$, and

$$\frac{\partial S}{\partial \nu^{\beta}} = h(\gamma) \operatorname{sgn}\left(\nu^{\beta}\right). \tag{10.23}$$

10.6. Derivative of the resolved shear

The derivative of the resolved shear is given as

$$\frac{\partial \tau^{\beta}_{\mathrm{n+1}}}{\partial \nu^{\alpha}_{\mathrm{n+1}}} = \frac{\partial \tau^{\beta}_{\mathrm{n+1}}}{\partial \mathbf{C}^{\mathrm{e}}_{\mathrm{n+1}}} : \frac{\partial \mathbf{C}^{\mathrm{e}}_{\mathrm{n+1}}}{\partial \nu^{\alpha}_{\mathrm{n+1}}}, \tag{10.24}$$

where

$$\frac{\partial \tau^{\beta}_{\mathrm{n+1}}}{\partial \mathbf{C}^{\mathrm{e}}_{\mathrm{n+1}}} = \frac{1}{2}\lambda\left(\mathbf{C}^{\mathrm{e}}_{\mathrm{n+1}} : \mathbf{P}^{\alpha}\right)\mathbf{I} + \delta^{I}_{\mathrm{n+1}}\mathbf{P}^{\alpha} + 2\mu\left(\mathbf{C}^{\mathrm{e}}_{\mathrm{n+1}}\mathbf{P}^{\alpha}\right)^{\mathrm{SYM}} \tag{10.25}$$

$$\frac{\partial \mathbf{C}^{\mathrm{e}}_{\mathrm{n+1}}}{\partial \nu^{\alpha}_{\mathrm{n+1}}} = 2\left(\left(\bar{\mathbf{F}}_{\mathbf{p}}\right)^{-T}\mathbf{C}^{\mathbf{et}}\frac{\partial\left(\bar{\mathbf{F}}_{\mathbf{p}}\right)^{-\mathbf{1}}}{\partial \nu^{\alpha}_{\mathrm{n+1}}}\right) \tag{10.26}$$

$$\frac{\partial\left(\bar{\mathbf{F}}_{\mathbf{p}}\right)^{-\mathbf{1}}}{\partial \nu^{\alpha}_{\mathrm{n+1}}} = -\left(\mathbf{I} + (1-\theta)\boldsymbol{\Lambda}\right)^{-1}\mathbf{Z}^{\beta}\left(\theta\mathbf{I} + (1-\theta)\left(\bar{F}_p\right)^{-1}\right). \tag{10.27}$$

More detail on the finding of the above derivatives, equations (10.25) to (10.27), are given in Appendix B.

10.7. Newton increment parameter

The slip rate and the resolved shear are constrained to have the same sign

$$\operatorname{sgn}(\nu^{\alpha}) = \operatorname{sgn}(\tau^{\alpha}). \tag{10.28}$$

In order to satisfy this constraint, the Newton increment of the solution is scaled by a parameter $0 < s \leq 1$. Depending on the hardening law, this is written as

$$\begin{pmatrix} \nu^{\beta} \\ S^{\lambda} \end{pmatrix}_{i+1} = \begin{pmatrix} \nu^{\beta} \\ S^{\lambda} \end{pmatrix}_{i} + s\begin{pmatrix} \Delta\nu^{\beta} \\ \Delta S^{\lambda} \end{pmatrix} \text{ or } \left(\nu^{\beta}\right)_{i+1} = \left(\nu^{\beta}\right)_{i} + s\left(\Delta\nu^{\beta}\right) \tag{10.29}$$

The incremental parameter, s, is chosen such that the constraint in equation (10.28) is satisfied.

10.8. Ramping the rate sensitivity parameter

Due to the power law rate sensitivity, a very small rate sensitivity parameter $m \ll 1$ will mean that the convergence of the Newton method is not guaranteed. To solve the problem, the rate sensitivity is solved for a larger rate sensitivity parameter. Upon convergence of the residual, the rate sensitivity parameter is decreased by some factor c

$$m_k \to \frac{1}{c} m_k \tag{10.30}$$

and the solution is used as an initial solution for a new Newton method. Upon convergence of the new residual the process is repeated until the intended rate sensitivity parameter is reached. This procedure is called ramping. An outline of the procedure used to solve for the unknowns in the slip-systems is given in Algorithm 10.1.

10.9. Fixed point algorithm

Due to the co-dependence of equations 8.5 and 8.6, an initial guess for the Newton–Raphson algorithm is not obvious. In addition to this, any initial choice has to satisfy the condition

$$\operatorname{sgn}(\nu^{\alpha}_{\mathrm{n+1}}) = \operatorname{sgn}(\tau^{\alpha}_{\mathrm{n+1}}). \tag{10.31}$$

The decision was made to use a fixed-point algorithm to find the initial guess for the Newton–Raphson algorithm and, if the fixed point algorithm's guess has converged to a sufficient degree, avoid using the Newton–Raphson algorithm altogether.

10.9.1. Outline

Consider the following equation

$$f(x) = x, \tag{10.32}$$

where $f(x)$ is a Lipschitz continuous function. A fixed point iteration to approximate the value of x that satisfies this equation is

$$x_{i+1} = f(x_i),\ i = 0, 1, 2, \cdots . \tag{10.33}$$

Convergence is guaranteed if the Lipschitz constant $L < 1$. The fixed point iterations of each of the hardening rules have a similar structure to the Newton–Raphson scheme. Due to the implicit dependence of the implicit rule the fixed point iteration must be solved as a coupled set of equations, i.e.

$$\begin{pmatrix} \nu^{\alpha}_{\mathrm{n+1}} \\ S^{\lambda}_{\mathrm{n+1}} \end{pmatrix}_{i+1} = \begin{pmatrix} d_0 \left(\frac{|\tau^{\alpha}_{\mathrm{n+1}}|}{S^{\alpha}_{\mathrm{n+1}}} \right)^{\frac{1}{m}} \operatorname{sgn}\left(\tau^{\alpha}_{\mathrm{n+1}}\right) \\ S^{\lambda}_{n} + \Delta t \sum_{\beta=1}^{N} \left(\chi^{\lambda\beta} + q\left(1 - \chi^{\lambda\beta}\right) \right) h\left(S^{\beta}_{\mathrm{n+1}}\right) |\nu^{\beta}_{\mathrm{n+1}}| \end{pmatrix}_{i}. \tag{10.34}$$

The other two hardening rules have an explicit expression for the hardening S^{α}_{n+1} and thus can be solved with the iteration

$$\left(\nu^{\alpha}_{\mathrm{n+1}}\right)_{i+1} = \left(d_0 \left(\frac{|\tau^{\alpha}_{\mathrm{n+1}}|}{S^{\alpha}_{\mathrm{n+1}}}\right)^{\frac{1}{m}} \operatorname{sgn}\left(\tau^{\alpha}_{\mathrm{n+1}}\right)\right)_{i} . \tag{10.35}$$

The initial value used for this algorithm is the value of the variable at $t = 0$, i.e. S_0 or d_0. After every iteration is complete the Lipschitz constant, L, is calculated. If there is no convergence, i.e. $L \geq 1$, then the fixed point algorithm is abandoned and the Newton–Raphson method is used with the final approximation of the fixed point algorithm as the initial guess for the Newton–Raphson scheme. If there is convergence, $L < 1$, then the fixed point algorithm can continue for one more iteration, etc. A summary of the entire corrector algorithm is shown in algorithm 10.1.

Algorithm 10.1 The corrector algorithm.

1. If the rate sensitivity parameter m is small, $m < 0.5$, then use a larger value $m_k = 0.5$ otherwise $m_k = m$
2. Initialization for $i = 0$, iterate with a fixed point algorithm:
   - Calculate the Lipschitz constant L
     - IF $L < 1$ continue to the next iteration in the fixed point algorithm
     - IF ν^α and S^α have converged to within acceptable tolerance then check the rate sensitivity parameter
       * IF $m_k = m$ then STOP,
       * Otherwise ramp the rate sensitivity parameter and continue the with the new value:

$$m_k \to \begin{cases} m & \text{if } m > \frac{1}{2}m_k \\ \frac{1}{2}m_k & \text{if } m < \frac{1}{2}m_k \end{cases}$$

       then continue with the fixed point algorithm.
     - IF $L > 1$ then continue to the next step
3. Increment iteration counter $i \to i + 1$ and set line search parameter $s = 1$
4. Determine $\bar{\mathbf{F}}^{\mathrm{p}\,-1}$ and update $\mathbf{F}^{\mathrm{p}\,-1}$ and $\mathbf{C}^{\mathbf{e}}$ with $\mathbf{\Lambda} = \sum_\alpha \nu^\alpha \mathbf{Z}^\alpha$
5. Compute resolved shear on each slip system α
6. IF $\operatorname{sgn}(\tau^\alpha) \neq \operatorname{sgn}(\nu^\alpha)$, increment the parameter s

$$s \to \frac{1}{2}s, \quad (\nu^\alpha)_i \to (\nu^\alpha)_i - s\,(\Delta\nu^\alpha)$$

   go to step 4
7. Compute the residuum
   - if $\nu^\beta \leq$ tolerance and $|\tau^\beta| < g$ then

$$R_\nu^\beta = -\nu^\beta + d_0 \left(\frac{\left\|\tau^\beta\right\|}{S^\beta} \right)^{\frac{1}{m_k}} \operatorname{sgn}\left(\tau^\beta\right)$$

   - else

$$R_\nu^\beta = -\left(\frac{\nu^\beta}{d_0 \operatorname{sgn}(\tau^\beta)} \right)^{m_k} + \frac{\left\|\tau^\beta\right\|}{S^\beta}$$

8. Check convergence
   - IF $|\mathbf{R}| <$ tolerance then check the rate sensitivity parameter
     - IF $m_k = m$ then STOP,
     - Otherwise ramp the rate sensitivity parameter and continue the with the new value:

$$m_k \to \begin{cases} m & \text{if } m > \frac{1}{2}m_k \\ \frac{1}{2}m_k & \text{if } m < \frac{1}{2}m_k \end{cases}$$

     then GO TO step 3
   - otherwise IF $|\mathbf{R}| >$ tolerance then continue to the next step
9. Perform a single Newton step

   a) Generate the Jacobi matrix

Implicit	Gurtin and Reddy, Isotropic
$\begin{pmatrix} \frac{\partial R_\nu^\beta}{\partial \nu^\alpha} & \frac{\partial R_\nu^\beta}{\partial S^\mu} \\ \frac{\partial R_S^\lambda}{\partial \nu^\alpha} & \frac{\partial R_S^\lambda}{\partial \nu^\mu} \end{pmatrix}$	$\left(\frac{\partial R_\nu^\beta}{\partial \nu^\alpha} \right)$

   b) solve for the newton increment

Implicit	Gurtin and Reddy, Isotropic
$\begin{pmatrix} \Delta\nu^\alpha \\ \Delta S^\mu \end{pmatrix} = -\begin{pmatrix} \frac{\partial R_\nu^\beta}{\partial \nu^\alpha} & \frac{\partial R_\nu^\beta}{\partial S^\mu} \\ \frac{\partial R_S^\lambda}{\partial \nu^\alpha} & \frac{\partial R_S^\lambda}{\partial \nu^\mu} \end{pmatrix}^{-1} \begin{pmatrix} R_\nu^\beta \\ R_S^\lambda \end{pmatrix}$	$(\Delta\nu^\alpha) = -\left(\frac{\partial R_\nu^\beta}{\partial \nu^\alpha} \right)^{-1} \left(R_\nu^\beta \right)$

   c) GO TO step 3

11. Implementation within an object oriented framework

11.1. Object oriented programming

Object oriented programming (OOP) is a paradigm of programming which is based on the manipulation of data structures called objects. Objects can contain functions and variables. The nature of the finite element method lends itself to an object oriented framework. Concepts such as reference elements and Gauss quadrature can easily be generalized and made into objects, which can then act over an entire mesh of elements. Generality is, in fact, a major priority that must be kept in mind within OOP.

11.2. DEAL.II

The differential equation analysis library (DEAL.II) is an extensive open-source finite element library. First created by Wolfgang Bangerth [7], it has dozens of contributers and is widely used in many academic and commercial projects. The library takes full advantage of the object oriented nature of the finite element method. It is written in the C++ programming language.

11.3. Multi-threading

Currently most desktop computers have more that one processor (or "core"). This means that to take full advantage of the resources of a computer, a piece of code must be written in a way that allows for it to be executed on all of the cores available to it. This is called multi-threading. In the case of this project this was implemented using Intel's threaded building blocks (TBB) library. The implementation is very straight forward. TBB provides a "wrapper", to which there is input a set of functions that can be implemented independently of each other and at the same time. TBB then controls the execution of these functions in parallel.

Part III.

Results

12. Validation of the numerical method

Before an investigation into the hardening rules can be done, the FEM approximation of the problem must be validated against results from the literature. Two benchmark problems are investigated. The first is a creep problem, in which an elastoplastic material is instantaneously loaded with a constant force. The material then proceeds to creep plastically. The second problem involves a unit element which is sheared to a very large extent. The FEM code was written to solve three-dimensional problems, but these problems are two-dimensional plane strain problems. Thus all degrees of freedom in the third dimension are constrained to have zero displacement.

12.1. Creep problem

This problem is described in [10]. A load is instantaneously applied to the top face of a box. Under this constant load the material continues to deform plastically, this is called creeping. The crystalline material is assumed to have only two slip systems, oriented at 60^o from each other (a diagram of this problem is shown in Figure 12.1). The material is defined to have a

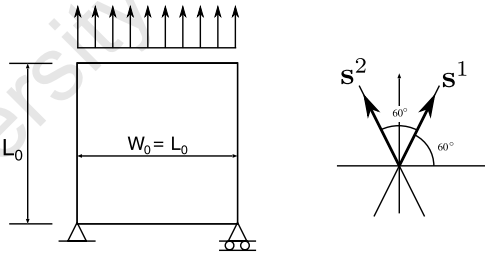

Figure 12.1.: Diagram of the creep problem

constant hardening (as described in section 10.4). The material parameters are shown in Table 12.1. This problem provides validation for the predictor part of the code and provides some

Shear modulus:	G	80.769 GPa
Bulk modulus:	K	175 GPa
Reference shear stress:	S	.18 GPa
Reference shear strain rate:	$\dot{\gamma}_0$	$0.002\,\mathrm{h}^{-1}$
Rate sensitivity parameter:	m	0.1961

Table 12.1.: Material parameters for the creep problem.

superficial validation of the corrector part. Since the hardening here is constant, the corrector part still needs a more rigorous examination. This is done in later sections. The results of this

test are compared with the results in [10]. These results are shown in Figure 12.2, where there is a good agreement.

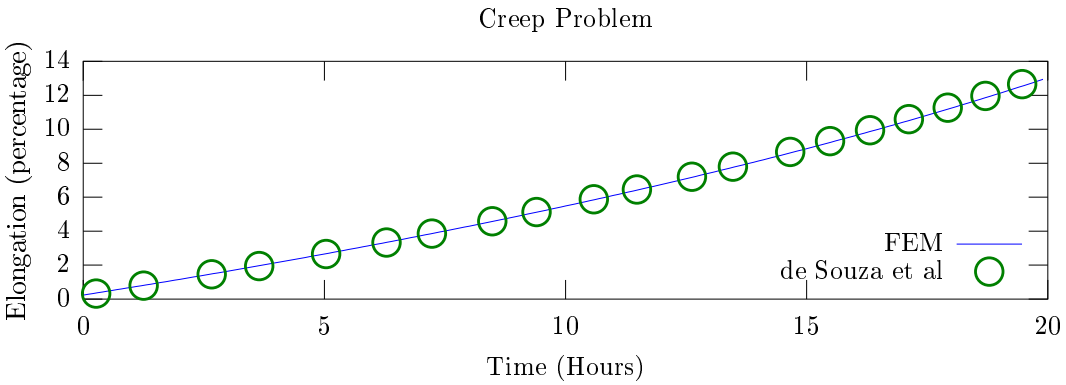

Figure 12.2.: Comparison of results for the creep problem. Here the percentage elongation of the material over a period of 20 hours is shown. Note the agreement with the results from de Souza et al. [10].

12.2. 2-D shear problem

This problem involves a single finite element that is undergoing a shear deformation, as described in [36]. A diagram of the problem is shown in Figure 12.3. The element is made to deform with a deformation gradient of

$$\mathbf{F} = \mathbf{1} + \epsilon \mathbf{e_1} \otimes \mathbf{e_2} \text{ with } 0 \leq \epsilon \leq \epsilon_{\max}. \tag{12.1}$$

This deformation is applied over 100 time-steps ($\Delta t = 5/100$) with a shear velocity $\dot{\epsilon} = 1$ until the maximum shear of $\epsilon_{\max} = 5$ is obtained. Since the deformation gradient is known everywhere in the domain, the finite element method is not necessary for this problem. The problem is a test of the corrector part of the algorithm. The isotropic hardening law (Section 7.3) is used. As in the previous example two slip systems, oriented at 60^o from each other, are used. The material parameters used are listed in Table 12.2. A comparison of the results from the code and the results from [36] is shown in Figure 12.4, where a good agreement can be seen.

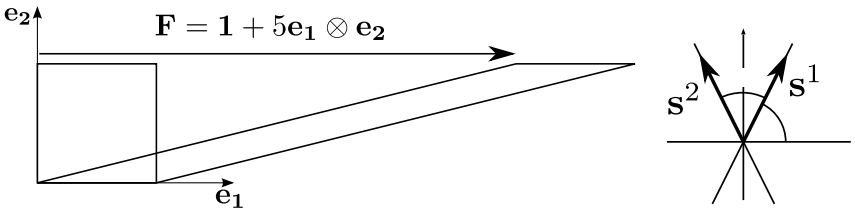

Figure 12.3.: Diagram for the 2-D shear problem.

Shear modulus:	G	23.427 GPa
Bulk modulus:	K	50.723 GPa
Reference shear stress:	τ_0	60.84 MPa
Saturation strength:	τ_∞	109.51 MPa
Initial hardening rate:	h_0	541.48
Reference shear strain rate:	$\dot{\gamma}_0$	0.001 s^{-1}
Rate sensitivity parameter:	m	0.005

Table 12.2.: Material parameters for the shear problem.

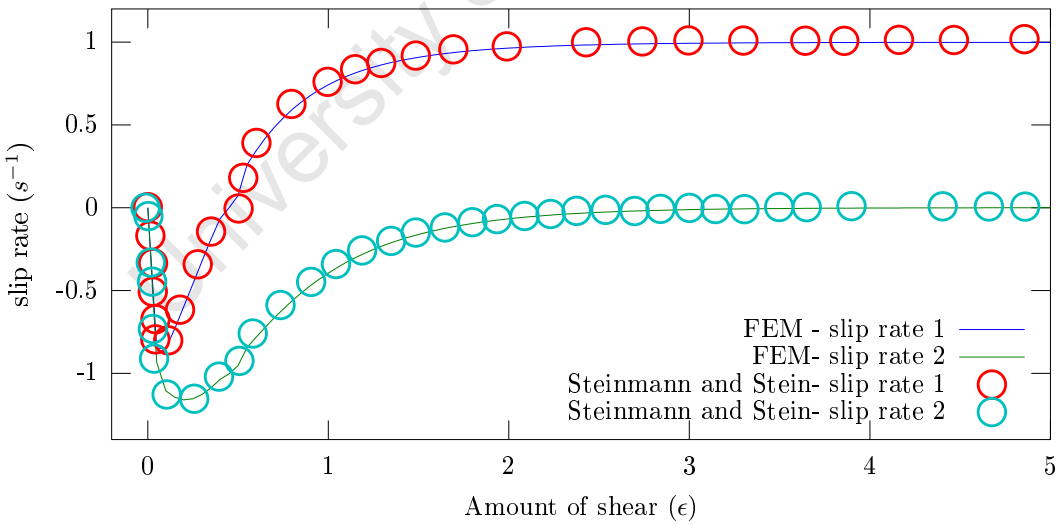

Figure 12.4.: Comparison of results for the 2-D shear problem. Here the slip rates of the two slip systems versus shear are shown.

13. Model problems

13.1. Calibration of the hardening rules

In order to compare the hardening laws, the material parameters need to be calibrated. This calibration is done by looking at a single slip system, where the hardening in each hardening law can be solved for exactly. Given a set of parameters for one hardening law, the parameters for the other hardening law can be found by using a non-linear least-squares fitting algorithm. For the case of single slip the implicit hardening law and the law by Gurtin and Reddy have the same form, given by

$$S(\gamma_{\text{acc}}) = S_s \left(1 - \frac{1}{\frac{h_0}{S_s}\gamma_{\text{acc}} + \frac{S_s}{S_s - S_0}}\right), \tag{13.1}$$

with parameters

$$a = 2, \quad h_0 = 180\text{MPa}, \quad S_s = 148\text{MPa}, \quad S_0 = 16\text{MPa}, \tag{13.2}$$

as suggested in [14]. For one slip-system the isotropic hardening law takes the form

$$S\left(\gamma_{\text{acc}}\right) = \tau_0 + (\tau_\infty - \tau_0) \tanh\left(\frac{h_0 \gamma_{\text{acc}}}{\tau_\infty - \tau_0}\right). \tag{13.3}$$

The parameters h_0, τ_∞ were found by fitting equation 13.3 to equation 13.1 with the parameters listed in equation 13.2. The value of the initial slip resistance τ_0 was not fitted, and is assumed to be the same for both hardening rules $S_0 = \tau_0 = 16\text{MPa}$.. The fit was done in Octave using the "leasqr" function of the optimization package [9].

13.2. Spherical indentation

This problem models a rigid spherical object which indents the top of a box-shaped single crystal material. The indentor is assumed to be perfectly bonded to the material. This results in a spherically-shaped deformation at the middle of the top of the box. Figure 13.2 shows a diagram of the problem. Due to symmetry a quarter of the box is modelled. A quarter of the box is a cube of length $L = 1\,\text{m}$, the domain Ω is thus $\Omega = (0, L)^3$. The $z = 0$ face has homogeneous Dirichlet boundary conditions imposed. Symmetry boundary conditions are imposed on the $x = 0$ and $y = 0$ faces. Since the area of the box in contact with the sphere changes over time, the region on the $z = L$ face (on which Dirichlet boundary boundary conditions are imposed) will also be

τ_∞	$104.494(42)\,\text{MPa}$
h_0	$98.246(77)\,\text{MPa}$

Table 13.1.: Fitted parameters for the isotropic law, with standard deviation in brackets.

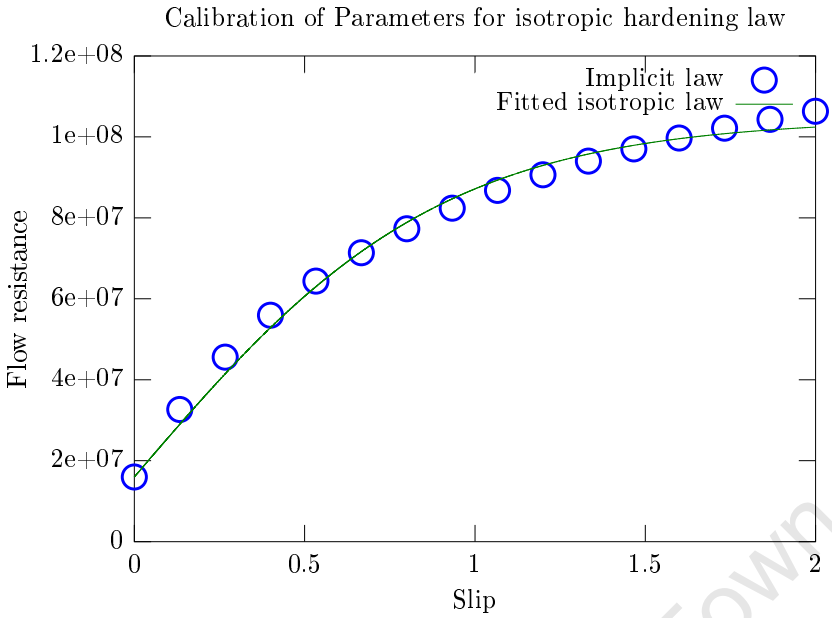

Figure 13.1.: Calibration of the isotropic hardening law on a single slip-system. Here the hardening for the isotropic law with the fitted parameters and the hardening for the Implicit/Gurtin-Reddy law are shown. The fit is good, thus a comparison of the hardening laws can now be made.

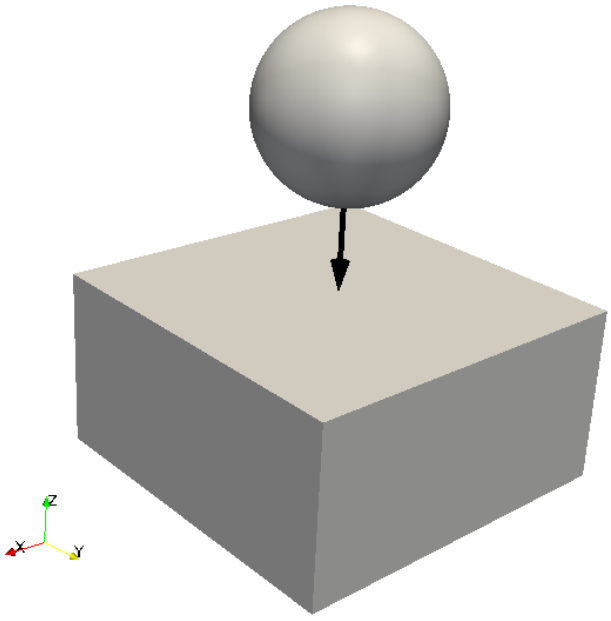

Figure 13.2.: Diagram of the indentation problem.

changing over time. Two regions on the top face are defined

$$\Gamma_D(t) \in \partial\Omega,\ \sqrt{x^2+y^2} \leq \sqrt{R^2-(L-ht)^2},\ z=L$$
$$\Gamma_N(t) \in \partial\Omega,\ \sqrt{x^2+y^2} > \sqrt{R^2-(L-ht)^2},\ z=L$$

here $R = 0.5$m is the radius of the sphere and h is a parameter that is related to the indentation depth. A non-homogeneous Dirichlet boundary on $\Gamma_D(t)$ is then defined as

$$\mathbf{u}(x,y,L) = \left(0, 0, \sqrt{R^2-(x^2+y^2)} + (L-ht)\right) \text{ on } \Gamma_D(t), \tag{13.4}$$

and a free boundary is defined on $\Gamma_N(t)$

$$\boldsymbol{\sigma}\mathbf{n} = \bar{\mathbf{t}} = \mathbf{0} \text{ on } \Gamma_N(t). \tag{13.5}$$

The problem is studied with the first three hardening laws that are described in chapter 7. For each hardening law the problem is solved using a single slip-system, a dual slip-system and an FCC crystal with 12 slip-systems. The material parameters have been calibrated to be the same for the case of a single slip-system. The results from this case can thus be used to validate the calibration.

13.2.1. Single slip-system crystal

The problem was solved with a crystal containing only one slip-system with normal $\mathbf{m} = (1,0,0)$ and slip-direction $\mathbf{s} = (0,1,1)$. As previously mentioned, this is used to validate the calibration between the hardening laws. It is expected that the results for the different hardening laws should be similar. This is indeed what is shown in Figure 13.3, which shows the slip (γ^α) and the flow resistance (S^α) for each of the hardening laws. For a single slip-system the Gurtin and Reddy formulation and the implicit formulation are the same, so identical results for both are expected. This is what is observed, for slip and flow resistance the results for the two rules are exactly the same. There is a slight difference, however, with the calibrated isotropic law. At the end of the simulation the flow resistance differs by about 2MPa. This is most probably due to the inexactness of the fit done in the calibration. The slip, however, shows very little difference between the hardening laws. From these results it can be concluded that the calibration was successful, and therefore a comparison of the hardening laws can be made for more complicated crystal structures.

13.2.2. Dual slip-system crystal

The purpose of testing the problem with dual slip-systems is mainly to confirm that the calibration has worked correctly. In this case, however, identical results for the Gurtin and Reddy formulation and the implicit formulation are no longer expected. The orientation of the slip-systems in the crystal are shown in Table 13.2. Figure (13.4) shows three graphs with the flow resistance for each hardening law. As expected, the Gurtin and Reddy formulation and the implicit formulations now give different results. The flow resistance for the first slip-system seems to

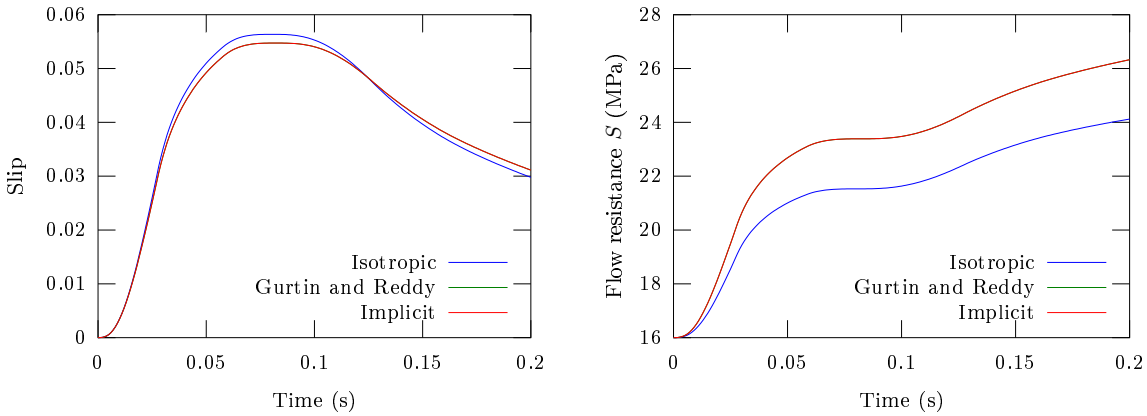

(a) Slip (γ^α) (b) Flow resistance (S^α)

Figure 13.3.: Comparison of slip (γ^α) and flow resistance (S^α) for each hardening law at the point $(0, 0, L)$ in the spherical indentation problem with a single slip-system crystal structure.

slip system	**s**	**m**
1	$\frac{1}{\sqrt{5}}(0, 1, 2)$	$\frac{1}{\sqrt{5}}(0, 2, -1)$
2	$\frac{1}{\sqrt{5}}(0, 1, -2)$	$\frac{1}{\sqrt{5}}(0, 2, 1)$

Table 13.2.: Dual slip-system orientations

follow the same path for both cases, but the values for the second slip-system differ significantly. For the implicit law the second flow resistance has a value larger than the first, and for Gurtin and Reddy's description it has a smaller value. This large difference, however doesn't carry over to the slips, Figure 13.5, which show very similar results for all three hardening laws.

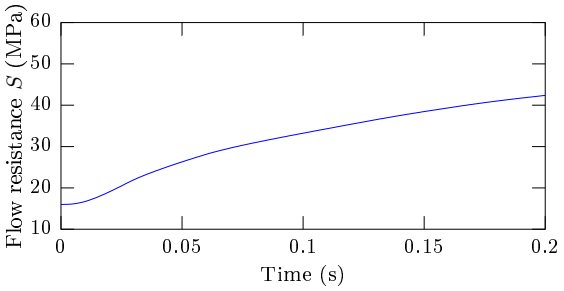

(a) Flow resistance for Isotropic hardening law

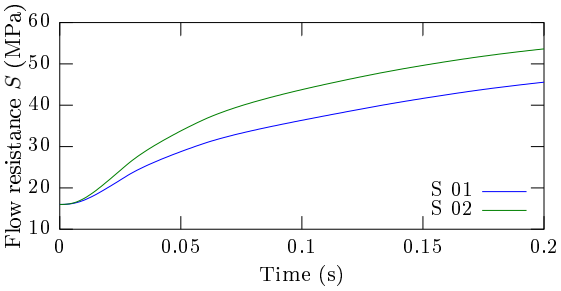

(b) Flow resistance for Implicit hardening law

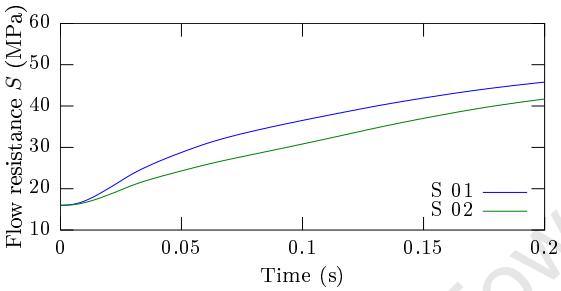

(c) Flow resistance for Gurtin & Reddy hardening law

Figure 13.4.: Comparison of flow resistance for each hardening law at the point $(0, 0, L)$ in the spherical indentation problem with a dual slip-system crystal structure

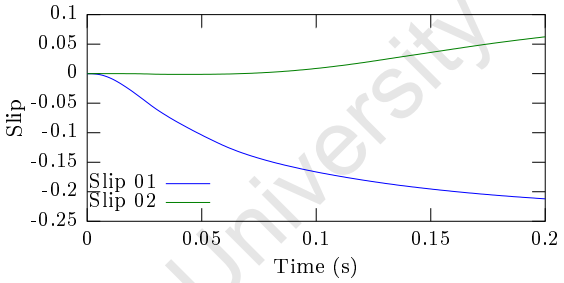

(a) Slip for Isotropic hardening law

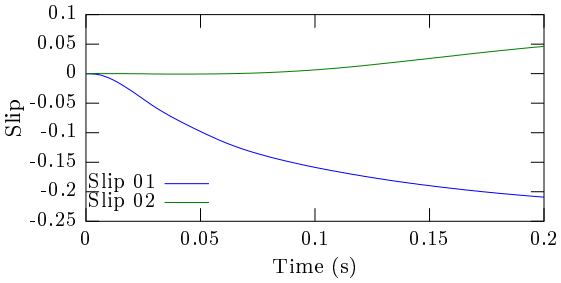

(b) Slip for Implicit hardening law

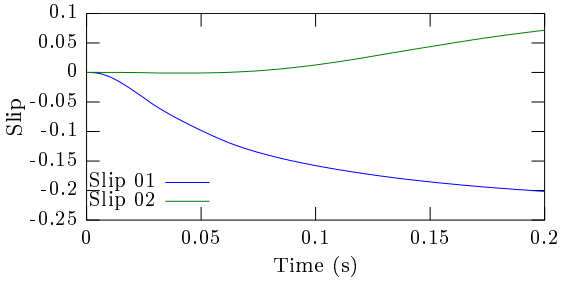

(c) Slip for Gurtin & Reddy hardening law

Figure 13.5.: Comparison of slip for each hardening law at the point $(0, 0, L)$ in the spherical indentation problem with a dual slip-system crystal structure

13.2.3. FCC crystal

For the FCC crystal significant differences between the hardening rules are expected. The orientations of the slip-systems are shown in Table 4.1. Figures 13.6 and 13.7 show some views of the model, solved using Gurtin and Reddy's rule, at the final time-step. Figure 13.6 shows the vertical component of the Cauchy stress ($\boldsymbol{\sigma}$), and Figure 13.7 shows the slip on one of the slip systems. It shows that there is a large amount of slip directly beneath the indenter. Figure 13.9 shows the flow resistance for the three hardening rules. Gurtin and Reddy's formulation seems to give flow resistances that range over a wider set of values. At the last time step this range is from 50MPa to 85MPa. This is a significant difference to the range of the implicit hardening rule, which ranges from 60MPa to 70MPa. Despite this large difference in flow resistance, it shows very similar results for the slip, which is shown in Figure 13.8. Although there is a distinct difference between the results, they are still qualitatively similar in that they have relatively similar amounts of activity on each slip-system.

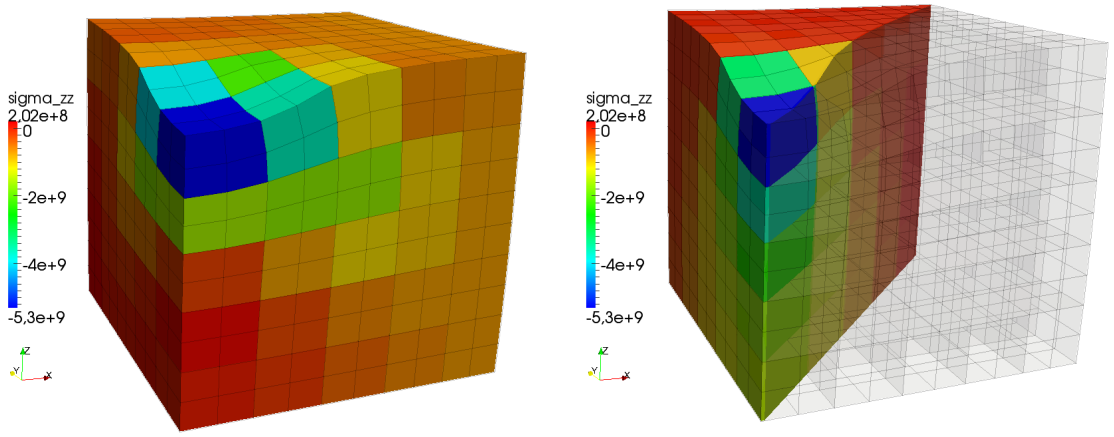

(a) View showing σ_{zz} (b) Sectioned view showing σ_{zz}

Figure 13.6.: Two views of the vertical component of stress (σ_{zz}) at time $t = 0.2$ for the spherical indentation problem with an FCC crystal structure.

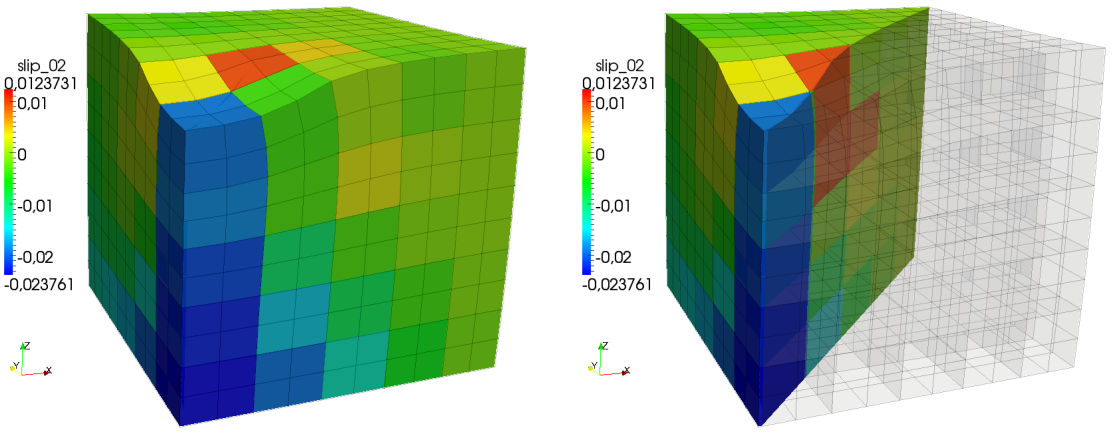

(a) View showing σ_{zz} (b) Sectioned view showing σ_{zz}

Figure 13.7.: Two views of the slip (γ^α) on the slip-system with $\mathbf{m}^\alpha = (1, 1, 1)$ and $\mathbf{s}^\alpha = (-1, 0, 1)$ at time $t = 0.2$ for the spherical indentation problem with an FCC crystal structure.

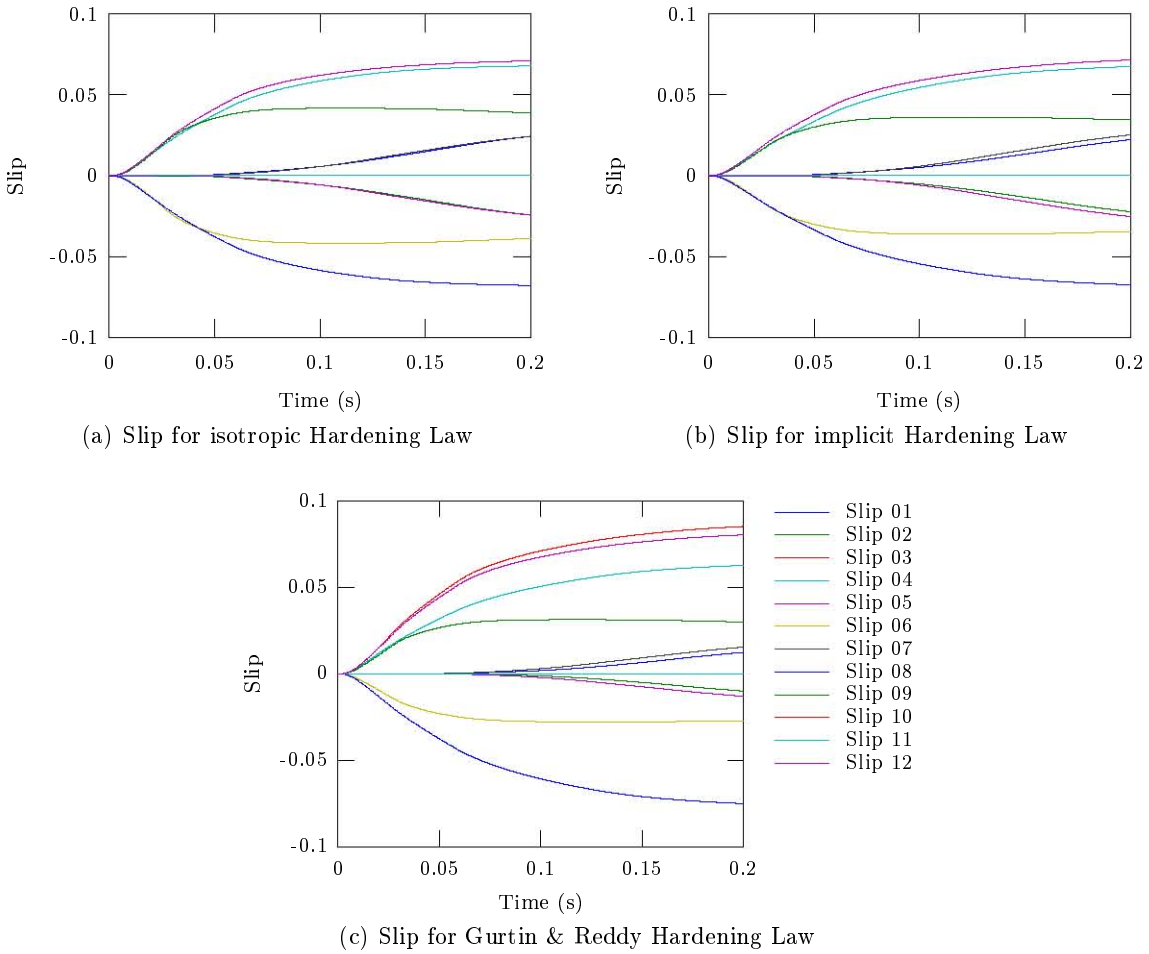

(a) Slip for isotropic Hardening Law

(b) Slip for implicit Hardening Law

(c) Slip for Gurtin & Reddy Hardening Law

Figure 13.8.: Comparison of Slip for each hardening law at the point $(0, 0, L)$ in the spherical indentation problem with an FCC crystal structure

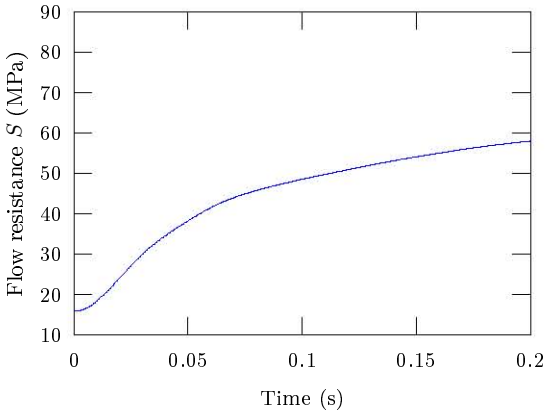

(a) Flow resistance for isotropic hardening law

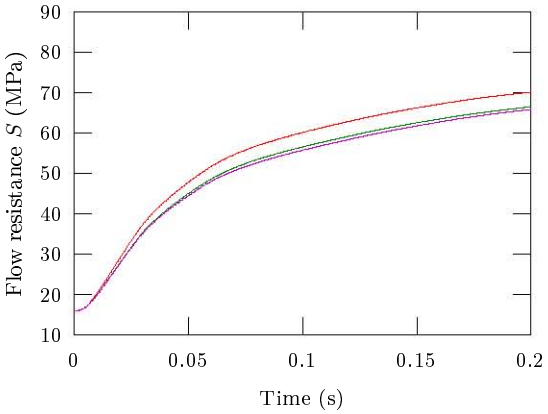

(b) Flow resistance for implicit hardening law

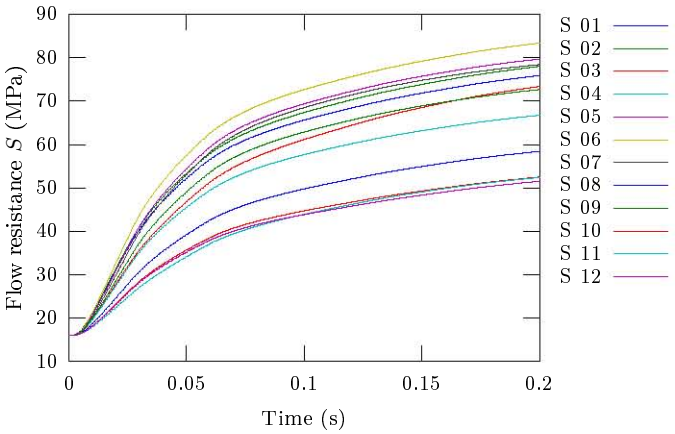

(c) Flow resistance for Gurtin & Reddy hardening law

Figure 13.9.: Comparison of flow resistance (S^α) for each hardening law at the point $(0, 0, L)$ in the spherical indentation problem with an FCC crystal structure

13.3. 3-D shear problem

The 3-D shear problem models a bar that is undergoing a shear deformation. This problem is described by Reddy et al. in [31]. The bar has dimensions $\Omega = (0, L)^2 \times (0, 3L)$, $L = 0.1\,\mathrm{m}$. Homogeneous Dirichlet boundary conditions are imposed on the $z = 0$ face and a displacement on the $z = L$ face that shears the bar in the y direction, shears back to the original position, and then shears in the y direction again

$$u(x, y, L) = \begin{cases} t(0, L, 0) & \text{if } t < \frac{1}{3}t_{\max} \\ (\frac{1}{3}t_{\max} - t)(0, L, 0) & \text{if } t > \frac{1}{3}t_{\max} \text{ and } t < \frac{2}{3}t_{\max} \\ (t - \frac{2}{3}t_{\max})(0, L, 0) & \text{if } t > \frac{2}{3}t_{\max}, \end{cases} \tag{13.6}$$

where $t_{\max}$ is the end time of the simulation. The $x = 0$ face has symmetry boundary conditions imposed, and the rest of the faces have free Neumann boundaries. A Diagram of the problem is shown in Figure 13.10. This problem is solved for each of the three hardening laws and with two different arrangements of crystal, the single-slip crystal and the FCC crystal. As with the

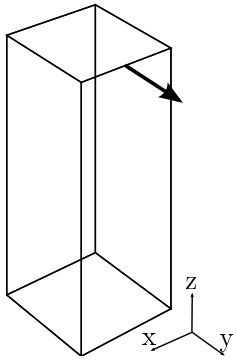

Figure 13.10.: Diagram of the 3-D shear problem.

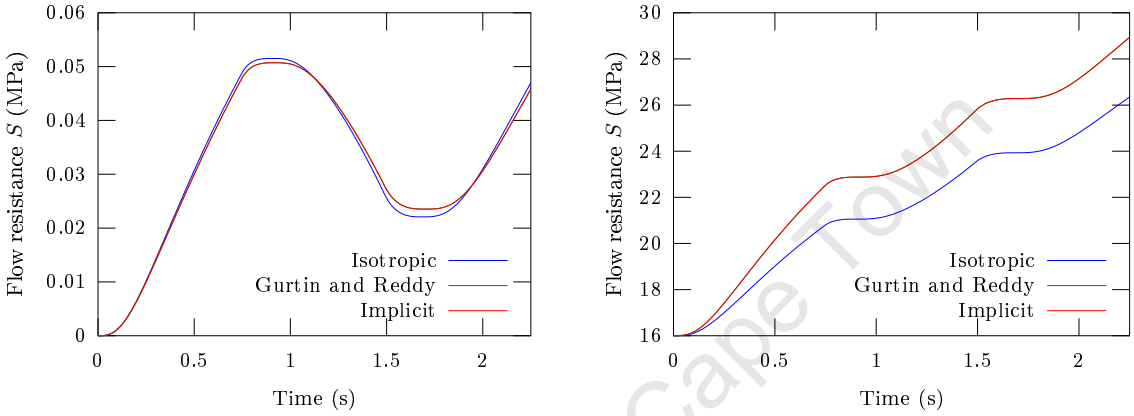

(a) Slip (γ^α) (b) Flow resistance (S^α)

Figure 13.11.: Comparison of slip (γ^α) and Flow resistance (S^α) for each hardening law at the point $(0.9L, 0.9L, 2.9L)$ in the 3D shear problem with a single slip-system crystal structure

spherical indentation problem the single slip-system case provides validation of the calibration of the hardening laws.

13.3.1. Single slip-system crystal

The slip system in this case has a normal $\mathbf{m} = (1, 0, 0)$ and slip direction $\mathbf{s} = (0, 0, 1)$. Figure 13.11 shows the slip (γ) and the flow resistance (S) for the three hardening laws. As with the spherical indentation problem, the Gurtin and Reddy's rule and the implicit rule give exactly the same results, as expected. A small difference in the flow resistance can be seen. Finally, despite this difference, a good match between the slips of the three hardening laws is observed. Thus it can be concluded that the calibration has been successful for this problem.

13.3.2. FCC crystal

A useful measure for the 3D Shear problem is that of the reaction force on the face that is being sheared. Figure 13.12 shows the component of this force in the direction of shear (y direction), for each of the three hardening rules. The plastic response of the material is clear in this graph.

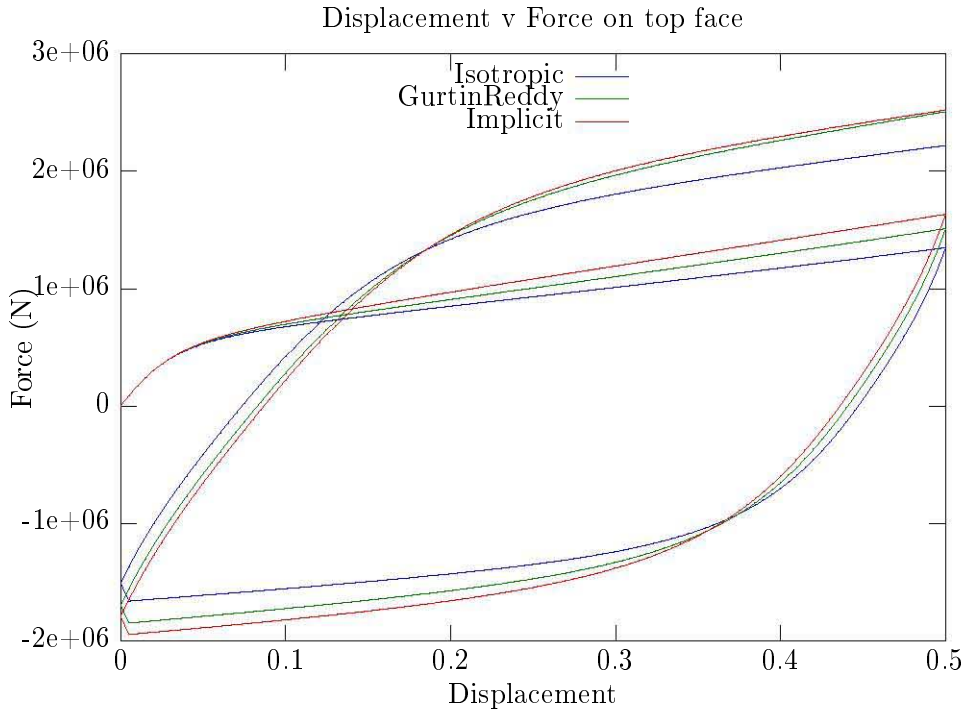

Figure 13.12.: Comparison of the reaction force on the top face in the direction of shear, for the three hardening rules with an FCC crystal structure.

A purely elastic material would have zero force once the material is returned to the original state. There is a large negative force, indicating that the material is resisting the deformation. The hardening of the material is also apparent in this graph. The elastic regime gets larger at the second loop, which means that the material is now less prone to a plastic response. The three hardening rules give a very similar response in this graph.

Figures 13.13 and 13.14 show the component of the stress in the direction of shear ($\boldsymbol{\sigma}_{yz}$) and the slip on one of the slip systems, for Gurtin and Reddy's hardening rule and the implicit hardening rule. Both figures show that the two hardening rules produce very similar results over the domain.

Figures 13.15 and 13.16 show the evolution of the flow resistance and the slip for all three hardening laws at the point (0.9L,0.9L,2.9L) on the domain. The changes in the direction of shear are clear in these graphs, they are the areas where the rate of slip goes to zero in the slip graphs and the areas where there is an inflection in the flow resistance graphs. The results here are very similar in nature to the results from the spherical indentation problem. The flow resistance for the slip-systems of the Gurtin and Reddy rule span a wider range than the implicit rule. Despite this significant difference, the slips are qualitatively the same for all three rules.

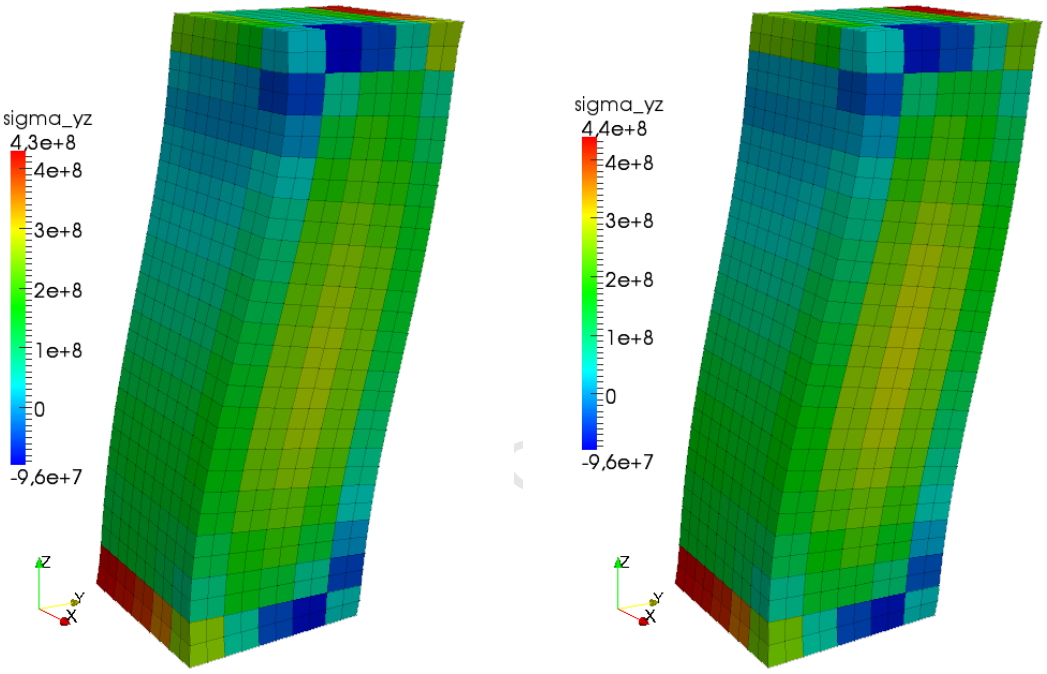

(a) Gurtin and Reddy hardening - $\boldsymbol{\sigma}_{yz}$

(b) Implicit hardening - $\boldsymbol{\sigma}_{yz}$

Figure 13.13.: Comparison of the shear component of stress ($\boldsymbol{\sigma}_{yz}$) at time $t = 0.75$ for the 3D shear problem with an FCC crystal structure.

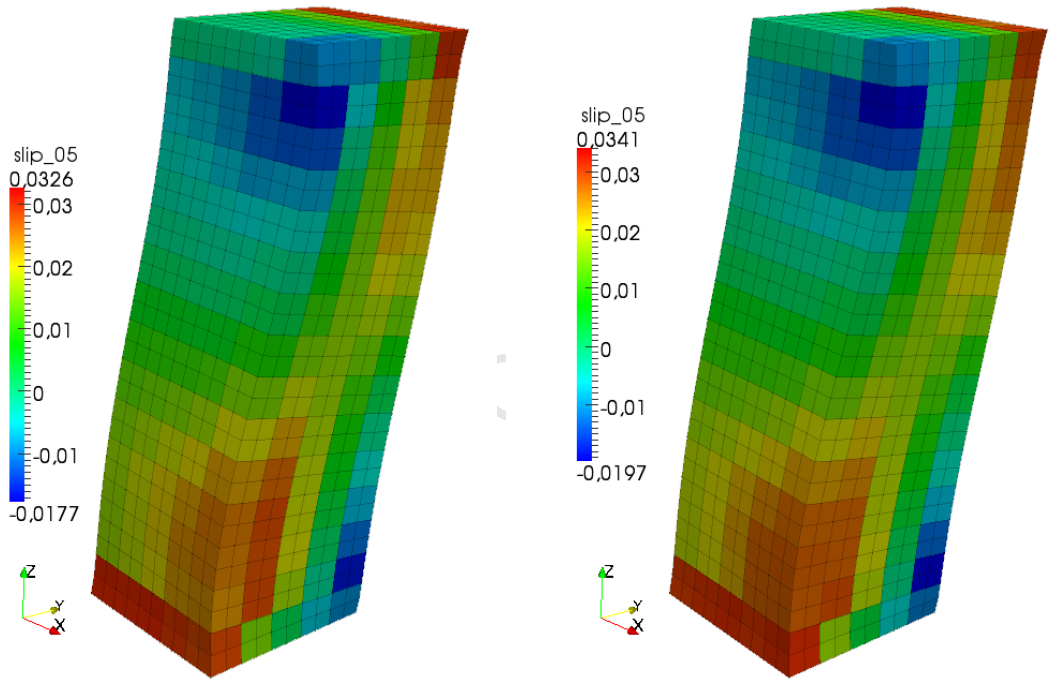

(a) Gurtin and Reddy hardening - γ^5

(b) Implicit hardening - γ^5

Figure 13.14.: Comparison of the slip (γ^5) on the slip-system with $\mathbf{m}^5 = (1, 0, 1)$ and $\mathbf{s}^5 = (-1, 1, 1)$ at time $t = 0.75$ for the 3D shear problem with an FCC crystal structure.

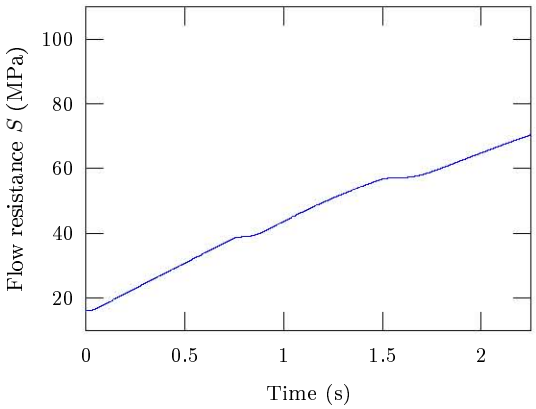

(a) Flow resistance for isotropic hardening law

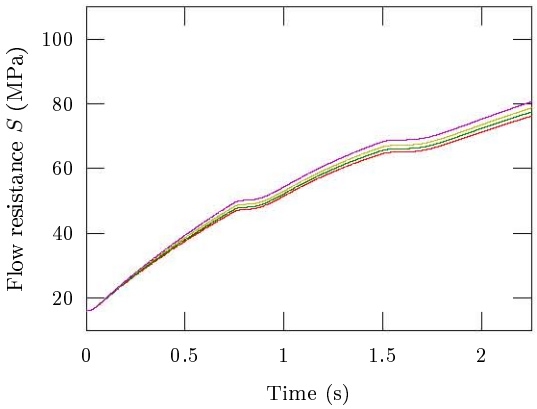

(b) Flow resistance for implicit hardening law

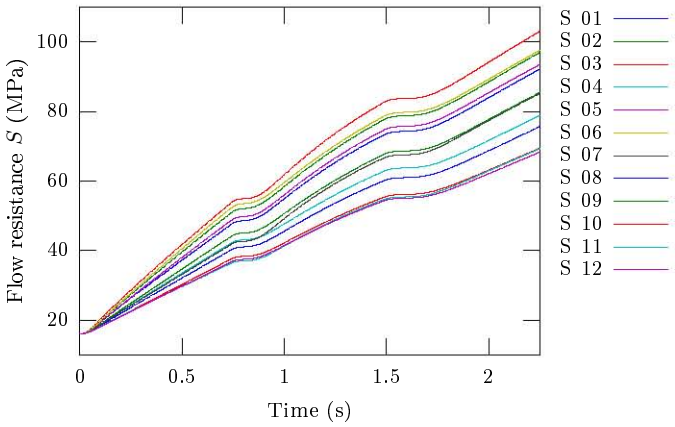

(c) Flow resistance for Gurtin & Reddy hardening law

Figure 13.15.: Comparison of flow resistance (S^α) for each hardening law at the point $(0.4L, 0.4L, 1.4L)$ in the 3D shear problem with an FCC crystal structure

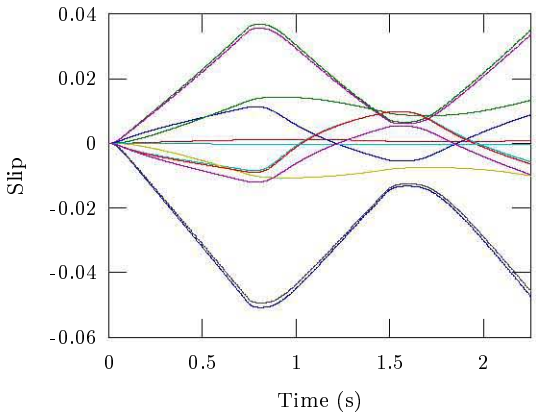

(a) Slip for isotropic hardening law

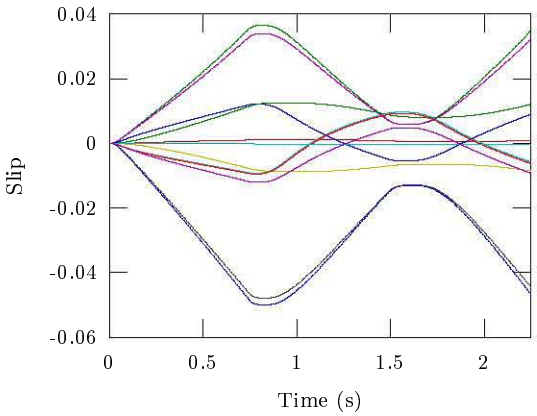

(b) Slip for implicit hardening law

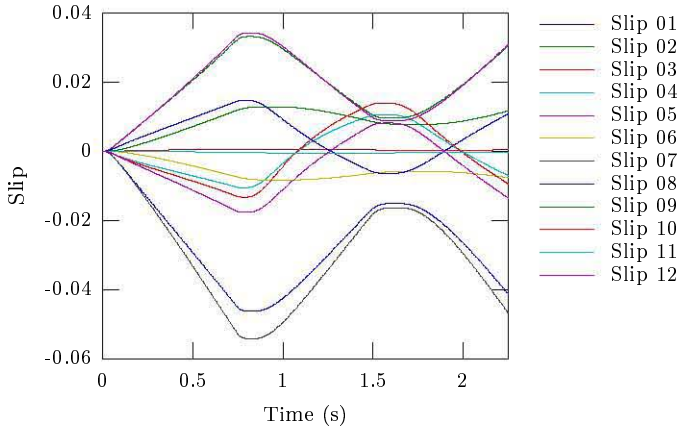

(c) Slip for Gurtin & Reddy hardening law

Figure 13.16.: Comparison of Slip for each hardening law at the point $(0.4L, 0.4L, 1.4L)$ in the 3D shear problem with an FCC crystal structure

Part IV.

Discussion and Conclusion

14. Discussion and conclusion

The finite element method coupled with a Newton–Raphson scheme in a predictor-corrector algorithm was used to solve the equations that describe single-crystal viscoplasticity under large deformations. This was based on the numerical method described in [36]. The underlying theory of continuum mechanics was described in Part I of this thesis. A detailed overview of the numerical method was given in Part II. Three different rules for hardening were studied. The first is an isotropic rule, dependent only on the accumulated slip, as described in [36]. The second is an implicit rule, in which the rate of flow resistance is dependent on the flow resistance itself. The third hardening rule is a novel one, described by Gurtin and Reddy in [14], in which the flow resistance is dependent on the slip accumulated on each slip system.

The numerical algorithm that was used to solve the corrector part of the method involved first finding an estimate using a fixed-point algorithm. If the fixed-point algorithm had not converged then the last result was used as the initial estimate for a Newton–Raphson scheme. This approach was found to be very efficient, the corrector part of the numerical method is the most computationally expensive, the Newton–Raphson scheme being the major contributor to this. In general the problems with fewer slip systems, such as the single and dual slip-system cases, were found to converge after a few iterations in the fixed point algorithm. Thus the use of the Newton–Raphson scheme could be avoided altogether. The FCC crystal, however, did require the Newton–Raphson scheme in order to obtain convergence.

The numerical method was validated by comparing with the results from the two-dimensional shear problem in [36] and the two-dimensional creep problem in [8]. The results from the numerical method agree very well with the results from the literature. In order to examine the hardening laws, two different models were studied, a box with the top surface being deformed by a spherical indenter and a bar that is undergoing a shear deformation. These models were solved with the three hardening rules, and with different crystal structures. Of particular interest are the results of the front centred cubic (FCC) crystals. These show a significant difference in the evolution of the flow resistance between Gurtin and Reddy's hardening rule and the implicit hardening rule. The flow resistances for the slip-systems in Gurtin and Reddy's rule spread out over a larger range when compared to that of the implicit rule. Despite this the evolution of the slips and the reaction force for each hardening rule (including the isotropic rule) is very similar.

Possible directions for this work in the future could involve extending the formulation of plasticity to a gradient theory, e.g. [13]. It would also be interesting to have a more detailed look at the algorithms required to solve for cases in which the rate sensitivity parameter (m) in the constitutive equation is very small. Some tests were done with some of the problems having the rate sensitivity at a very small value generally failed when using the algorithm described in this thesis. It is suspected that this is probably due to the fact that low values of the rate sensitivity parameters approximate the rate-independent constitutive equations. Most probably

what is required is that some kind of active set search algorithm should be used, as described in [26].

A. Calculation of the spatial algorithmic material operator

Using equation (9.11), and substituting equation (49) of [36] the following is obtained

$$J\left(\mathcal{E}_2^a\right)_{ijkl} = 2 \underset{iAjBkClD}{\mathbb{F}} \left(\underbrace{\frac{\partial\left(\delta_I^{\mathrm{n}+1}\right)}{\partial \hat{C}^{\mathrm{e}}{}_{CD}} \bar{C}^{\mathrm{p}-1}_{AB}}_{A} + \underbrace{\delta_I^{\mathrm{n}+1} \frac{\partial \bar{C}^{\mathrm{p}-1}_{AB}}{\partial \hat{C}^{\mathrm{e}}{}_{CD}}}_{B} + \underbrace{\mu \frac{\partial}{\partial \hat{C}^{\mathrm{e}}{}_{CD}} \left(\bar{C}^{\mathrm{p}-1}_{AE} \hat{C}^{\mathrm{e}}{}_{EG} \bar{C}^{\mathrm{p}-1}_{GB} \right)}_{C} \right), \tag{A.1}$$

Here the 8th order tensor $\underset{iAjBkClD}{\mathbb{F}} = \hat{F}^{\mathrm{e}}{}_{iA} \hat{F}^{\mathrm{e}}{}_{jB} \hat{F}^{\mathrm{e}}{}_{kC} \hat{F}^{\mathrm{e}}{}_{lD}$ is used. Now, focusing only at the first term (term A)

$$\begin{aligned}
& 2 \underset{iAjBkClD}{\mathbb{F}} \left(\frac{\partial\left(\frac{1}{2}\lambda\left(\left(C_e^{\mathrm{n}+1}\right)_{HH} - 3\right) - \mu\right)}{\partial \hat{C}^{\mathrm{e}}{}_{CD}} \bar{C}^{\mathrm{p}-1}_{AB} \right) \\
=& \lambda \underset{iAjBkClD}{\mathbb{F}} \left(\frac{\partial\left(C_e^{\mathrm{n}+1}\right)_{HH}}{\partial \hat{C}^{\mathrm{e}}{}_{CD}} \bar{C}^{\mathrm{p}-1}_{AB} \right) \\
=& \lambda \underset{iAjBkClD}{\mathbb{F}} \left(\frac{\partial\left(\bar{F}^{\mathrm{p}-1}_{MH} \hat{C}^{\mathrm{e}}{}_{MN} \bar{F}^{\mathrm{p}-1}_{NH}\right)}{\partial \hat{C}^{\mathrm{e}}{}_{CD}} \bar{C}^{\mathrm{p}-1}_{AB} \right) \\
=& \lambda \underset{iAjBkClD}{\mathbb{F}} \left(\left(\bar{C}^{\mathrm{p}-1}_{CD} + \frac{\partial \bar{F}^{\mathrm{p}-1}_{MH}}{\partial \hat{C}^{\mathrm{e}}{}_{CD}} \hat{C}^{\mathrm{e}}{}_{MN} \bar{F}^{\mathrm{p}-1}_{NH} + \bar{F}^{\mathrm{p}-1}_{MH} \hat{C}^{\mathrm{e}}{}_{MN} \frac{\partial \bar{F}^{\mathrm{p}-1}_{NH}}{\partial \hat{C}^{\mathrm{e}}{}_{CD}} \right) \bar{C}^{\mathrm{p}-1}_{AB} \right) \\
=& \lambda \underset{iAjBkClD}{\mathbb{F}} \left(\left(\bar{C}^{\mathrm{p}-1}_{CD} + \hat{C}^{\mathrm{e}}{}_{MN} \underbrace{\left(\frac{\partial \bar{F}^{\mathrm{p}-1}_{MH}}{\partial \nu^\beta} \bar{F}^{\mathrm{p}-1}_{NH} + \bar{F}^{\mathrm{p}-1}_{MH} \frac{\partial \bar{F}^{\mathrm{p}-1}_{NH}}{\partial \nu^\beta} \right)}_{X} \left(\frac{\partial \nu^\beta}{\partial \hat{C}^{\mathrm{e}}{}_{CD}} \right) \right) \bar{C}^{\mathrm{p}-1}_{AB} \right)
\end{aligned}$$

Equation (52) in [36] shows that $\partial_{\nu^\beta}\left(\bar{C}^{\mathrm{p}}\right)^{-1} = 2\left(\left(\partial_{\nu^\beta}\left(\bar{F}^{\mathrm{p}-1}\right)\right)\bar{F}^{\mathrm{p}-1}\right)^{\mathrm{sym}}$, which is the same as X, so

$$\begin{aligned}
=& \lambda \underset{iAjBkClD}{\mathbb{F}} \left(\hat{F}^{\mathrm{e}-1}_{AO} B^{\mathrm{e}}_{OP} \hat{F}^{\mathrm{e}-1}_{BP} \right) \left(\hat{F}^{\mathrm{e}-1}_{CM} B^{\mathrm{e}}_{MN} \hat{F}^{\mathrm{e}-1}_{DN} \right) + \lambda \underset{iAjBkClD}{\mathbb{F}} \left(\hat{C}^{\mathrm{e}}{}_{MN} \frac{\partial \bar{C}^{\mathrm{p}-1}_{MN}}{\partial \nu^\beta} \frac{\partial \nu^\beta}{\partial \hat{C}^{\mathrm{e}}{}_{CD}} \right) \bar{C}^{\mathrm{p}-1}_{AB} \\
=& \lambda \delta_{iO} \delta_{jP} \left(B^{\mathrm{e}}_{OP}\right) \left(B^{\mathrm{e}}_{MN}\right) \delta_{kM} \delta_{lN} + \lambda \hat{F}^{\mathrm{e}}{}_{kC} \hat{F}^{\mathrm{e}}{}_{lD} \left(\hat{C}^{\mathrm{e}}{}_{MN} \frac{\partial \bar{C}^{\mathrm{p}-1}_{MN}}{\partial \nu^\beta} \frac{\partial \nu^\beta}{\partial \hat{C}^{\mathrm{e}}{}_{CD}} \right) \left(\bar{C}^{\mathrm{p}-1}_{AB} \hat{F}^{\mathrm{e}}{}_{kC} \hat{F}^{\mathrm{e}}{}_{lD} \right)
\end{aligned}$$

A. Calculation of the spatial algorithmic material operator

$$
\begin{aligned}
=&\lambda B^{\mathrm{e}}_{ij}B^{\mathrm{e}}_{kl}+\lambda \hat{F}^{\mathrm{e}}{}_{kC}\hat{F}^{\mathrm{e}}{}_{lD}\left(\hat{C}^{\mathrm{e}}{}_{MN}\frac{\partial \bar{C}^{\mathrm{p}-1}_{MN}}{\partial \nu^{\beta}}\frac{\partial \nu^{\beta}}{\partial \hat{C}^{\mathrm{e}}{}_{CD}}\right)B^{\mathrm{e}}_{ij}\\
=&\lambda B^{\mathrm{e}}_{ij}B^{\mathrm{e}}_{kl}+\sum_{\beta}\left(\lambda \hat{F}^{\mathrm{e}}{}_{kC}\hat{F}^{\mathrm{e}}{}_{lD}\hat{C}^{\mathrm{e}}{}_{MN}\frac{\partial \bar{C}^{\mathrm{p}-1}_{MN}}{\partial \nu^{\beta}}B^{\mathrm{e}}_{ij}\right)\left(\frac{\partial \nu^{\beta}}{\partial \hat{C}^{\mathrm{e}}{}_{CD}}\right).
\end{aligned}
$$

Now the second term (term B) of equation (A.1) will be examined

$$
\begin{aligned}
&2\underset{iAjBkClD}{\mathbb{F}}\left(\delta^{\mathrm{n}+1}_{I}\frac{\partial \bar{C}^{\mathrm{p}-1}_{AB}}{\partial \hat{C}^{\mathrm{e}}{}_{CD}}\right)\\
=&2\underset{iAjBkClD}{\mathbb{F}}\left(\delta^{\mathrm{n}+1}_{I}\sum_{\beta}\frac{\partial \bar{C}^{\mathrm{p}-1}_{AB}}{\partial \nu^{\beta}}\frac{\partial \nu^{\beta}}{\partial \hat{C}^{\mathrm{e}}{}_{CD}}\right)\\
=&\sum_{\beta}\left(\underset{iAjBkClD}{\mathbb{F}}\left(2\delta^{\mathrm{n}+1}_{I}\frac{\partial \bar{C}^{\mathrm{p}-1}_{AB}}{\partial \nu^{\beta}}\right)\right)\left(\frac{\partial \nu^{\beta}}{\partial \hat{C}^{\mathrm{e}}{}_{CD}}\right).
\end{aligned}
$$

Lastly the third term (term C) of equation (A.1) is

$$
\begin{aligned}
&2\underset{iAjBkClD}{\mathbb{F}}\left(\mu\frac{\partial}{\partial \hat{C}^{\mathrm{e}}{}_{CD}}\left(\bar{C}^{\mathrm{p}-1}_{AE}\hat{C}^{\mathrm{e}}{}_{EG}\bar{C}^{\mathrm{p}-1}_{GB}\right)\right)\\
=&2\mu\underset{iAjBkClD}{\mathbb{F}}\left(\left(\frac{\partial \bar{C}^{\mathrm{p}-1}_{AE}}{\partial \hat{C}^{\mathrm{e}}{}_{CD}}\hat{C}^{\mathrm{e}}{}_{EG}\bar{C}^{\mathrm{p}-1}_{GB}\right)+\left(\bar{C}^{\mathrm{p}-1}_{AE}\frac{\partial \hat{C}^{\mathrm{e}}{}_{EG}}{\partial \hat{C}^{\mathrm{e}}{}_{CD}}\bar{C}^{\mathrm{p}-1}_{GB}\right)\right.\\
&\left.+\left(\bar{C}^{\mathrm{p}-1}_{AE}\hat{C}^{\mathrm{e}}{}_{EG}\frac{\partial \bar{C}^{\mathrm{p}-1}_{GB}}{\partial \hat{C}^{\mathrm{e}}{}_{CD}}\right)\right)\\
=&2\mu\underset{iAjBkClD}{\mathbb{F}}\left(\left(\bar{C}^{\mathrm{p}-1}_{AE}\frac{1}{2}\left(\delta_{EC}\delta_{GD}+\delta_{ED}\delta_{GC}\right)\bar{C}^{\mathrm{p}-1}_{GB}\right)\right.\\
&\left.+\sum_{\beta}\left(\left(\frac{\partial \bar{C}^{\mathrm{p}-1}_{AE}}{\partial \nu^{\beta}}\hat{C}^{\mathrm{e}}{}_{EG}\bar{C}^{\mathrm{p}-1}_{GB}\right)+\left(\bar{C}^{\mathrm{p}-1}_{AE}\hat{C}^{\mathrm{e}}{}_{EG}\frac{\partial \bar{C}^{\mathrm{p}-1}_{GB}}{\partial \nu^{\beta}}\right)\right)\left(\frac{\partial \nu^{\beta}}{\partial \hat{C}^{\mathrm{e}}{}_{CD}}\right)\right)\\
&=2\mu\underset{iAjBkClD}{\mathbb{F}}\left(\frac{1}{2}\left(\bar{C}^{\mathrm{p}-1}_{AC}\bar{C}^{\mathrm{p}-1}_{DB}+\bar{C}^{\mathrm{p}-1}_{AD}\bar{C}^{\mathrm{p}-1}_{CB}\right)\right.\\
&\left.+\sum_{\beta}\left(2\left(\frac{\partial \bar{C}^{\mathrm{p}-1}_{AE}}{\partial \nu^{\beta}}\hat{C}^{\mathrm{e}}{}_{EG}\bar{C}^{\mathrm{p}-1}_{GB}\right)^{\mathrm{SYM}}\right)\left(\frac{\partial \nu^{\beta}}{\partial \hat{C}^{\mathrm{e}}{}_{CD}}\right)\right)\\
&=\mu\left(B^{\mathrm{e}}_{ik}B^{\mathrm{e}}_{lj}+B^{\mathrm{e}}_{il}B^{\mathrm{e}}_{kj}\right)+\sum_{\beta}\left(4\mu\underset{iAjBkClD}{\mathbb{F}}\left(\frac{\partial \bar{C}^{\mathrm{p}-1}_{AE}}{\partial \nu^{\beta}}\hat{C}^{\mathrm{e}}{}_{EG}\bar{C}^{\mathrm{p}-1}_{GB}\right)^{\mathrm{SYM}}\right)\left(\frac{\partial \nu^{\beta}}{\partial \hat{C}^{\mathrm{e}}{}_{CD}}\right)
\end{aligned}
$$

Finally, joining all of these back together, the spatial algorithmic material operator is

$$
\begin{aligned}
J\left(\mathcal{E}^{a}_{2}\right)_{ijkl}=&\lambda B^{\mathrm{e}}_{ij}B^{\mathrm{e}}_{kl}+\mu\left(B^{\mathrm{e}}_{ik}B^{\mathrm{e}}_{lj}+B^{\mathrm{e}}_{il}B^{\mathrm{e}}_{kj}\right)\\
&+\sum_{\beta}\left(\underset{iAjBkClD}{\mathbb{F}}\left(\left(4\mu\frac{\partial \bar{C}^{\mathrm{p}-1}_{AE}}{\partial \nu^{\beta}}\hat{C}^{\mathrm{e}}{}_{EG}\bar{C}^{\mathrm{p}-1}_{GB}\right)^{\mathrm{SYM}}+2\delta^{\mathrm{n}+1}_{I}\frac{\partial \bar{C}^{\mathrm{p}-1}_{AB}}{\partial \nu^{\beta}}\right)\right.\right.\\
&\left.\left.+\left(\lambda \hat{F}^{\mathrm{e}}{}_{kC}\hat{F}^{\mathrm{e}}{}_{lD}\hat{C}^{\mathrm{e}}{}_{MN}\frac{\partial \bar{C}^{\mathrm{p}-1}_{MN}}{\partial \nu^{\beta}}B^{\mathrm{e}}_{ij}\right)\right)\left(\frac{\partial \nu^{\beta}}{\partial \hat{C}^{\mathrm{e}}{}_{CD}}\right),
\end{aligned}
$$

where the derivative $\frac{\partial \nu^{\beta}}{\partial \hat{C^{e}}_{CD}}$ is shown in Appendix B.

B. Calculating the derivative of the resolved shear

Recall equation (10.24)

$$\frac{\partial \tau^{\beta}_{\mathrm{n+1}}}{\partial \nu^{\alpha}_{\mathrm{n+1}}} = \frac{\partial \tau^{\beta}_{\mathrm{n+1}}}{\partial \mathbf{C}^{\mathrm{e}}_{\mathrm{n+1}}} : \frac{\partial \mathbf{C}^{\mathrm{e}}_{\mathrm{n+1}}}{\partial \nu^{\alpha}_{\mathrm{n+1}}}.$$

First note that the resolved shear can be rewritten as follows

$$\begin{aligned}
\tau^{\alpha}_{\mathrm{n+1}} &= \mathbf{F}^{\mathrm{e}}{}_{\mathrm{n+1}} \mathbf{s}^{\alpha} \boldsymbol{\sigma}_{\mathbf{n+1}} \mathbf{F}^{\mathrm{e}}{}_{\mathrm{n+1}}{}^{-1} \mathbf{m}^{\alpha} \\
&= \mathbf{F}^{\mathrm{e}}{}_{\mathrm{n+1}}{}^{T} \boldsymbol{\sigma}_{\mathbf{n+1}} \mathbf{F}^{\mathrm{e}}{}_{\mathrm{n+1}}{}^{-T} : (\mathbf{s}^{\alpha} \otimes \mathbf{m}^{\alpha}) \\
&= \mathbf{F}^{\mathrm{e}}{}_{\mathrm{n+1}}{}^{T} \left(\left(\mathbf{F}^{\mathrm{e}}{}_{\mathrm{n+1}} \right) \mathbf{F}^{\mathrm{e}}{}_{\mathrm{n+1}}{}^{-1} \right) \boldsymbol{\sigma}_{\mathbf{n+1}} \mathbf{F}^{\mathrm{e}}{}_{\mathrm{n+1}}{}^{-T} : (\mathbf{s}^{\alpha} \otimes \mathbf{m}^{\alpha}) \\
&= \mathbf{C}^{\mathrm{e}}_{\mathrm{n+1}} \mathbf{S}^{\mathrm{e}}_{\mathrm{n+1}} : (\mathbf{s}^{\alpha} \otimes \mathbf{m}^{\alpha}) .
\end{aligned} \tag{B.1}$$

Recall that for the St. Venant-Kirchhoff model of elasticity, the second Piola-Kirchoff stress is given as

$$\mathbf{S}^{\mathrm{e}}_{\mathrm{n+1}} = \frac{1}{2} \lambda \mathrm{tr} \left(\mathbf{C}^{\mathrm{e}}_{\mathrm{n+1}} - \mathbf{I} \right) \mathbf{I} + \mu \left(\mathbf{C}^{\mathrm{e}}_{\mathrm{n+1}} - \mathbf{I} \right), \tag{B.2}$$

so the resolved shear is

$$\tau^{\beta}_{\mathrm{n+1}} = \left(\frac{1}{2} \lambda \mathrm{tr} \left(\mathbf{C}^{\mathrm{e}}_{\mathrm{n+1}} - \mathbf{I} \right) \mathbf{C}^{\mathrm{e}}_{\mathrm{n+1}} + \mu \mathbf{C}^{\mathrm{e}}_{\mathrm{n+1}} \left(\mathbf{C}^{\mathrm{e}}_{\mathrm{n+1}} - \mathbf{I} \right) \right) : (\mathbf{s}^{\alpha} \otimes \mathbf{m}^{\alpha}), \tag{B.3}$$

and in indicial form

$$\tau^{\beta}_{\mathrm{n+1}} = \left(\frac{1}{2} \lambda \left(\left(C^{\mathrm{e}}_{\mathrm{n+1}} \right)_{\phi\phi} - \delta_{\phi\phi} \right) \left(C^{\mathrm{e}}_{\mathrm{n+1}} \right)_{\gamma\psi} + \mu \left(C^{\mathrm{e}}_{\mathrm{n+1}} \right)_{\gamma\xi} \left(\left(C^{\mathrm{e}}_{\mathrm{n+1}} \right)_{\xi\psi} - \delta_{\xi\psi} \right) \right) s^{\beta}_{\gamma} m^{\beta}_{\psi}. \tag{B.4}$$

The derivative $\partial_{\mathbf{C}^{\mathrm{e}}} \tau^{\beta}_{\mathrm{n+1}}$ is thus

$$\begin{aligned}
\frac{\partial \tau^{\beta}_{\mathrm{n+1}}}{\partial \left(C^{\mathrm{e}}_{\mathrm{n+1}} \right)_{\omega\rho}} =& \left(\frac{1}{2} \lambda \left(\left(\left(C^{\mathrm{e}}_{\mathrm{n+1}} \right)_{\phi\phi} - \delta_{\phi\phi} \right) \frac{1}{2} \left(\delta_{\gamma\omega} \delta_{\psi\rho} + \delta_{\gamma\rho} \delta_{\psi\omega} \right) + \delta_{\omega\rho} \left(C^{\mathrm{e}}_{\mathrm{n+1}} \right)_{\gamma\psi} \right) \right. \\
&\left. + \mu \left(\frac{1}{2} \left(\delta_{\gamma\omega} \delta_{\xi\rho} + \delta_{\gamma\rho} \delta_{\xi\omega} \right) \left(\left(C^{\mathrm{e}}_{\mathrm{n+1}} \right)_{\xi\psi} - \delta_{\xi\psi} \right) + \frac{1}{2} \left(C^{\mathrm{e}}_{\mathrm{n+1}} \right)_{\gamma\xi} \left(\delta_{\xi\omega} \delta_{\psi\rho} + \delta_{\xi\rho} \delta_{\psi\omega} \right) \right) \right) s^{\beta}_{\gamma} m^{\beta}_{\psi} \\
=& \frac{1}{2} \lambda \left(\left(C^{\mathrm{e}}_{\mathrm{n+1}} \right)_{\phi\phi} - \delta_{\phi\phi} \right) \frac{1}{2} \left(s^{\beta}_{\omega} m^{\beta}_{\rho} + s^{\beta}_{\rho} m^{\beta}_{\omega} \right) + \frac{1}{2} \lambda \delta_{\omega\rho} \left(C^{\mathrm{e}}_{\mathrm{n+1}} \right)_{\gamma\psi} s^{\beta}_{\gamma} m^{\beta}_{\psi} \\
&+ \mu \frac{1}{2} \left(\left(\left(C^{\mathrm{e}}_{\mathrm{n+1}} \right)_{\rho\psi} - \delta_{\rho\psi} \right) s^{\beta}_{\omega} m^{\beta}_{\psi} + \left(\left(C^{\mathrm{e}}_{\mathrm{n+1}} \right)_{\omega\psi} - \delta_{\omega\psi} \right) s^{\beta}_{\rho} m^{\beta}_{\psi} \right) \\
&+ \mu \frac{1}{2} \left(\left(C^{\mathrm{e}}_{\mathrm{n+1}} \right)_{\gamma\omega} s^{\beta}_{\gamma} m^{\beta}_{\rho} + \left(C^{\mathrm{e}}_{\mathrm{n+1}} \right)_{\gamma\rho} s^{\beta}_{\gamma} m^{\beta}_{\omega} \right) \\
=& \frac{1}{2} \lambda \left(\left(C^{\mathrm{e}}_{\mathrm{n+1}} \right)_{\phi\phi} - \delta_{\phi\phi} \right) \frac{1}{2} \left(s^{\beta}_{\omega} m^{\beta}_{\rho} + s^{\beta}_{\rho} m^{\beta}_{\omega} \right) + \frac{1}{2} \lambda \delta_{\omega\rho} \left(C^{\mathrm{e}}_{\mathrm{n+1}} \right)_{\gamma\psi} s^{\beta}_{\gamma} m^{\beta}_{\psi}
\end{aligned}$$

$$
\begin{aligned}
&+\mu\frac{1}{2}\left(\left(C^{\mathrm{e}}_{\mathrm{n+1}}\right)_{\rho\psi}s^{\beta}_{\omega}m^{\beta}_{\psi}-s^{\beta}_{\omega}m^{\beta}_{\rho}+\left(C^{\mathrm{e}}_{\mathrm{n+1}}\right)_{\omega\psi}s^{\beta}_{\rho}m^{\beta}_{\psi}-s^{\beta}_{\rho}m^{\beta}_{\omega}\right)\\
&+\mu\frac{1}{2}\left(\left(C^{\mathrm{e}}_{\mathrm{n+1}}\right)_{\gamma\omega}s^{\beta}_{\gamma}m^{\beta}_{\rho}+\left(C^{\mathrm{e}}_{\mathrm{n+1}}\right)_{\gamma\rho}s^{\beta}_{\gamma}m^{\beta}_{\omega}\right)\\
=&\frac{1}{2}\lambda\left(\left(C^{\mathrm{e}}_{\mathrm{n+1}}\right)_{\phi\phi}-\delta_{\phi\phi}\right)\frac{1}{2}\left(s^{\beta}_{\omega}m^{\beta}_{\rho}+s^{\beta}_{\rho}m^{\beta}_{\omega}\right)+\frac{1}{2}\lambda\delta_{\omega\rho}\left(C^{\mathrm{e}}_{\mathrm{n+1}}\right)_{\gamma\psi}s^{\beta}_{\gamma}m^{\beta}_{\psi}\\
&+\mu\frac{1}{2}\left(\left(C^{\mathrm{e}}_{\mathrm{n+1}}\right)_{\rho\psi}s^{\beta}_{\omega}m^{\beta}_{\psi}+\left(C^{\mathrm{e}}_{\mathrm{n+1}}\right)_{\gamma\rho}s^{\beta}_{\gamma}m^{\beta}_{\omega}+\left(C^{\mathrm{e}}_{\mathrm{n+1}}\right)_{\omega\psi}s^{\beta}_{\rho}m^{\beta}_{\psi}+\left(C^{\mathrm{e}}_{\mathrm{n+1}}\right)_{\gamma\omega}s^{\beta}_{\gamma}m^{\beta}_{\rho}\right)\\
&-\mu\frac{1}{2}\left(s^{\beta}_{\rho}m^{\beta}_{\omega}+s^{\beta}_{\omega}m^{\beta}_{\rho}\right)
\end{aligned}
$$

Keeping in mind that $\mathbf{C^e}$ is symmetric, this can be rewritten in vector form as

$$
\begin{aligned}
\frac{\partial\tau^{\beta}_{\mathrm{n+1}}}{\partial\mathbf{C}^{\mathrm{e}}_{\mathrm{n+1}}}=&\frac{1}{2}\lambda\mathrm{tr}\left(\mathbf{C}^{\mathrm{e}}_{\mathrm{n+1}}-\mathbf{I}\right)\mathbf{P}^{\beta}+\frac{1}{2}\lambda\left(\mathbf{C}^{\mathrm{e}}_{\mathrm{n+1}}:\mathbf{P}^{\beta}\right)\mathbf{I}\\
&+\mu\frac{1}{2}\left(\mathbf{Z}{\mathbf{C}^{\mathrm{e}}_{\mathrm{n+1}}}^{T}+\mathbf{Z}^{T}{\mathbf{C}^{\mathrm{e}}_{\mathrm{n+1}}}^{T}+\mathbf{C}^{\mathrm{e}}_{\mathrm{n+1}}\mathbf{Z}^{T}+\mathbf{C}^{\mathrm{e}}_{\mathrm{n+1}}\mathbf{Z}\right)\\
&-\mu\mathbf{P}^{\beta}\\
=&\frac{1}{2}\lambda\mathrm{tr}\left(\mathbf{C}^{\mathrm{e}}_{\mathrm{n+1}}-\mathbf{I}\right)\mathbf{P}^{\beta}+\frac{1}{2}\lambda\left(\mathbf{C}^{\mathrm{e}}_{\mathrm{n+1}}:\mathbf{P}^{\beta}\right)\mathbf{I}\\
&+\mu\frac{1}{2}\left(2\left(\mathbf{C}^{\mathrm{e}}_{\mathrm{n+1}}\mathbf{P}^{\beta}\right)^{T}+2\mathbf{C}^{\mathrm{e}}_{\mathrm{n+1}}\mathbf{P}^{\beta}\right)\\
&-\mu\mathbf{P}^{\beta}\\
=&\frac{1}{2}\lambda\mathrm{tr}\left(\mathbf{C}^{\mathrm{e}}_{\mathrm{n+1}}-\mathbf{I}\right)\mathbf{P}^{\beta}+\frac{1}{2}\lambda\left(\mathbf{C}^{\mathrm{e}}_{\mathrm{n+1}}:\mathbf{P}^{\beta}\right)\mathbf{I}\\
&+\mu 2\left(\mathbf{C}^{\mathrm{e}}_{\mathrm{n+1}}\mathbf{P}^{\beta}\right)^{\mathrm{SYM}}-\mu\mathbf{P}^{\beta}\\
=&\left(\mathbf{S}^{\mathrm{e}}_{\mathrm{n+1}}\mathbf{P}^{\beta}\right)^{\mathrm{SYM}}+\frac{1}{2}\lambda\left(\mathbf{C}^{\mathrm{e}}_{\mathrm{n+1}}:\mathbf{P}^{\beta}\right)\mathbf{I}+\mu\left(\mathbf{C}^{\mathrm{e}}_{\mathrm{n+1}}\mathbf{P}^{\beta}\right)^{\mathrm{SYM}}.
\end{aligned}
\tag{B.5}
$$

Next $\partial_{\nu^{\alpha}}\mathbf{C}^{\mathrm{e}}_{\mathrm{n+1}}$ is found. First note that

$$
\mathbf{C}^{\mathrm{e}}_{\mathrm{n+1}}=\bar{\mathbf{F}}^{\mathrm{p}-T}\hat{\mathbf{C}}^{\mathrm{e}}\bar{\mathbf{F}}^{\mathrm{p}-1},
\tag{B.6}
$$

therefore the derivative is

$$
\begin{aligned}
\frac{\partial\mathbf{C}^{\mathrm{e}}_{\mathrm{n+1}}}{\partial\nu^{\alpha}_{\mathrm{n+1}}}&=\frac{\partial\bar{\mathbf{F}}^{\mathrm{p}-T}}{\partial\nu^{\alpha}_{\mathrm{n+1}}}\hat{\mathbf{C}}^{\mathrm{e}}\bar{\mathbf{F}}^{\mathrm{p}-1}+\bar{\mathbf{F}}^{\mathrm{p}-T}\hat{\mathbf{C}}^{\mathrm{e}}\frac{\partial\bar{\mathbf{F}}^{\mathrm{p}-1}}{\partial\nu^{\alpha}_{\mathrm{n+1}}}\\
&=2\left(\bar{\mathbf{F}}^{\mathrm{p}-T}\hat{\mathbf{C}}^{\mathrm{e}}\frac{\partial\bar{\mathbf{F}}^{\mathrm{p}-1}}{\partial\nu^{\alpha}_{\mathrm{n+1}}}\right)^{\mathrm{SYM}},
\end{aligned}
\tag{B.7}
$$

where

$$
\begin{aligned}
\frac{\partial\bar{\mathbf{F}}^{\mathrm{p}-1}}{\partial\nu^{\alpha}_{\mathrm{n+1}}}=&\frac{\partial}{\partial\nu^{\alpha}_{\mathrm{n+1}}}\left(\left(\mathbf{I}+(1-\theta)\boldsymbol{\Lambda}\right)^{-1}\left(\mathbf{I}-\theta\boldsymbol{\Lambda}\right)\right)\\
=&\frac{\partial\left(\mathbf{I}+(1-\theta)\boldsymbol{\Lambda}\right)^{-1}}{\partial\nu^{\alpha}_{\mathrm{n+1}}}\left(\mathbf{I}-\theta\boldsymbol{\Lambda}\right)+\left(\mathbf{I}+(1-\theta)\boldsymbol{\Lambda}\right)^{-1}\frac{\partial\left(\mathbf{I}-\theta\boldsymbol{\Lambda}\right)}{\partial\nu^{\alpha}_{\mathrm{n+1}}}\\
=&\frac{\partial\left(\mathbf{I}+(1-\theta)\boldsymbol{\Lambda}\right)^{-1}}{\partial\left(\mathbf{I}+(1-\theta)\boldsymbol{\Lambda}\right)}\frac{\partial\left(\mathbf{I}+(1-\theta)\boldsymbol{\Lambda}\right)}{\partial\nu^{\alpha}_{\mathrm{n+1}}}\left(\mathbf{I}-\theta\boldsymbol{\Lambda}\right)
\end{aligned}
$$

$$
\begin{aligned}
&+ \left(\mathbf{I} + (1-\theta)\,\mathbf{\Lambda}\right)^{-1} (-\theta)\, \frac{\partial \mathbf{\Lambda}}{\partial \nu^{\alpha}_{\mathrm{n+1}}} \\
&= - \left(\mathbf{I} + (1-\theta)\,\mathbf{\Lambda}\right)^{-1} (1-\theta)\, \frac{\partial \mathbf{\Lambda}}{\partial \nu^{\alpha}_{\mathrm{n+1}}} \left(\mathbf{I} + (1-\theta)\,\mathbf{\Lambda}\right)^{-1} \left(\mathbf{I} - \theta \mathbf{\Lambda}\right) \\
&\quad + \left(\mathbf{I} + (1-\theta)\,\mathbf{\Lambda}\right)^{-1} (-\theta)\, \frac{\partial \mathbf{\Lambda}}{\partial \nu^{\alpha}_{\mathrm{n+1}}} \\
&= - \left(\mathbf{I} + (1-\theta)\,\mathbf{\Lambda}\right)^{-1} \frac{\partial \mathbf{\Lambda}}{\partial \nu^{\alpha}_{\mathrm{n+1}}} \left(\theta + (1-\theta) \left(\bar{\mathbf{F}}_{\mathbf{p}}\right)^{-1}\right) \\
&= - \Delta t \left(\mathbf{I} + (1-\theta)\,\mathbf{\Lambda}\right)^{-1} \mathbf{Z}^{\alpha} \left(\theta + (1-\theta) \left(\bar{\mathbf{F}}_{\mathbf{p}}\right)^{-1}\right). \qquad \text{(B.8)}
\end{aligned}
$$

Bibliography

[1] L. Anand and M. Kothari. A computational procedure for rate-independant crystal plasticity. *Journal of the Mechanics and Physics of Solids*, 44:525–558, 1996.

[2] R.J. Asaro and J.R. Rice. Strain localization in ductile single crystals. *Journal of the Mechanics and Physics of Solids*, 25(5):309–338, 1977.

[3] Robert J Asaro. Micromechanics of crystals and polycrystals. *Advances in Applied Mechanics*, 23:1–115, 1983.

[4] Robert J Asaro. Crystal plasticity. *Journal of Applied Mechanics*, 50:921, 1983.

[5] Robert J Asaro and A Needleman. Texture development and strain hardening in rate-dependent polycrystals. *Acta Metallurgica*, 33(6):923–953, 1985.

[6] W. Bangerth. DEAL II, the step-8 tutorial program. Online, February 2013. URL `http://www.dealii.org/7.2.0/doxygen/tutorial/index.html`.

[7] W. Bangerth, R Hartmann, and G. Kanschat. deal.II — a general-purpose object-oriented finite element library. *ACM Transactions on Mathematical Software*, 33(4), 1999.

[8] F. Brezzi and M. Fortin. *Mixed and Hybrid Finite Element Methods*. Springer series in computational mathematics. Springer-Verlag, 1991.

[9] Octave community. Gnu/octave, 2012. URL `www.gnu.org/software/octave/`.

[10] E.A. de Souza Neto, D. Peric, and D.R.J. Owen. *Computational Methods for Plasticity: Theory and Applications*. Wiley, 2011.

[11] D.C. Drucker. *A More Fundamental Approach to Plastic Stress-strain Relations*. Division of Applied Mathematics, Brown University, 1951.

[12] M.E. Gurtin. A finite-deformation, gradient theory of single-crystal plasticity with free energy dependent on densities of geometrically necessary dislocations. *International Journal of Plasticity*, 24(4):702 – 725, 2008.

[13] M.E. Gurtin. A finite-deformation, gradient theory of single-crystal plasticity with free energy dependent on the accumulation of geometrically necessary dislocations. *International Journal of Plasticity*, 26:1073–1096, 2010.

[14] M.E. Gurtin and B.D. Reddy. Gradient single-crystal plasticity within a Mises-Hill framework based on a new formulation of self and latent hardening. *In Review*, 2013.

[15] M.E. Gurtin, E. Fried, and L. Anand. *The Mechanics and Thermodynamics of Continua*. Cambridge University Press, 2010. Chapter 110.

[16] W. Han and B.D. Reddy. *Plasticity: Mathematical Theory and Numerical Analysis*. Springer, New York, second edition, 2013.

[17] R. Hill. Generalized constitutive relations for incremental deformation of metal crystals by multislip. *Journal of the Mechanics and Physics of Solids*, 14(2):95–102, 1966.

[18] R. Hill. *The Mathematical Theory of Plasticity*. Oxford Classic Texts in the Physical Sciences Series. Clarendon Press, 1998.

[19] R. Hill and J.R. Rice. Constitutive analysis of elastic-plastic crystals at arbitrary strain. *Journal of the Mechanics and Physics of Solids*, 20(6):401–413, 1972.

[20] G.A. Holzapfel. *Nonlinear Solid Mechanics: A Continuum Approach for Engineering*. John Wiley & Sons, 2000.

[21] E. Kröner. Allgemeine kontinuumstheorie der Versetzungen und Eigenspannungen. *Archive for Rational Mechanics and Analysis*, 4(4):273–334, 1960.

[22] E.H. Lee. Elastic-plastic deformations at finite strains. *Journal of Applied Mechanics*, 36: 1–6, 1969.

[23] G. Maenchen and S. Sacks. The tensor code. *Methods of Computational Physics*, 3:181–210, 1964.

[24] Jean Mandel. Généralisation de la théorie de plasticité de WT Koiter. *International Journal of Solids and structures*, 1(3):273–295, 1965.

[25] C. Miehe. Exponential map algorithm for stress updates in anisotropic multiplicative elastoplasticity for single crystals. *International Journal for Numerical Methods in Engineering*, 39(19):3367–3390, 1996.

[26] C. Miehe and J. Schröder. A comparative study of stress update algorithms for rate-independent and rate-dependent crystal plasticity. *International Journal for Numerical Methods in Engineering*, 50(2):273–298, 2001.

[27] D. Peirce, R.J. Asaro, and A. Needleman. Material rate dependence and localized deformation in crystalline solids. *Acta Metallurgica*, 31(12):1951–1976, 1983.

[28] W. Prager. Recent developments in the mathematical theory of plasticity. *Journal of Applied Physics*, 20(3):235–241, 1949.

[29] Ludwig Prandtl. Spannungsverteilung in plastischen Körpern. In *Proceedings of the 1st International Congress on Applied Mechanics, Delft*, pages 43–54, 1924.

[30] Ludwig Prandtl. Ein Gedankenmodell zur kinetischen Theorie der festen Körper. *Zeitschrift für Angewandte Mathematik und Mechanik*, 8(2):85–106, 1928.

[31] B.D. Reddy, C. Wieners, and B. Wohlmuth. Finite element analysis and algorithms for single-crystal strain-gradient plasticity. *International Journal for Numerical Methods in Engineering*, 90(6):784–804, 2012.

[32] A. Reuss. Berücksichtigung der elastischen Formänderung in der Plastizitätstheorie. *Zeitschrift für Angewandte Mathematik und Mechanik*, 10:266–274, 1930.

[33] J.R. Rice. Inelastic constitutive relations for solids: an internal-variable theory and its application to metal plasticity. *Journal of the Mechanics and Physics of Solids*, 19(6):433–455, 1971.

[34] J.C. Simo. Numerical analysis and simulation of plasticity. In P.G. Ciarlet and J.L. Lions, editors, *Numerical Methods for Solids (Part 3) Numerical Methods for Fluids (Part 1)*, volume 6 of *Handbook of Numerical Analysis*, pages 183 – 499. Elsevier, 1998.

[35] J.C. Simo and R.L Taylor. Consistent tangent operators for rate-independent elastoplasticity. *Computer methods in applied mechanics and engineering*, 48(1):101–118, 1985.

[36] P. Steinmann and E. Stein. On the numerical treatment and analysis of finite deformation ductile single crystal plasticity. *Computer Methods in Applied Mechanics and Engineering*, 129(3):235–254, 1996.

[37] G.I. Taylor and C.F. Elam. Bakerian lecture. the distortion of an aluminium crystal during a tensile test. *Proceedings of the Royal Society of London. Series A*, 102(719):643–667, 1923.

[38] G.I. Taylor and C.F. Elam. The plastic extension and fracture of aluminium crystals. *Proceedings of the Royal Society of London. Series A*, 108(745):28–51, 1925.

[39] S.G.I. Taylor. Plastic strain in metals. *The Journal of the Institute of Metals*, LXII:307–324, 1938.

[40] C. Truesdell, W. Noll, and S. Antman. *The Non-Linear Field Theories of Mechanics*. Number v. 3 in The non-linear field theories of mechanics. Springer, 2004.

[41] R. von Mises. Mechanik der festen Körper im plastisch deformablen Zustand. *Göttin. Nachr. Math. Phys*, 1:582–592, 1913.

[42] R. von Mises. Mechanik der plastischen Formänderung von Kristallen. *Zeitschrift für Angewandte Mathematik und Mechanik, B*, 8:161–185, 1928.

[43] G. Weber and L. Anand. Finite deformation constitutive equations and a time integration procedure for isotropic, hyperelastic-viscoplastic solids. *Computer Methods in Applied Mechanics and Engineering*, 79(2):173–202, 1990.

[44] M.L. Wilkins. Computation of elastic–plastic flow. *Methods of Computational Physics*, 1964.